People's Democratic Republic of Algeria

Ministry of Higher Education and Scientific Research

University of Ibn Khaldoun -Tiaret-

Faculty of Material Science

كلية علوم المادة

Physics Department

قسم الفيزياء

Project

Master

Promotion: Physics

Specialty: Material Physics

Presented by: SAFA SARA

Subject

ab-initio and experimental investigations of the physical properties of cobalt Sulfides

Presented in 30/06/2025, before the jury composed from:

Mr. M. Bousmaha	*President*	*Professor*	*UNIV. Tiaret*
Mr. M. Bezzarrouk	*Examiner*	*Associate Pr*	*UNIV. Tiaret*
Mr. A. Ammari	*Supervisor*	*Associate Pr*	*UNIV. Tiaret*
Mr. G. Benabdellah	*Co-Supervisor*	*Associate Pr*	*UNIV. Tiaret*

Scholar Year: 2024-2025

Dedication

To the twelve years old me you did it CHAMP

To the pillars of my life, my dear parents and brothers Mohamed and Zakaria, who have been my supports in my journey and the reason for my existence.

I dedicate this humble work to you with all love and appreciation.

And to my dear grandmother , who planted in me the love of science and knowledge, and her last words to me were like a beacon that illuminated my path, «Pay attention to your studies", your words will always remain in my heart.

To my friends and classmates for their support and encouragement

Also to the world of physics, this great universe that never ceases to amaze us,

I seek to be a part of you in a special way, armed with knowledge and passion to explore your infinite secrets.

Acknowledgement

Full praise and profound gratitude to the Almighty Allah who granted me with strength, patience and willingness to undertake and accomplish this study.

First of all, I would like to deeply thank my supervisor **Dr.AMMARI AbdelKader** for his full devotion, constant guidance and above all the remarkable support during the various stages of this project and the trust placed in me. Without your keen criticism, advice, collaboration, and patience, this dissertation would have never been accomplished. **Dr.BENABDELLAH Gholamellah** to have co-direct this work, I would express my gratitude for your precious interventions and thoughtful peace of advice.

Also, I am equally thankful to the members of the jury, **Pr. M.BOUSMAHA Hocine** and **Dr. BEZZEROUK Mohamed El amine**, for their time and effort for reviewing and evaluating the present work.

My thanks also go to **Pr. El-H. BELARBI,** the director of Synthesis and Catalysis laboratory. University Ibn Khaldoun Tiaret, for the measure of XRD and UV-visible measurements. Also, my thanks go to **Pr. B. BENRABAH,** the director of Physical Engineering laboratory, University Ibn Khaldoun Tiaret, for the FTIR measurements.

We would like to thank **Dr Ahmed SAFA** for his technical support in the realisation of the electronic part for our experimental setup.

My sincere thanks to the technical staff of the chemistry lab. Especially **Mr. LARBI AbdelKader,** whose expertise in managing laboratory equipment was crucial for my experiments. Their patience and readiness to assist at all times have left a profound impact on the completion of my project.

Finally, I would also like to thank the staff of the Department of Physics at University of Ibn Khaldoun-Tiaret, whose resources and assistance have been invaluable. There are many people who have helped me and supported me from near and far. I express my deep gratitude to them.

My thanks to all of you

SAFA SARA

Abbreviations

TMS: Transition Metal Sulfide

TMO: Transition Metal Oxide

TMCh: Transition Metal Chalcogenide

TMD: Transition Metal Dichalcogenide

SCs: Super Capacitors

KM : kubelka-Munk

uma: unite mass atomic

SRAM: Static Random Access Memory

DRAM: Dynamic Random Access Memory

CPU: Central Processing Unit

GPU: Graphics Processing Unit

MOF: Metal Organic Framework

HRETM: High Resolution Transmission Electron Microscope

EDLC: Electric Double-Layer Capacitor

CCP: Cubic Close Packed

HCP: Hexagonal Closed Packed

SQUID: Superconducting Quantum Interface Device

XRD: X-Ray Diffraction Analysis

XRR: X-Ray Reflectometry

UV-VIS-NIR: Ultraviolet-Visible-Nearinfrared

UVDRS: UV-Diffuse Reflectance Spectroscopy

FTIR: Fourier-Transform Infrared

TEM: Transmission Electron Microscopy

SEM: Scanning Electron Microscopy

XPS: X-Ray Photoelectron Spectroscopy

EDX: Energy Dispersive Spectroscopy Analysis

BET: Brunauer Emmett Teller

FESEM: Field Emission Scanning Electron Microscopy

PL : Photo-Luminescence

VASP**:**Vienna Ab-initio Simulation Package**.**

SAM : Scanning Auger Microscopy

ICP-OES: Inductively Coupled Plasma Optical Emission Spectroscopy

ERM: Electrical Resistivity Measurement

DSSC: Dye Synthesis Solar Cells

HER: Hydrogen Evolution Reaction

OER: Oxygen Evolution Reaction

ORR: Oxygen Reduction Reaction

CBD: Chemical Bath Deposition

PVD: Physical Vapour Deposition

QE: Quantum Espresso.

DFT: Density Function Theory

GGA: Generalized Gradient Approximation

LDA: Local Density Approximation

LSDA: Local Spin Density Approximation

HSE06: Heyd–Scuseria–Ernzerhof hybrid functional

SCCVD: Single Crystal Chemical Vapor Deposition

HRTEM: High-Resolution Transmission Electron Microscopy

KS: Kohn-Sham

SSSP: Standard Solid State Pseudo Potential

DFPT: Density Functional Perturbation Theory

FSP: Flame Spray Pyrolysis

ESP: Electrostatic Spray Pyrolysis

PSP: Pneumatic Spray Pyrolysis

VFSP: Vortex Flame Spray Pyrolysis

USP: Ultrasonic Spray Pyrolysis

DOS: Density Of State

CB: Conduction Band

CV: Valence Band

NP: Nano Particle

FWHM: Full Width at Half Maximum

PBEsol: Perdew–Burke–Ernzerhof for solids

Symbols List:

σ: Electrical conductivity

ρ: Electrical resistivity

Eg: Band gap width

d_{hkl}: Interspacing between atomic planes

θ: Bragg angle

n: Integer number

λ: Wave length

ν: $wavenumber$

T: Temperature

M: Metallic atom

R: Alkyl radical

h: Planck's constant (h = 6.63×10^{-34} J·s)

c: Speed of light (c = 3×10^{8} m/s)

a, b, c: Crystal lattice parameters

d: Layer thickness

α (hν): Absorption coefficient

ν : Absorption frequency

T: Transmission

A: Absorption

V: Electrical voltage

I: Electrical current

ρ: Resistivity

D: Crystalline size

℃: $Degree\ celsius$

H: Hamiltonian

ψ: $Eigen\ vecteur$

E: Eigenvalue

V: Potential

e: Electron

m_i: $mass\ of\ the\ electron\ i$

m_α: $mass\ of\ the\ nucleus\ \alpha$

Z_α: Atom charge

$\rho\ (r)$: Electronic density

E_F: Fermi energy

C: Concentration

V: Volume

M: Molar mass

T: Temperature

t: Time

E_0: Total energy.

B: Modulus of compressibility.

V_0: Equilibrium volume.

$g_i^t(E)$: State number

$g^{out}(E)$: Number of states (electrons) in the interstitial area

(hkl): Miller indice of plans

α: absorption coefficient

r: Refractive index

$\varepsilon_1(w), \varepsilon_2(w)$: The real and imaginary parts of the dielectric function.

Sommaire

Introduction 4
I.1.Cobalt sulfide CoS: 4
I.1.1.Preparation methods: 4
I.1.2.Structural properties: 4
I.1.3.Optoelectronic properties: 6
I.2.Cobalt sulfide CoS_2: 7
I.2.1.Preparation methods: 7
I.2.2.Structural properties: 7
I.2.3.Optoelectronic properties: 9
I.3.Cobalt sulfide Co_3S_4: 9
I.3.1.Preparation methods: 9
I.3.2.Structural properties: 10
I.3.3.Optoelectronic properties: 11
I.4.Cobalt sulfide Co_9S_8: 11
I.4.1.Preparation methods: 11
I.4.2.Structural properties: 11
I.4.3.Optoelectronic properties: 13
II. The density functional theory DFT 16
II.1. Overview 16
II.2.The Schrödinger equation 16
II.2.1.Adiabatic Born-Oppenheimer approximation 16
II.2.2 Hartree and Hartree-Fock approximation 17
II.3.Mathematical formalism 18
II.3.1.The Hohenberg and Kohn theorems 18
II.3.2.Khon and Sham equations 19
II.3.3.The exchange and correlation function 20
II.3.4.DFT numerical resolution approach 21
II.4.The pseudopotential method 22
II.4.1.Introduction 22
II.4.2.The Principe 22
II.4.3.the construction of pseudopotentiel method 22

II.4.4.Examples of pseudopotentiel method 22
II.5.Quantum Espresso Coding QE: 23
II.5.1. INTRODUCTION 23
II.5.2.What can be done by QE: 23
III.1.Thin Films: 26
III.1.1.Formation of thin films: 26
III.1.1.1.Island growth: 26
III.1.1.2.Layer growth: 27
III.1.1.3. Stranski-Krastanov (layer & island): 27
III.1.2. Thin films structures: 27
III.1.2.1.Single Crystalline structure: 28
III.1.2.2.Poly crystalline structure: 28
III.1.2.3.Amorph structure: 28
III.1.3. Types of thin films and Applications: 28
III.1.3.1.Mechanical Thin Films: 28
III.1.3.2.Optical Thin Films: 28
III.1.3.3.Electronic Thin Films: 29
III.1.3.4.Magnetic Thin Films: 29
III.1.3.5.Thermal Thin Films: 29
III.1.3.6.Chemical Thin Films: 29
III.2.Sol-Gel synthesis method: 31
III.2.1.Sol-Gel process steps: 31
III.2.1.1.Homogeneous solution: 31
III.1.1.2.Hydrolysis (sol formation): 31
III.2.1.3.Condensation(Gel formation): 32
III.2.1.4.Gelation: 32
III.2.1.5.Drying and formation of xerogel: 32
III.2.1.6.Calcination : 33
III.2.2.The influenced parameters on the sol gel method 33
III.2.3.Advantages&disadventages of Sol-Gel Method 34
III.2.3.1.Pros: 34
III.2.3.2.Cons: 34
III.2.4.Application of the Nanomaterial’s prepared by Sol-Gel Method: 35

III.3.Deposition by sol Gel synthesis 35
III.3.1.Spin Coating: 36
III.3.2.Dip Coating: 36
III.3.3.Spray Pyrolysis Deposition: 37
III.3.3.1.History: 37
III.3.3.2.Principe: 37
III.3.3.3.The pros and cons of Spray Pyrolysis: 38
III.3.3.4.thermal annealing 39
III.4.Synthesis of cobalt sulphide thin films 40
III.4.1.Solutions preparation 40
III.4.2.Substrate choice 42
III.4.2.1.Cleaning of substrates: 42
III.4.3Layer Deposition: 42
III.4.4. Elaboration of an Ultrasonic Spray Pyrolysis (USP) Device 43
III.4.4.Deposition parameters: 44
III.5.Characterisation techniques: 45
III.5.1.Principles and instrumentation for UV-Vis-IR: 45
III.5.2. Fourier Transform Infrared Spectroscopy (FTIR): 47
III.5.3. X-Ray diffraction (XRD): 50
III.5.4.Profilometry: 52
IV.3 Electronic properties: 58
IV.3.1 Structure of bands energy: 59
IV.4.1. Density of state: 65
IV.2.Expiremental part 68
IV.2.1.X Ray diffraction (XRD): 68
IV.2.2.Profilometry measurements: 69
IV.2.3.Fourier Transform Infrared Spectroscopy (FTIR): 70
IV.2.4. UV-Vis spectroscopy Analysis: 71
Conclusion: 78

Figure List

Figure I.1: *Optimized crystal structure of Cobalt Mon-sulfide CoS in a) Tetragonal phase b) Hexagonal phase.* 6
Figure I.2: *Crystal structure of CoS_2.* 9
Figure I.3: *Crystal Structure of Cobalt Sulfide Co_3S_4 with cobalt atom in bleu and Sulfide* 10
Figure I.4: *The cubic structure of Co_9S_8 where the cobalt is represented in bleu and Sulfide with yellow atoms.* 13
Figure II.5: *A flowcharts representing the Numerical procedure for solving the Kohn-Sham equations.* 21
Figure II.6: *Schematic diagram of a pseudo potential and wave function (ψ) bleu compared to the pseudo wave function (Ψ_pseudo) calculated in the pseudo potential (V pseudo) (red).*[34] 23
Figure III.7: *Basic modes of thin films growth a) Volmer- Weber or layer growth, b) Franck-Van der Merwe growth, c) Stranski-Krastanov mode.* 27
Figure III.8: *Thin films applications diagram*[40] 30
Figure III.9: *Schematic of different stages of Sol-Gel process.* 33
Figure III.10: *Schematic Diagram of spin coating process.* 36
Figure III.11: *Schematic illustration of the Dip coating process.* 37
Figure III.12: *Schematic Diagram of Spray Pyrolysis setup.* 38
Figure III.13: Nabertherm oven 39
Figure III.14: *Thin layer production protocol.* 41
Figure III.15: *Scheme of depositing samples by Ultrasonic Spray Pyrolysis (USP) method: from colloidal solution.* 43
Figure III.16*: Instrument used to create thin cobalt sulphide layers using ultrasonic spray pyrolysis (USP).* 44
Figure III.17: *Various types of UV-VIS-IR spectrophotometry.* 46
Figure III.18: *Spectrophotometer of double beam type SHIMADZU (UV-1650PC).* 47
Figure III.19: *Schematic diagram of Michelson interferometer.* 48
Figure III.20: *Infrared Spectroscopy set up type SHIMADZU -8400.* 49
Figure III.21: *W.L.Bragg low demonstration.* 50

Figure III.22: *Diagram of XRD setup*[56]. 51
Figure III.23: *XRD instrument (Rigaku MINIFLEX 600).* 52
Figure III.24: *Profilometer process.* 52
Figure IV.25: *Variation of the total energy as a function of the unit-cell volume of various phases of cobalt sulfide* 56
Figure IV.26: *Energy versus volume of CoS both structure.* 58
Figure IV.27: Band structure of hexagonal CoS 59
Figure IV.28: Band structure of hexagonal CoS, calculated using GGA+U 59
Figure IV.29: Band structure of tetragonal CoS 60
Figure IV.30: Band structure of tetragonal CoS, calculated using GGA+U 60
Figure IV.31: Band structure of cubic CoS_2 61
Figure IV.32: Band structure of cubic CoS_2 , calculated using GGA+U 61
Figure IV.33: Band structure of tetragonal Co_2S_3 62
Figure IV.34: Band structure of tetragonal Co_2S_3, calculated using GGA+U 62
Figure IV.35: Band structure of spinel Co_3S_4 63
Figure IV.36: Band structure of spinel Co_3S_4, calculated using GGA+U 63
Figure IV.37: Band structure of cubic Co_9S_8 64
Figure IV.38: Band structure of cubic Co_9S_8 , calculated using GGA+U 64
Figure IV.39: *Partial density of state of cobalt sulfide phases* 67
Figure IV.40: *Total density of state plots of cobalt sulfide phases* 68
Figure IV.41: *Diffractogramme (DRX) of Co_9S_8* 69
Figure IV.42: DEKTAK profilometry instrument. 70
Figure IV.43: *FTIR spectrum of Co_9S_8* 71
Figure IV.44: *Impact of Annealing and Deposition duration on the Optical Transmittance of Synthesised Films.* 72
Figure IV.45: *Direct and indirect band gap in variation of deposition duration* 73
Figure IV.46: *Direct and indirect band gap of variation in annealing duration* 74

Table List

Table I.1: *Element composition and Mass Distribution of CoS.* 4
Table I.2: *Different morphology of cobalt sulfide CoS* 5
Table I.3: *Element composition and Mass Distribution of CoS_2.* 7
Table I.4: *Different morphology of cobalt sulfide CoS_2* 8
Table I.5: *Element composition and Mass Distribution of Co_3S_4.* 10
Table I.6: *Different morphology of cobalt sulfide Co_3S_4.* 11
Table I.7: *Element composition and Mass Distribution of Co_9S_8.* 11
Table I.8: *Different morphology of cobalt sulfide Co_9S_8.* 12
Table I.9: *Literature summary of Structural and Electronic Properties of Cobalt Sulfide* 14
Table IV.10: *Lattice parameters a,b,c(Å), compressibility modulus B(GPa) and its derivative Bp* 57
Table IV.11: *Comparison between the results of our work with the previous study.* 57
Table IV.12: *Nature of gap for Hex CoS, CoS_2, Co_3S_4 and Co_9S_8* 65
Table IV.13: *Reflection angles with the (hkl) of hexagonal cobalt sulfide Co_9S_8* 69
Table IV.14: Thickness of different thin films 70
Table IV.15: *Table show collectively analysis of the deposition Co_9S_8 at various conditions and its optical behaviour.* 75

GENERAL

INTRODUCTION

Introduction

The fast growth has created an urgent need for the development of novel materials and devices capable of efficient and reliable optoelectronic properties [1-2]. Transition Metal Oxides (TMOs) have drawn significant attention due to their diverse range of properties and applications. The partially filled d orbitals of the transition metal ions, with highly electronegative oxygen atoms, give rise to unique electronic structures that lead to multiple applications due to their magnetic, optical, and structural properties.[3] , but many advances challenges remain to be addressed in the synthesis and characterization of this materials. Transition metal oxide TMOs like ZnO, CuO,NiO, CoO, , [4], [5].The Fe cobalt oxide Co have shown a crucial potential in $2O3$ $Al2O3$ Ox various applications, especially in energy storage and catalyst, Their exceptional properties and versatility make them ideal candidates for a wide range of technological advancements. On the other hand, there has been a discernible increase in research on nanocrystals made of transition metal sulfide (TMS) compounds. Their attractive properties in the environment and the development of renewable energy solutions, are the reason for this increased attention. The abundance of materials with easily tunable electrical-optical, physical, and chemical properties is primarily responsible for this. TMSs are semiconducting compounds in which a metal cation is coordinated by the anion sulfur[12]. Cobalt sulfides include different phases: CoS, CoS_2, Co_4S_3,Co_9S_8, Co_3S_4, Co_2S_3, $Co_{1-x}S_x$ and Co_2S_7. The complex structure of these various phases is reflected on their huge field of applications, It may be utilized as an active electrode material in a variety of technologies, including dye-sensitized solar cells DSSCs, super capacitors, and batteries [13], organic solar cells [14], water splitter to produce hydrogen [15], electrocatalysts (HER, OER, ORR) [13, 16], diluted magnetic materials [17]. Lithium-sulfur (Li-S) batteries have garnered significant research interest owing to their exceptional energy density, positioning them as a compelling candidate for next-generation energy storage technology [18]. Cobalt sulfide is also an attractive material for biomedical applications [19]. In 2022, cobalt sulfide (CoS) has been chosen to build a composite with magnetite (Fe3O4). According to research reported by M.S.Gopika and S. Savitha Pillai, It would be crucial to look into the characteristics of the composites of cobalt sulfide and ferrous oxide (Fe3O4) for bio-related applications [19]. Furthermore, Ahmed et al (2025), reported the use of cobalt sulfide to successfully enhance the solar cells performance[14]. Cobalt sulfides have being considered as electrode materials for supercapacitors, and the construction of amorphous/crystalline heterointerfaces in cobalt

sulfide is a helpful way to enhance ion/electron transport and reaction kinetics to improve supercapacitor performance [6].

In addition, cobalt sulfide-cobalt ferrite-reduced graphene oxide (CoS-$CoFe_2O_4$-rGO) nanocomposites have been developed as electrodes for all-solid-state asymmetric supercapacitors[7].Numerous reports have been devoted to the synthesis and the study of cobalt sulfides:Shajaripour Jaberi et al. (2023) address various approaches to the synthesis of CoS_2 to be applied as transition metal dichalcogenide (TMD) [13]. The properties of CoS_2 thin films synthesized by adsorption-diffusion method was reported by Vaiciukynaite et al., in 2024. Furthermore, the cobalt sulfide Co3S4 has been synthesized using spray pyrolysis technique [22]. The result of this study shows the impact of glass temperature on the properties of cobalt sulfide. The Co_9S_8 hexagonal phase has been successfully synthesized by a one-step and convenient self-template strategy, which explain the faster diffusion rate of Co2+ from inside to outside than S2- from solution to the inside [23]. Based on our bibliographic research, we have concluded that these phases are still under investigation and a lot of work and progress has to be done using various approaches to fully understand the properties of cobalt sulfides phases. Therefore, the present work aims to focus on studying structural and electronic properties of different cobalt sulfide phases.

Our manuscript is organized in four chapters, as follows:

● In the first chapter we presented some generalities on various phases of cobalt sulfides.

● In the second chapter we will discuss calculation methods including approximations for solving the Schrödinger equation using density functional theory (DFT). Finally, the based ab-initio Quantum ESPRESSO code used in our study was presented.

● In the third chapter, we describe the experimental techniques and methods used to prepare our samples. Then, the characterization techniques applied to analyze the properties were briefly presented.

● The last chapter is devoted to the presentations of our data and their interpretations.

Finally, the manuscript is corroborated with a general conclusion to highlight the main results

CHAPTER I

REVIEW OF COBALT SULFIDE

Introduction

In recent years, the cobalt sulfide is an important transition metal chalcognide and dichalcogenides, it has multiphase structures such as: CoS, CoS_2, Co_2S_3, Co_4S_3, Co_3S_4, and Co_9S_8. These compounds are commonly known as Co_xS_y. However, this substance has drawn the curiosity of researchers in light of its vast potential for use in a numerous areas.

To understand the decomposition, structural and electronic properties of the cobalt sulfide phases we based on the formula Co_xS_y where x value represented the proportion of sulfide in the compound.

I.1.Cobalt sulfide CoS:

Cobalt sulfide can be used in many applications as example Dadi et al reported that it has a hugh impact in Dye Sensitized Solar Cells (DSSCs) [1], It is useful for Hydrogen Evaluation Reaction (HER) and Oxygen Evaluation Reaction (OER) [2], adding to the previous uses it has a properties that makes it suitable in supercapacitor[3].

I.1.1.Preparation methods:

Many studied have been successfully carried out the various properties of cobalt monosulfide using three different technique specifically the Hydrothermal method[4] [3] Chemical Bath Deposition (CBD) [2] [5]and simulation method basing on the density function theory and quantum espresso (QE) [1].

I.1.2.Structural properties:

The details examination of the structural properties of cobalt sulfide CoS are based on the in-depth understanding of its element composition, the following table shows the constituent element with their percentages.

Table I.1: ***Element composition and Mass Distribution of CoS.***

Element	Symbol	Atomic masse (Uma)	Number of atom	Masse percentage
Cobalt	Co	58.933	1	64.76652
Sulfide	S	32.06	1	35.23348

The crystalline structure of cobalt sulfide CoS depend on the method of examination, Gopika and savitha [4]reported that this phase has a hexagonal structure in space group $P6_3/mmc$ with the lattice parameter a=b=3.3710 **Å** and c=5.1809 **Å** , this structure show different morphology are shown in the table below as example starflower,balls,fuzzy balls in the average diameter size 2.16,1.25,3 μm respectively , by the same method but different temperature from 160 to 220℃ in stand of a fixed temperature 180℃ as the previous study the cobalt monosulfide show a hexagonal phase and a high Cristallinty at 200℃ additionally it exhibit an amorphousness structure in less temperature, nonetheless when the temperature increase more the stability of material disappeared which is threw out by Alshoaibi [3] , more than that Patil et Bathula and Abza et al groups applied the (CBD) technique ,the first group come out with hexagonal phase structure of $CoS_{1.0365}$ nanorod array according to JCPDS, PDF no. 75-0605 , they have been reported the formation of cobalt oxy-sulfide on the surface of the material and the other group given out the hexagonal phase by varying the deposition time from 2h to 3.5h and the average particle size is noted 52.8-22.5 nm. In addition, Jaipurite phase contain sulfur lattice S_2^{-2} hcp and the cobalt atom filled all the octahedral holes [6].

Table I.2: ***Different morphology of cobalt sulfide CoS***

Material	Morphology	D (nm)	Ref
CoS	Star flower	$2.16*10^3$	[4]
	Balls	$1.25*10^3$	[4]
	Fuzzy balls	$3*10^3$	[4]
	Nano- particles	52.8-22.8	[5]
	1D-Nanorod array	-	[2]
	Nano-Structure	8-24	[3]

However ,there were some variation in the cell parameter of cobalt sulfide a=b=3.53A^0 and c=4.8A^0 , when Dadi and his collaborator studied it using the ab-intio and DFT they noted that the CoS belongs under the space group P4/nmm with Wyckoff positions 2a and 2c of cobalt Co and sulfide S are respectively 0; 0; 0 and 0.5; 0; 0.765095, which correspondence to tetragonal structure[1].

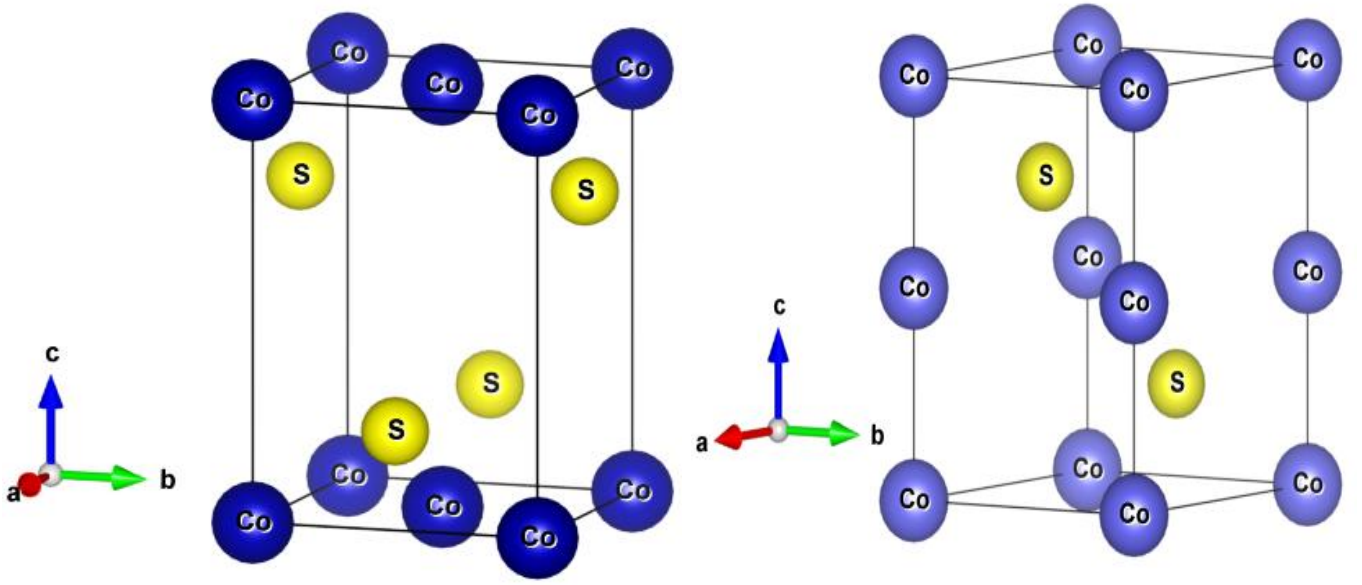

a) Tetragonal structure of Cos

b) Hexagonal structure of Cos

Figure I. 1: ***Optimized crystal structure of Cobalt Mon-sulfide CoS in a) Tetragonal phase b) Hexagonal phase.***

I.1.3.Optoelectronic properties:

Band gap energy of the sample were estimated by using two different experimental technique Gopika et savitha [4] use the kubelka-Munk (KM) function and the values are noted respectively 1.27 , 1.16 , 1.07 ev ; While Abza and his co-worker[5]reported a higher energy gap then the group of Gopika 1.55 ,1.65, 1.75 ev and this increase is properly due to the variation in morphology of the structure and the particle size , when they measured the electronic resistivity by the two probe method at room temperature declared that only the samples prepared at 2.5h to 3h are classified in semi-conductor material $\rho = 5 * 10^4$, $5 * 10^3\ \Omega.cm$.In other hand when Dadi et al use Ab-intio ,they bring out the value of the energy band gap similar to the previous one via GGA and Heyd–Scuseria–Ernzerhof hybrid functional (HSE06) method are 1.63 , 1.69 ev respectively, the dielectric behavior of CoS were calculated by the realtion of Kramer Kronig wich take on consideration the reel and imagenery value ε_1(W)=11.85 and ε_2 (w)=0.13 [1].

The magnetic properties play a crucial role to improve the various uses of cobalt monosulfide CoS.

Gopika and savitha studied given out that the CoS show a paramagnetic behavior at room temperature but when the temperature decrease it will have a transition from a state where the magnetic spin are slightly misaligned to a state where it exhibit a weak ferromagnetic and this change is due to the unique crystallography of the material[4].

I.2.Cobalt sulfide CoS_2:

Cobalt disulfide has been explored as an attractive material for its special properties and the large area of applications such as the super capacitors[7], transistors[8], it can be used in electro-catalyst for oxygen evaluation reaction (OER) [9], for hydrogen evaluation reaction (HER)[10] lithium ion batteries and solar cells [11].

I.2.1.Preparation methods:

Wide range application of the material has a high relation with the method used to perform it, it existed the precipitation method, Hydrothermal technique and wet method [11]and others(physicochemical deposition methods were used, such as chemical vapor , aerosol chemical vapor , electrochemical , spray pyrolysis , sol-gel , microwave-assisted , wet methods such as chemical bath deposition or sequential adsorption and reaction of the ion layer are the widely method use in synthesis of this sample).

I.2.2.Structural properties:

The structural characteristics of cobalt disulfide CoS_2 are presented in the table blow to provide the basic information of its elements.

Table I.3: ***Element composition and Mass Distribution of CoS_2.***

Element	Symbol	Atomic masse (uma)	Number of atom	Masse percentage%
Cobalt	Co	58.933	1	47.89237
Sulfide	S	32.06	2	52.10763

In 2022 ,Agboola et al mentioned in their studied that the CoS_2 has a cubic phase which is in well agreement with JCPDS no. 041–1471 in a cottony and spherical shape[7] ,while it existe other morphology of cobalt Sulfide were mentioned in table (I.2). The cattierite phase

structure exhibits a pyrite structure in group space Pa3- with octahedral holes filled with cobalt and S_2^{-2} units in ccp packing.[6]

Table I.4: ***Different morphology of cobalt sulfide CoS_2***

Material	Morphology	D (nm)	Ref
CoS_2	Spherical Shape	-	[7]
	2D-van der walls nano-sheets	-	[8]
	Thin films	-	[11]
	Nano-Particles	5-7	[9]
	Nano-particles	24.24	[12]

The study of Vaiciukynaite et al [13]confirmed this phase by using the absorption diffusion method at 80℃ but if the temperature decrease the sample show a large accumulation on the surface which means that the morphology of CoS_2 was influenced by the condition of their formation .Meanwhile, Wang and his collaborator's reported that the sample crystalized in the structure of van der Waals synthesized under a specific condition (growth temperature from 720 to 780℃) using Single Crystal Chemical Vapor Deposition (SCCVD) [8]. However, recent research indicates that CoS_2 experiences significant structural deterioration during long-term environmental storage as well as high-temperature operation. Phase changes (e.g., $CoS_2 \rightarrow Co_9S_8$) are caused by sulphur loss due to gaseous S_2 emissions at high temperature, while room-temperature aging causes surface oxidation and sulfur[14] in contrast with other group when they used different conditions of synthesis technique ,they put on the air the difficulties to transform it to CCP linneaite Co_3S_4 or cobalt pentlandite Co_9S_8 [6].

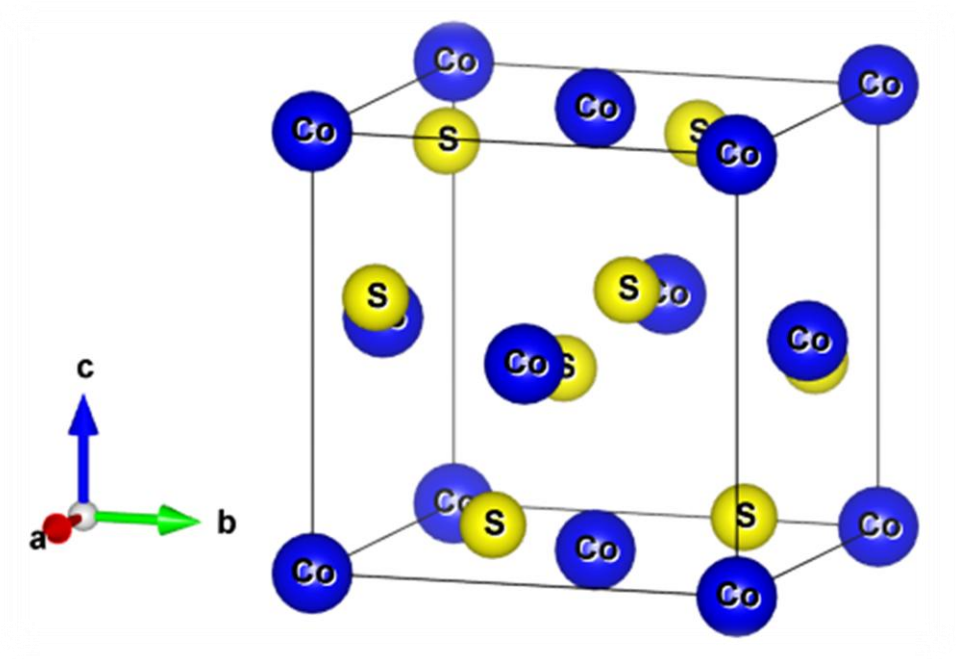

Figure I.2: ***Crystal structure of CoS_2.***

I.2.3.Optoelectronic properties:

Wang et al reported that the electronic conductivity has a high relation with thickness and the temperature of synthesis of the material for example when they used the CoS_2 in the size of 5.1 nm at room temperature the electronic conductivity was $2.6 * 10^6\ s/m$ however when they used 34.1 nm show less conductivity around $2.1 * 10^6\ s/m$ [8].These semi-conductor due to their stoichiometric diversity have optical band gap in average of 1.38-2.7 ev[11].

I.3.Cobalt sulfide Co_3S_4:

The cobalt sulfide show a crucial potential for its applications in energy storage (batteries, super capacitors, and photovoltaic solar cells) [15] [16]also for the biosensors[17].

I.3.1.Preparation methods:

The various phases of cobalt sulfide have higher depended to the technique used. The material Co_3S_4 can be prepared using one step vulcanization process[15]Hydrothermal technique [17]spray pyrolysis method[16] .

I.3.2.Structural properties:

In the aim to understand the structural properties of the cobalt sulfide Co_3S_4 we have to know the distribution of each element in the compound, the parameters that describe it are summarize in the following table.

Table I.5: ***Element composition and Mass Distribution of Co_3S_4.***

Element	Symbol	Atomic masse (uma)	Number of atom	Masse percentage%
Cobalt	Co	58.933	3	57.95947
Sulfide	S	32.06	4	42.04053

Cobalt sulfide Co_3S_4 exhibit spinel structure characteristics in cubic crystal system in well agreement with the standard card JCPDS No42-1448 with ccp sulfurs and cation atom of cobalt in $1/4$ of tetrahedral holes and half of the octahedral hols[6] which is confirmed by the group of Abdelouahab[16] , Hucheng Li et al use one step process and mentioned that the broadened peaks of Co_3S_4 indicate nanocristalline nature with a microsphere morphology that enhance its surface area with high porousity nature allowing for efficient electrolyte penetration and exposing abundant active sites which makes tham ideal for batteries and SC. Meanwhile other morphology was mentioned in table I.7.On other side, when they applied HRTEM image they noted interplanar spacing of 0.232 nm and 0.286 nm corresponding to the plan (400) and (311) respectively [18].

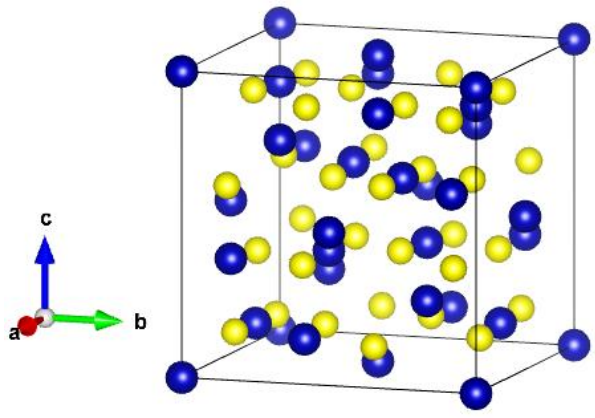

Figure I.3: ***Crystal Structure of Cobalt Sulfide Co_3S_4 with cobalt atom in bleu and Sulfide atom in yellow.***

Table I.6: ***Different morphology of cobalt sulfide Co_3S_4.***

Material	Morphology	D (nm)	Ref
Co_3S_4	Thin films	9.586-20.842	[16]
	Hollow dodecahedral	500	[19]
	Hollow Nano-Structure	-	[15]
	Nano-Particules	-	[17]

I.3.3.Optoelectronic properties:

CP et al mentioned that the hexagonal Co_3S_4 is a semiconductor with low conductivity which is less suitable in electrode materials that require efficient charge transfer in contrast with Abdelouahab and his coworkers[16] found that the cubic phase has an important electronic properties the electronic conductivity $\sigma = 2.56 * 10^3 - 9.61 * 10^4 s/cm$ and band gap energy ranged from 1.76 to 1.72 ev makes the sample a good candidate for super capacitors.

I.4.Cobalt sulfide Co_9S_8:

In recent years, the use of cobalt sulfide has grown to involve a several technological uses including Lithium ion batteries[20], photo catalytic in electrochemical reaction such as OER and HER[21].

I.4.1.Preparation methods:

The material Co_9S_8 can be prepared with two methods. Chemical Bath Deposition (CBD) and Hydrothermal technique.

I.4.2.Structural properties:

The crystalline studied depend on the composition of the different element within the material; the following table highlighted the key data of the cobalt and sulfide in the Co_9S_8 compound.

Table I.7: ***Element composition and Mass Distribution of Co_9S_8.***

Element	Symbol	Atomic masse (uma)	Number of atom	Masse percentage%
Cobalt	Co	58.933	9	67.40533
Sulfide	S	32.06	8	32.59467

More than that, the technique used and its condition are also curcial for example Abza et al[5] have reported a cubic phase with crystalline size 10.95 nm of cobalt sulfide using CBD method which agree with the study in 2023 where the lattice constant comes out to be a=9.4 A in group space Fm3m and they mentioned that the crystalline size increased by doping it with Al and Zn from 11.5 nm to 28.8 nm[22] the S atoms form a close-packed cubic array with the Co atoms centering half of the tetrahedral holes and 1/8 of the octahedral holes,also ccp Cobalt pentlandite (Co_9S_8) is considered as an intermediate to ccp linnaeite (Co_3S_4) [6] [23]. In like yang et al [20]denoted a cubic phase with an average size 14.72nm to 17.03 nm and this growth was explained by the beneficial effect of Na2EDTA in the development of Co_9S_8 using the hydrothermal technique .its morphologies was summarized in table I.9.

Table I.8: ***Different morphology of cobalt sulfide Co_9S_8.***

Material	Morphology	D(nm)	Ref
Co_9S_8	Nano-Particles	10.95	[5]
	Nano Sheets	14.72-17.03	[20]
	Micro-sphere	-	[21]

While tang and his collaborator reported an hexagonal structure which confirmed by JCPDS No 30-0443 card in space of group P-3m1(164) with lattice parameters are respectively a=b=0.3183 nm and c=0.4652 nm ,the formation of Co_9S_8 attributed to the diffusion of Co^{2+} out ward from the inner and S^{2-} from outside to the core was mentioned [21]. This material have drown much attention by improving the catalytic performance due to the presence of S vacancies in Co_9S_8 which can create an additional active sites and in the degradation of Rhoda mine B (RhB) due to the larger specific surface area (13.74 m^2/g) [21].

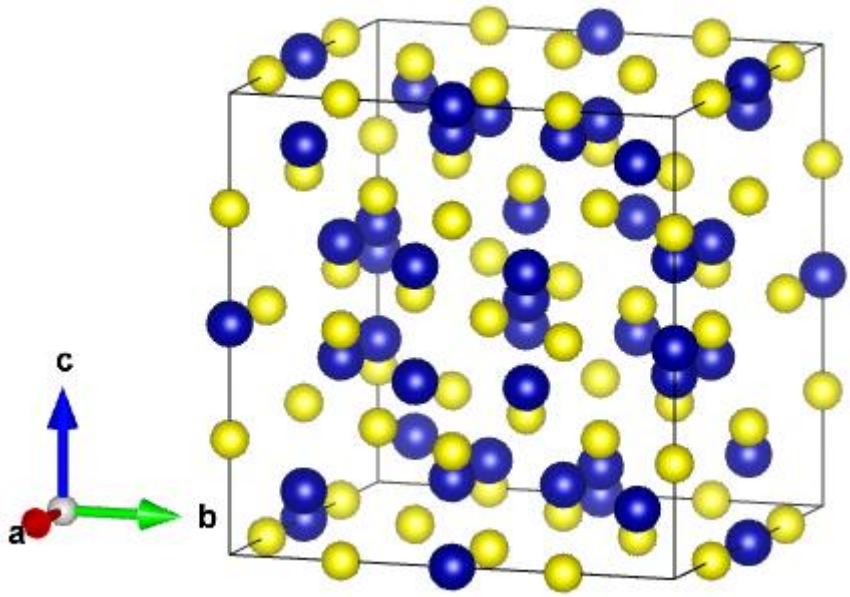

Figure I.4: ***The cubic structure of Co_9S_8 where the cobalt is represented in bleu and Sulfide with yellow atoms.***

I.4.3.Optoelectronic properties:

The band gap energy of cobalt sulfide varied from 1.28 to 1.3 ev [21] ,[5]depending on the stoichiometry and the synthesis condition with an electronic conductivity $\sigma = 7.6923 * 10^{-5}$ s/m including in the range of semiconductors materials.

There are a large number of studies about the magnetic behavior of cobalt sulfide Co_9S_8 which confirm its potential applications in magnetic field.

Robert Heidelberg mentioned that the material has the behavior of an antiferromagnetic and that happened when the Neel temperature is higher than the decomposition temperature ,Meanwhile Erika Dotkuva and his coworker studied the magnetic properties of it using mechanical chemistry based on superconducting quantum interface devices (SQUID)magnetometer and they conclude that the temperature depend to the magnetization state, at room temperature the sample support paramagnetic properties and under this temperature the cobalt sulfide show a transition from paramagnetic to ferromagnetic material [24].

The following table brings a summary on different cobalt sulfides phases:

Table I.9: ***Literature summary of Structural and Electronic Properties of Cobalt Sulfide***

Phases	Structure	Conductivity S/Cm	Gap Energy $E_g(eV)$
COS[5]	Hexagonal [5] tetragonal[1]	$5.88 * 10^{-7}$ [5] Chemical Bath Deposition	1.75 [5] 1.63-1.69[1]
COS_2 [7]	Cubic[7]	$8.26 * 10^{-8}$[7] Hydrothermal Technique $2.6 * 10^{4}$[8] SCCVD	1.38-2.7[11]
Co_2S_3			
Co_2S_7	-	-	-
Co_3S_4 [25]	Cubic[25] hexagonal[17]	$0.89 * 10^{3}$ [16] SPD $2.56 * 10^{3} - 9.61 * 10^{4}$[17]	1.82 [16] 1.76 to 1.72[17]
Co_4S_3	-	-	-
Co_9S_8 [5]	Cubic[5] hexagonal[21]	$7.692 * 10^{-5}$ [5]Chemical Bath Depostion	1.3[5] 2.03[26] 2.81[27] 1.28[21]

CHAPTER II

FORMALIZATION & CALCULATION METHODS

II. The density functional theory DFT

II.1. Overview

Density functional theory (DFT) introduced by Hohenberg and Kohn in 1964 and later developed by Kohn and Sham in 1965[28]. The purpose of this theory is to replace the multi-electron wave function with the electron density as the basis for calculation, thus reducing the multi-body problem to a single-body problem, which determines the total energy. However the Ground-state properties such as its electronic structure and ionization energy of a system are the result of our calculations. The ab-initio Methods used for solving the Schrödinger equation. In this chapter, we will discuss DFT method with various levels of approximation, allowing for the treatment of large systems (complex systems).

II.2.The Schrödinger equation

It is necessary to solve the Schrödinger equation for a stationary system of N electrons, to study the characteristics of compounds.

This equation is expressed as follows:

$$H\psi = E\psi \qquad \text{II.1}$$

The Hamiltonian H is given by:

$$H = \boldsymbol{T_e} + \boldsymbol{V_{n-e}} + V_{e-e} + T_n + V_{n-n} \qquad \text{II.1.1}$$

E represents the system's eigenvalues, while ψ represents its eigenvectors. Nevertheless, when it comes to solve the Schrodinger equation it is necessary to follow certain approximations firstly we will base on the adiabatic Born-Oppenheimer approximation.

$$\boldsymbol{H = T_e + V_{n-e} + V_{e-e}} \qquad \text{II.2}$$

II.2.1.Adiabatic Born-Oppenheimer approximation

This hypothesis is based on the fact that the mass of any nucleus is significantly higher than that of an electron. For this reason, the motion of nuclei relative to electrons may be ignored; nuclei are assumed to be fixed. In this condition, nuclei have zero kinetic energy ($T_n = 0$) and a constant columbine energy V_{n-n} due to repulsion.

At this stage, we've progressed from solving the Schrödinger equation for a system with (N electrons + M nuclei) to solving the equation for a system with N electrons sensing the

potential of the nuclei .The Hamiltonian now only includes monoelectronic (T_e and V_{n-e}) and bi-electronic ($V_{e\text{-}e}$) contributions[29]:

Schrödinger's equation is then written:

$$\left[\frac{-\hbar}{2m_i}\sum_i \nabla_i^2 + \sum_{i.j}\frac{e^2}{|r_i - r_j|} - \sum_{i.\alpha}\frac{Z_\alpha e^2}{|r_i - r_\alpha|}\right]\psi = E\psi \qquad \text{II.3}$$

With $\begin{cases} m_i & the\ mass\ of\ the\ electron\ i \\ m_\alpha & the\ mass\ of\ the\ nucleus\ \alpha \\ Z_\alpha & the\ atom\ charge \end{cases}$

This approximation significantly reduces the number of variables required for interpreting the wave functionψ. Due to the complicated nature of electron-electron interactions, this approximation alone

Cannot solve Schrödinger's equation. As a result of this, it is frequently used alongside the Hartree approximation.

II.2.2 Hartree and Hartree-Fock approximation

In 1927, Hartree suggested a technique for estimating approximate poly-electronics as products of mono-electronic wave functions[30]. Each electron is allocated an orbital, and the entire wave function is expressed as a combination of mutually orthogonal single-particle wave functions:

$$\boldsymbol{\psi(r_1; r_2; \dots\dots\dots; r_n) = \psi_1(r_1)\psi_2(r_2)\dots\dots\dots\psi_n(\mathbf{r_n})} \qquad \text{II.4}$$

Then in 1930, Fock demonstrated that Hartree's method does not respect the principle of antisymmetry of the function. The antisymmetry principle of the onde function. Indeed, according to Pauli's exclusion principle two electrons cannot simultaneously be in the same quantum state.

The Hartree-Fock method provides an approximate solution of the Schrödinger equation of a quantum system with N electrons and M nuclei, in which the poly-electron wave function ψ_{HF} is written in the form of a Slater determinant consisting of monoelectronic orbital spin that respects the antisymmetry of the wave function[29]:

$$\psi(\boldsymbol{r_1}, \sigma_1; \boldsymbol{r_2}, \sigma_2; \dots\dots\dots; \boldsymbol{r_{ne}}, \sigma_{ne} = \frac{1}{\sqrt{n!}}\begin{vmatrix} \psi_1(\boldsymbol{r_1}, \sigma_1) & \psi_1(\boldsymbol{r_2}, \sigma_2)\dots\dots & \psi_1(\boldsymbol{r_{ne}}, \sigma_{ne}) \\ \psi_2(\boldsymbol{r_1}, \sigma_1) & \psi_2(\boldsymbol{r_2}, \sigma_2)\dots\dots & \psi_2(\boldsymbol{r_{ne}}, \sigma_{ne}) \\ \psi_3(\boldsymbol{r_1}, \sigma_1) & \psi_3(\boldsymbol{r_2}, \sigma_2)\dots\dots & \psi_3(\boldsymbol{r_{ne}}, \sigma_{ne}) \end{vmatrix} \qquad \text{II.5}$$

σ: $represents\ the\ electron\ spin$

Schrödinger's equation is show below

$$\left(-\frac{\hbar}{2m_i}\nabla^2 + V_i(r) + V_n(r)\right)\psi_i(\mathrm{r_i}) - \sum_j[\int d^3r'\psi_j^*(r')\psi_i(r)\frac{1}{|r-r'|}]\psi_j(r) = E_i\psi_i(\mathrm{r_i}) \quad \text{II.5.1}$$

The Hartree-Fock approximation simplifies the N-body problem to a one-body problem, where each electron is subject to an effective potential from other electrons. For complex calculations, density functional theory is utilized.

II.3.Mathematical formalism

II.3.1.The Hohenberg and Kohn theorems

The Hohenberg and Kohn theorems are the basis of Density functional theory DFT, and this approach can be applied to any system with a several interacting particle evaluating in a external potential.

First theorem

Hohenberg and Kohn showed that there exists a bijective correspondence between the external potential V_{ext} and the electron density $\rho(r)$, where V_{ext} can be represented as a ground state functional of $\boldsymbol{\rho}$ (r). Consequently, the total fundamental energy E is a unique functional of the electron density.

$$E(\rho_{fond}) = T_e(\rho_{fond}) + V_{ee}(\rho_{fond}) + \int V_{n-e}(r)\rho(r)d^3r$$

The independent terms of the system are grouped into Hohenberg and Kohn functional ($F_{HK}(\rho_{fond})$) as indicated below:

$$F_{HK}(\rho_{fond}) = T_e(\rho_{fond}) + V_{e-e}(\rho_{fond}) \quad \text{II.6}$$

Consequently

$$E(\rho_{fond}) = F_{HK}(\rho_{fond}) + \int V_{n-e}(r)\rho(r)d^3r \quad \text{II.7}$$

Where

$T_e(\rho_{fond})$: The kinetic energy

$V_{e-e}(\rho_{fond})$: Electron-electron interaction energy

$V_{n-e}(r)$: Nucleus -electron interaction energy

Second theorem

The aim of this theorem is to find out what the electronic density of the fundamental state, so that all the system's properties can be obtained. Nevertheless, Hohenberg and Kohn determined that the electronic density of the ground state depend on the minimum of the total energy[31].

$$E(\rho_0) = \min E(\rho) \quad \text{II.8}$$

II.3.2.Khon and Sham equations

Khon and Sham propose an approximation for F_{HK}.Where they consider the equivalence between a system of interacting electrons in an external potential V_{ext}(r) and a system of non-interacting electrons in an effective potential V_{eff}(r) . The reason for this interest comes from the fact that the expressions of the kinetic energy and the potential energy for this fictitious system are known. Then KS demonstrate that the electrons can be placed in an effective potential.

This leads us to model the problem in terms of three inter-dependent equations.

the Kohn-Sham equations:

The first equation

The definition for the effective potential where the electron placed

$$V_{eff}[\rho(r)] = V_H[\rho(r)] + V_{XC}[\rho(r)] + V_{ext}[\rho(r)] \qquad \text{II.9}$$

With :

$V_H[\rho(r)] = \frac{1}{2}\int \frac{e^2}{4\pi\varepsilon_0}\frac{\rho(r`)}{|r-r`|}dr`$ The Hartree potential of electrons.

$V_{XC}[\rho(r)] = \frac{\partial E_{XC}[\rho(r)]}{\partial[\rho(r)]}$ The Exchange-correlation potential.

The second equation

Uses the effective potential in the N single-electron Schrödinger equations to obtain the single-particle wave functions

$$\left[-\frac{1}{2}\nabla^2 + V_{eff}[\rho(r)]\right]\varphi_i(r) = \varepsilon_i\varphi_i(r) \qquad \text{II.10}$$

$$\left[-\frac{1}{2}\nabla^2 + V_H[\rho(r)] + V_{XC}[\rho(r)] + V_{ext}[\rho(r)]\right]\varphi_i(r) = \varepsilon_i\varphi_i(r) \qquad \text{II.11}$$

The terms on the right-hand side represent the non-interacting kinetic, electron-nucleus, Hartree, exchange-correlation, and nucleus-nucleus energies, respectively.[32] Where $\varepsilon i\ et\ \varphi_i(r)$ are, respectively, the energy of a Kohn- Sham orbital and the particle-specific wave function.

The final equation

The electron density $\rho(r) = \sum_{\varepsilon_i \le E_F}|\varphi_i(r)|^2$ II.12

II.3.3.The exchange and correlation function

To solve directly the equation of Khon and Sham is impossible because the exchange and correlation function is unknown, so for that we should use a practical approximation. The most commonly approximations are

- ✓ Local density approximation (LDA).
- ✓ Local spin density approximation (LSDA).
- ✓ Generalized gradient approximation (GGA).

II.3.3.1. Local density approximation (LDA).

khon and sham consider the solid close to the limit of a homogenous electron gas for which the exchange and correlation effects are local. So the principle of this approximation is to study an inhomogeneous system as locally homogeneous.

The exchange and correlation energy is expressed as a function of the exchange and correlation energy per particle.

$$E_{XC}^{LDA}[\rho(r)] = \int \varepsilon_{XC}^{LDA}[\rho(r)]\rho(r)d^3r \quad \text{.....II.13.1}$$

The exchange and correlation potentiel

$$V_{XC}^{LDA}(r) = \frac{\delta(\rho(r)\int \varepsilon_{XC}^{LDA}[\rho(r)]d^3r)}{\delta\rho(r)} \quad \text{.....II.13.2}$$

The characteristic of LDA approach

It allows properties such as equilibrium density, covalent bonds, and compressibility modulus to be written.

-There is also a version of the LDA that takes electronic spin into account. This is the LSDA local spin density approximation. The exchange and correlation becomes a functional of the two spin densities, up and down:

$$E_{XC}^{LSDA} \quad (\rho\uparrow, \rho\downarrow) = \int \rho(r)\, \varepsilon_{XC}(\rho\uparrow, \rho\downarrow)\, dr \quad \text{.....II.14}$$

II.3.3.2.The generalized gradient approximation GGA

The generalized gradient approximation module the exchange and correlation energy not only as a function of electron density electron density$\boldsymbol{\rho}$ (r) but also of its gradient. The scientists think about to improve the accuracy of LDA results.It is given by the following equation:

$$E_{XC}^{GGA}\rho(r) = \int f[\rho(r), |\nabla\rho(r)|]d^3r \text{.....II.15}$$

II.3.4.DFT numerical resolution approach

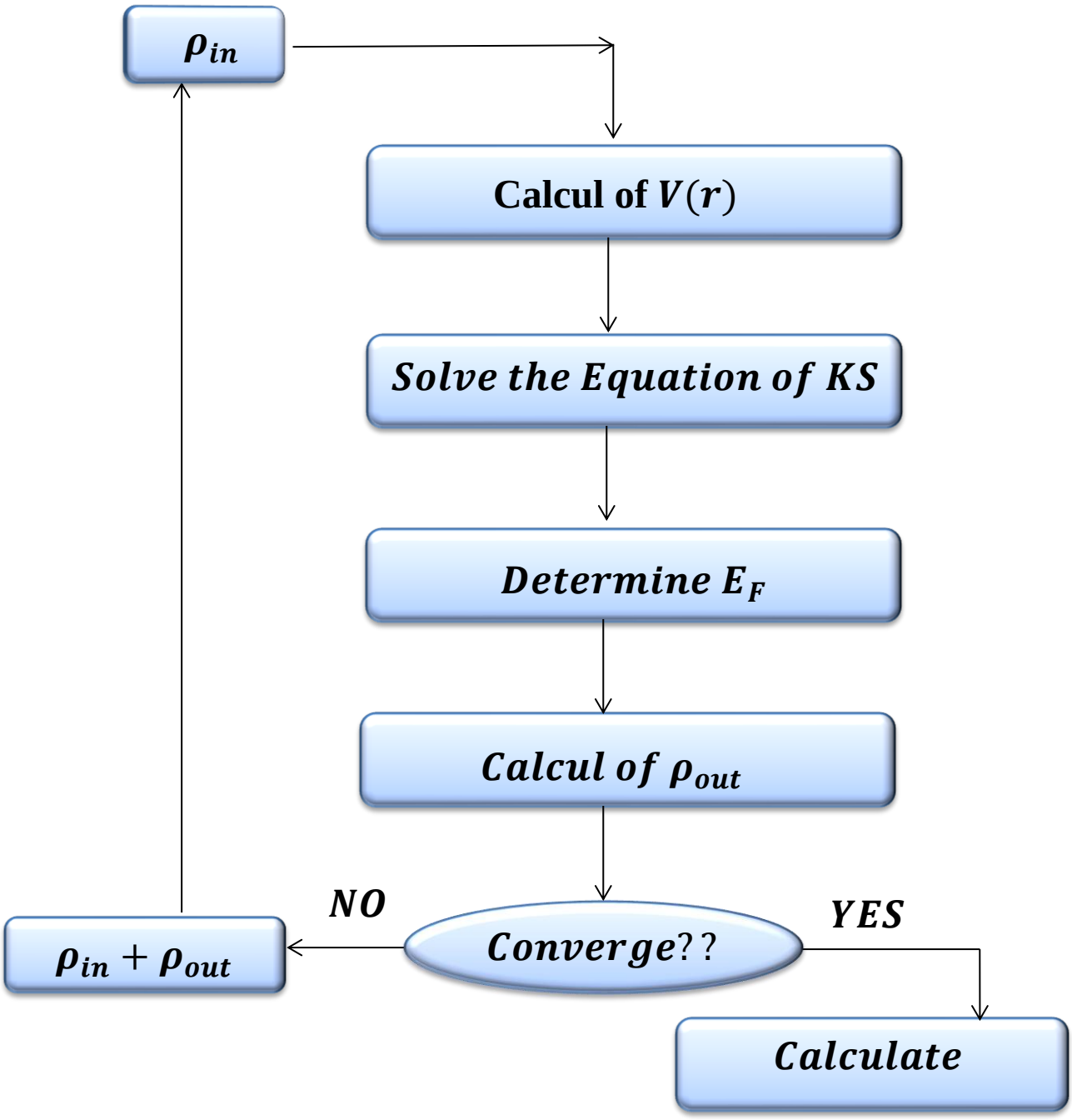

Figure II.5: *A flowcharts representing the Numerical procedure for solving the Kohn-Sham equations.*

II.4.The pseudopotential method

II.4.1.Introduction

Pseudo-potential method has gained significant success in DFT calculations and predictions of the fundamental state of a solid. The pseudo-potential method aims to obtain the valence states of a system without calculating the heart states, which are not necessary for describing physical properties. The pseudo-potentials' base is the approximate heart gel, assuming that the electronic states of electrons are insensible to the electronic configuration. In practice, the functions of electrons (r) are replaced by pseudo-functions (r), which are assigned an equal value to the atom's r-sphere and chosen to remove noeuds and oscillations due to the orthogonally of the functions. These pseudo-functions offer the advantage of being represented in Fourier space with a very reduced number of planes, reducing numerical calculations. The interaction between electrons and ions includes coulombic interaction, heart-valence resonance, and exchange-correlation. The higher the r-sphere, the less pseudo-functions and pseudo-potential are.

II.4.2.The Principe

The pseudo-potential principle involves separating electrons into valence and heart electrons, resulting in a new potential for the electrons in a reference atom configuration, which can be calculated multiple times, despite the minimal impact of the surrounding environment.[33]

II.4.3.the construction of pseudopotentiel method

The pseudo-potential must have certain properties[31] [33]:

- ✓ It must be additive, meaning it's the center of pseudo-potential when multiple atoms are present.
- ✓ It must be transferable, meaning it can be used in different chemical environments.
- ✓ It induces less potential variations than the real heart potential due to reduced planes.

II.4.4.Examples of pseudopotentiel method

- ✓ Pseudo-potential with conserved standard
- ✓ Ultra-soft pseudopotentials

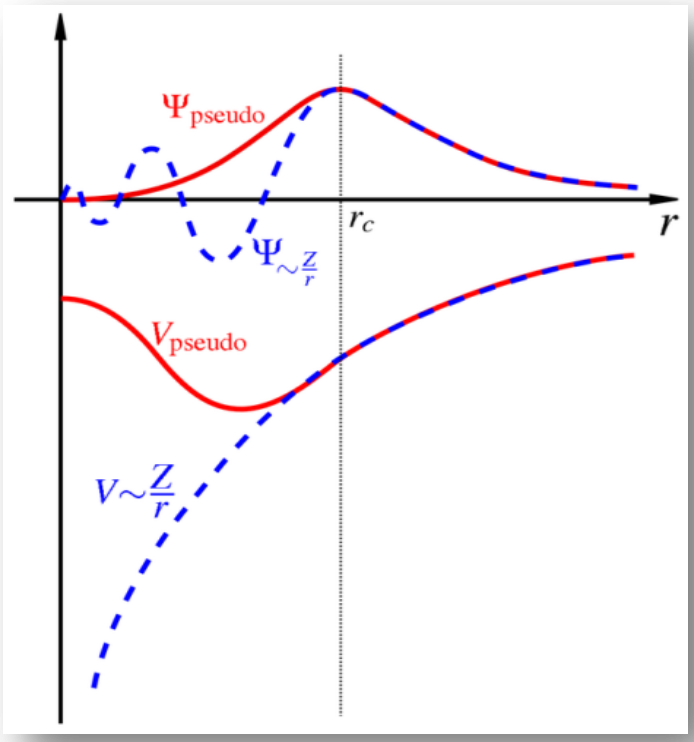

Figure II.6: ***Schematic diagram of a pseudo potential and wave function (ψ) bleu compared to the pseudo wave function (Ψ_pseudo) calculated in the pseudo potential (V pseudo) (red).***[34]

II.5.Quantum Espresso Coding QE:

II.5.1. INTRODUCTION

Quantum espresso is an integrated suite of Open-Source computer codes for electronic-structure calculations and materials modeling.is developed by Quantum espresso foundation QEF. It is based on density-functional theory, plane waves, and pseudo potentials, An excellent resource for PPs is Standard Solid State PPs (SSSP), a collection of the best verified PPs, maintained by THEOS and MARVEL on the Materials Cloud.[35]

II.5.2.What can be done by QE:

- ✓ Ground state calculations
- ✓ Structural Optimization: Modifying the geometry of a system to minimize total energy.

- ✓ Car-Parrinello molecular dynamics:
- ✓ Calculation of energy barriers and reaction pathways
- ✓ Calculation of phonon properties using Density Functional Perturbation Theory (DFPT)
- ✓ Spectroscopic properties: study of interactions between matter and electromagnetic radiation.
- ✓ GW calculations and solution of the Bethe-Salpeter equation for electronic excitations
- ✓ Quantum transport calculations using Wannier functions.

CHAPTER III

SYNTHESIS & CHARACTERIZATION

OF THIN FILMS

In this chapter, we present in the first section the description of the experimental procedure which led to the realization of cobalt sulphide thin films.

The following section is devoted to presenting the different techniques of characterization used in this work to study the physical properties of materials that brings out a deeper understanding to its structural composition and various properties which is crucial to optimize their performance in vast applications.

III.1.Thin Films:

Thin films are interesting due to the special physic-chemical characteristics acquired by the material. For this reason, thin films are playing a more and more important role in nanotechnology, they are useful in windows coating ,magnetic media, biomedical advices ,aerospace, solar cells……etc.

They also pose a challenge in the economic area due to the fact they are cheap in manufacturing terms and the relative simplicity of the procedures used to create them.

A thin layer of a given material is an element of that material whose one dimension, called the thickness, has been appreciably reduced to the point that it is expressed in units of some nanometers to a few micrometer and this small distance between the two limiting surfaces (quasi two-dimensional) causes a disturbance in the majority of its physical properties[36].

III.1.1.Formation of thin films:

The formation of thin films involves three basic modes of growth as illustrate in figure III.7:

a) Island or (Volmer- Weber).
b) Layer or (Frank van der Merwe).
c) Stranski- Krastanov.

III.1.1.1.Island growth:

Is the process by which the tiniest stable clusters form islands by nucleating on the substrate and growing in three dimensions 3D. In this case, the molecules or atoms are more bound to each other than to the substrate which called by multilayered. In this growth mode, the front becomes rough after a very short deposition time. In this regard, the frequently example of it was observed in graphite and alkali halide crystals.

III.1.1.2.Layer growth:

In this case, planar sheets are created as the smallest stable nucleus expands in two dimensions (2D).On the other hand, atoms that are highly mobile on the surface can diffuse widely, which allows them to further integrate at the edge of a terrace or island's steps so they are more strongly bonded to the substrate than to one another. In this instance, a layer's full expansion is therefore achievable. A second layer that is loosely bound covers the first full monolayer once it has formed. This procedure is repeated, producing what is commonly referred to as Franck-Van der Merwe growth (layer by layer). Single-crystal epitaxial growth of semiconductor films is one example.

III.1.1.3. Stranski-Krastanov (layer & island):

An intermediate combination of the layer and island growth mechanisms is the Stranski-Krastanov (layer plus island) process. Once one or more monolayers have formed, the layer's development eventually becomes unfavourable, leading to the formation of islands. One possible explanation for the two-to-three dimension shift is the disruption of the layer growth's monotonic binding energy decrease. For instance, strain energy builds up in the film as a result of a lattice mismatch between the substrate and the film. The island formation is caused then by the high energy at the deposited intermediate layer when it is released.[37]

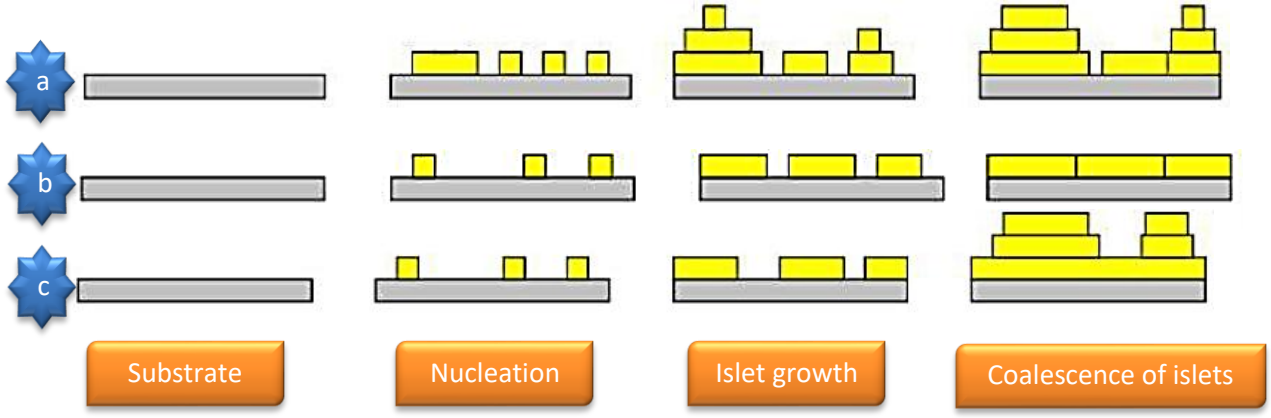

Figure III.7: ***Basic modes of thin films growth a) Volmer- Weber or layer growth, b) Franck-Van der Merwe growth, c) Stranski-Krastanov mode.***

III.1.2. Thin films structures:

The conditions of preparation affected the thin film's structure, as they do for all materials so we notice a single crystalline, poly crystalline and amorphous structure.

III.1.2.1.Single Crystalline structure:

Grain boundaries are absent in epitaxial (single-crystalline) need sluggish growth and high temperatures: superior thin films, including complicated oxides and III-V semiconductor films

III.1.2.2.Poly crystalline structure:

Thin films with grain sizes ranging from a few nanometres to cm. Thin films with a single crystal but a lot of flaws, such as dislocations, precipitates, and point defects. Single crystalline thin films that are almost flawless are something we frequently desire but do not always obtain. We might see regular grains or a variety of textures if we only look at polycrystalline thin films. Once more, we handle it when we encounter it. Lots of grain boundaries: Most elemental metals grown near room temperatures

III.1.2.3.Amorph structure:

Devoid of crystalline flaws due to the absence of crystalline structures typical insulators, like amorphous SiO2

III.1.3. Types of thin films and Applications:

III.1.3.1.Mechanical Thin Films:

Thin films made of hard, corrosion, and wear-resistant materials. Used In coating applications, mechanical thin films can be coated on almost any surface including metals, plastics, glass, etc. providing additional strength against friction and abrasion. The strong anti-corrosion properties also provide them with great versatility to be used in numerous and very diverse industries including aerospace engineering and transportation logistics.

III.1.3.2.Optical Thin Films:

Optical thin films are coatings that change the optical properties of surfaces in order to increase the effectiveness and efficiency of certain applications. Optical thin films are having a great impact on solar energy and the design of lightweight, flexible and sustainable solar panels. In general, optical thin films can do the following:

- Improve reflectivity or lessen glare depending on the type of coating.
- Protect surfaces against UV deterioration and fading due to sunlight.
- Increase the efficiency of solar cells, optical detectors and waveguides.
- Be used in computer monitors, anti-reflective coatings, and other optical devices.

Their versatility leads to use across industries from energy to electronics. An optical thin film with appropriate designs can increase performance, sustainability, and appearance.

III.1.3.3.Electronic Thin Films:

These thin films were better insulating than thick film components, allowing for efficient heat transfer in some applications. When utilized for circuitry, the thinness of the film increases the sensitivity of sensors and decreases power loss. This is what makes them very compatible with many substrates, including integrated circuits, insulators, semiconductors, piezoelectric drivers.

III.1.3.4.Magnetic Thin Films:

They are extremely thin, typically less than a nanometer in thickness, they have a lot of advantages such as being:

- Completely resistance to environmental influence
- Elements of great durability.

These qualities can be useful for acting in harsh equipment or long service in consumer items. There are many kinds of magnetic thin films that can be used in data storage devices, such as memory disks, sensing devices, and automation systems.

III.1.3.5.Thermal Thin Films:

Thermal thin films, also known as insulating thin films, are sophisticated coatings used to improve insulation, heat dissipation, and electrical resistance in many industries. They are manufactured from high-quality polymers with certain additives and are able to endure extreme thermal cycling and conditions, they are useful due to their:

- Excellent insulation and airtight seals.
- Improved heat dissipation to support effective thermal management.
- Flexible applications without the need to use adhesives or fabrics.
- Reduced energy consumption compared to insulating materials.

Thermal thin films are commonly found in industries creating insulation layers, and heat sinks used to improve efficiency and life span of a thermal system.

III.1.3.6.Chemical Thin Films:

Chemical thin films are flexible coatings that can offer a plethora of properties for a wide range of modern industries. These coatings provide durability, corrosion resistance, electrical conductivity, and optically active materials.

Some of the advantages above are:

- Prevent alloying, diffusion, corrosion, and oxidation.
- Can have custom composition that is developed for needs of the application.
- Advance the development of gas and liquid sensors.
- Allow engineers and manufacturers to start exploring possibilities as research advances.

Their versatility and protection offer method to all areas of technology -as we engineer and material scientists, move material development forward in new applications.[38], [39]

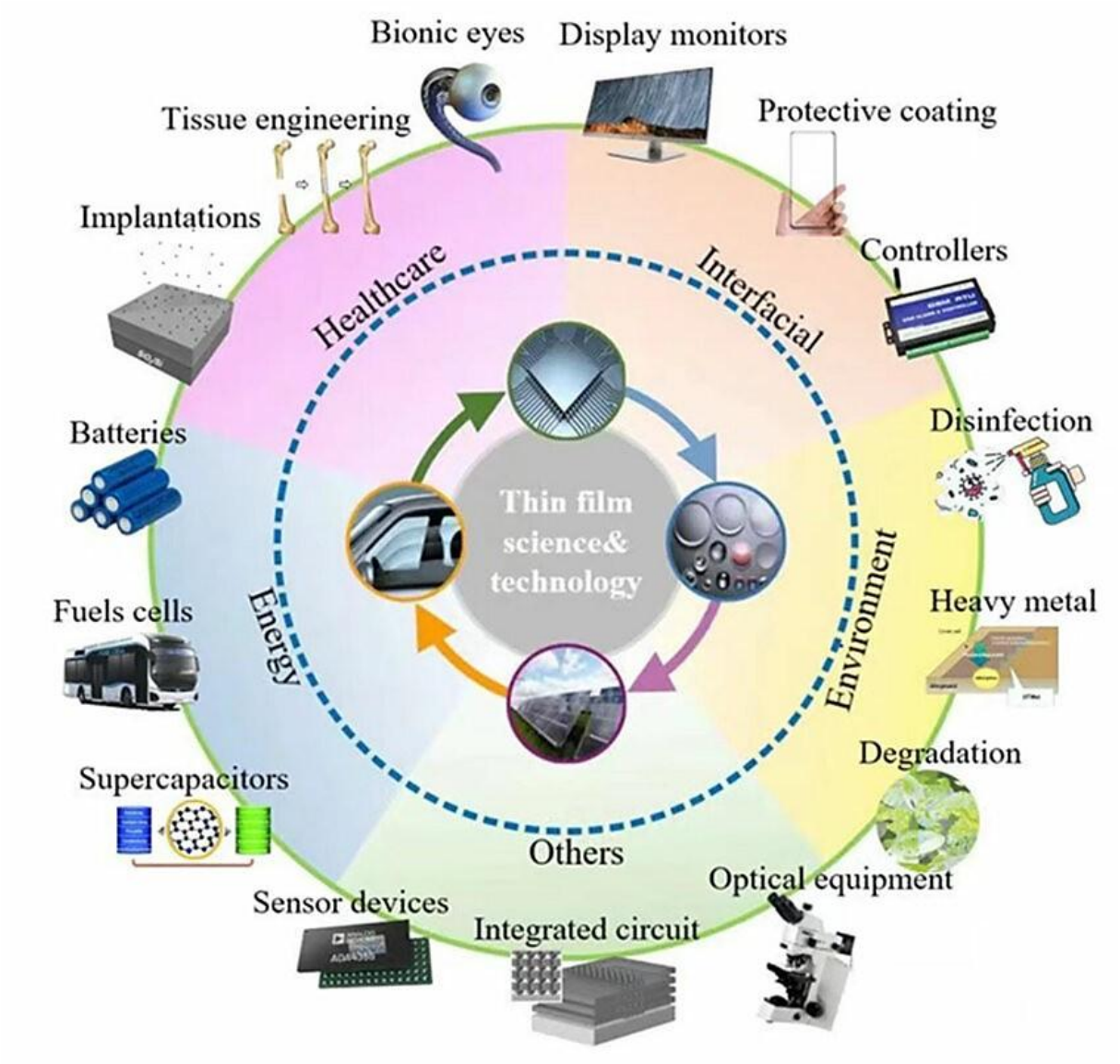

Figure III.8: ***Thin films applications diagram*****[40]**

III.2.Sol-Gel synthesis method:

The sol-gel process is a widely used wet chemical method in synthesis of nanoparticles and gives the highest level of control over size, shape, and composition. In this process, a liquid precursor (sol) becomes a solid gel network through a series of chemical processes. The properties of the synthesized nanoparticles are particularly useful in a variety of fields including materials science, biotechnology, and energy storage.[41]

The uniqueness of the Sol-Gel process, which is the abbreviation for Solution-Gelling, is that it is obtained in solution and at low temperature; therefore it is soft chemistry; of a solid or powder with a generally amorphous structure that produces an amorphous or crystalline material through subsequent thermal annealing.[42]

III.2.1.Sol-Gel process steps:

The sol-gel process typically involves several key steps:

III.2.1.1.Homogeneous solution:

An important aspect of the sol-gel process is to achieve a homogeneous solution of precursors and alcohols. To create this homogeneous solution, the solvent (usually containing water, alcohol, organic solvents, or a combination of these in varying ratios) is first mixed with the precursor in some type of container. it is often ideal to use mixtures of two solvents in specific concentrations such that the precursors are completely dissolved in. As an example, some metalorganic precursors must be dissolved in a water-soluble organic solvent first, and then the resulting solution can then be dissolved in water. If the organic precursor is metal salt, this can be added directly to the water and does not require an organic solvent. Metal oxide precursors can also be added and used this way, and while alkoxide precursors are more common, the sol-gel process can be completed in other fashions, in which a “relatively stable colloid” is used, instead of the homogeneous tuberculosis, for gel formation. Metal alkoxides, the precursors used in sol-gel process, belong to the family of organic metal compounds which can be defined as an organic base bonded to a metal or quasi-metal. An interesting example would be silicon tetroxide (OC2H5)4 ; this precursor is often referred to tetraethoxysilane (TEOS).[43]

III.1.1.2.Hydrolysis (sol formation): it involves the conversion of a homogeneous solution of the precursor into a colloidal solution

Under the influence of water or alcohol like ethanol the metal alkoxide undergoes hydrolysis and forms metal hydroxide bonds (where water molecules react with the metal alkoxide) as a result the metal-oxygen bonds of the precursor break and metal hydroxide or oxide species are formed. The generic reaction can be written as:

$$M\text{-}OR + H_2O \rightarrow M\text{-}OH + R\text{-}OH.$$

Where:

M-OR: represent metal alkoxide.

M-OH: represent metal hydroxide.

III.2.1.3.Condensation(Gel formation): The colloidal solution is held for aging and the metal hydroxide essentially condenses by chemical reaction (polymerisation); in other words the metal hydroxide groups undergo chemical change, where hydroxide links M - O - M and water molecules H_2O/R - OH are eliminated to form a three-dimensional network, where is the reaction can be divided into two categories [44]

a) Dehydration polycondensation:

$$M\text{-}OH + M\text{-}OH \rightarrow M\text{-}O\text{-}M + H2O$$

b) Dealcoholisation polycondensation

$$M\text{-}OH + M\text{-}OR \rightarrow M\text{-}O\text{-}M + R\text{-}OH.$$

This condensation reaction continues until it finally results in a coherent, rigid, porous, inorganic network completely covered with a liquid phase (This phase is also called gelation/transitions).

III.2.1.4.Gelation: The sol becomes a gel because of the growth of the network throughout the liquid phase; the gelation process can be controlled over adjusting factors like precursor concentration, solvent composition, PH and temperature …etc.

III.2.1.5.Drying and formation of xerogel: The gel is dried to evaporate the solvent and this process can be done by evaporation, supercritical drying or freeze-drying, as drying should be conducted under controlled conditions to avoid cracking or collapsing the gel framework. When the solvent is dehydrated at ambient conditions (Removal of R-OH groups) a xerogel is formed, and the subsequent thermal calcination.

III.2.1.6.Calcination : In most cases, the dry gel is subject to a thermal treatment called calcination at very high temperature; the organic compounds or at least residual, are removed and this elevated temperature induce to further crystallization and growth of the desired material and properties of the nanostructure materials take shape in this step. [45][46], [47]

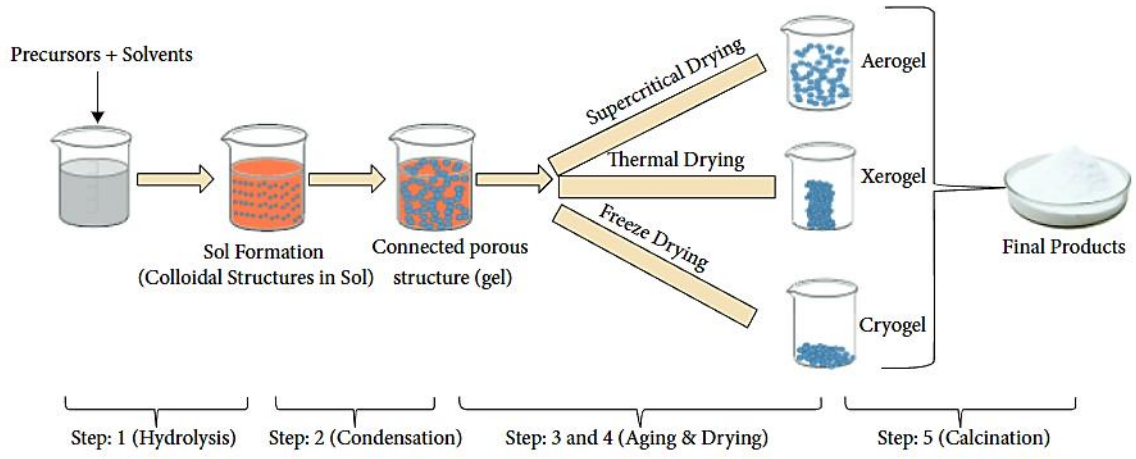

Figure III.9: ***Schematic of different stages of Sol-Gel process.***

III.2.2.The influenced parameters on the sol gel method

PH: Solutions can be dictated specifically by the pH

Solvent: Solvent will matter in the polycondensation process. First solvent helps the NPs stay dissolved.

Agitation: Gel networks can be formed domain wise during gel formation. Mixing would break the domain wise networks and then form a leigh network. Agitation helps with the chemical reaction in all parts of the solution and allows all the molecules to have the exact same quantity of chemicals.

Time: Time has an impact on different gelation processes because the solution has different amounts of time to produce gels. Gelation is a slow process. Accelerating reaction for a brief amount of time sometimes cannot produce a gel.

Temperature: Gelation is a slow process. Temperature speeds and changes the chemical kinetics of the reaction for the gel formation. Sometimes gelation needs a period of time for a week or more. Adequate temperature will reduce the gel forming timeframe. Temperature also helps bind the NPs to gel.

Catalysts: Catalysts act big in the chemical reactions to speed it up. Because acidic (H+) and base are catalysts in this case act differently with decreasing time to speed up the reaction.[46]

III.2.3.Advantages&disadventages of Sol-Gel Method

III.2.3.1.Pros:

i. Simplicity of the process.
ii. Preparation of high purity products.
iii. Very high production efficiency.
iv. Production of optical components with complex shapes.
v. Synthesis of uniform compounds in the form of composite oxides.
vi. Ability of designing and controlling chemical composition and obtaining a homogeneous composition.
vii. Ability of using the product with special shapes such as fiuch and aerogels
viii. Surface coverage
ix. Ability of using this process to synthesize amorphous materials in thin layers
x. Production of materials with modified physical properties, such as low thermal expansion coefficient, low UV absorption, and high optical transparency.
xi. Production of porous and rich materials with organic and polymeric compounds.
xii. High chemical reactivity of precursors due to process in solution phase.[47]

III.2.3.2.Cons:

Some of the disadvantages of the sol-gel technique involve the many chemical parameters necessary to be controlled in order to define the final structure of the material, revealing a certain complexity beneath the apparent simplicity of the process.

The major disadvantages of the sol-gel process are:

i. Obtaining thin layers requires several depositions and drying steps to achieve a thickness of several hundred nanometers, resulting in an increased risk of cracking since all the first deposited layers are exposed to successive annealing.
ii. Working with a relatively large volume of solvents.
iii. The generally long thermal annealing times, tend to increase the time for production.
iv. The limited availability of organometallic precursors on the commercial market, and it's quite high cost.[42]
v. Complete sulfurization can be difficult, often requiring a H2S atmosphere and high temperatures[48]

vi. Another drawback of this process is the understanding of the reaction [46]

III.2.4.Application of the Nanomaterial's prepared by Sol-Gel Method:

Optical Materials: High-purity glass and ceramic materials, needed for lenses, mirrors, and optical fibres, can be formulated using the sol-gel synthesis. The ability to control refractive index and transparency is very beneficial for these materials.

Coatings: Often, the development of protective and functional coatings (for example, for metals, glass and polymers, etc.) is accomplished via sol-gel techniques. These coatings could provide scratch resistance, anti-reflection, hydrophobicity, and other desired surface properties.

Catalysts and Sensors: Finally, sol-gel has the ability to produce porous materials that can be used as catalysts or as substrates for sensors. Their large surface area and the chemical functionality can be tailored for the specific catalytic reaction or detection of the chemical species of interest.

Biomedical Applications: Sol-gel derived materials are useful in drug delivery systems or bioactive coatings for implant materials. Significant research is being conducted in both areas where therapeutic agents can be released in a controlled manner and on implants where materials can promote bone growth. [47][49]

III.3.Deposition by sol Gel synthesis

Several methods can be used to deposit thin films on chosen substrates. Each has distinct features, and the choice of method will depend upon the characteristics of the substrate, such as geometry and size.

There are numerous methods for the fabrication of cobalt sulfide thin films, including techniques like chemical vapour deposition (CVD), physical vapour deposition (PVD), laser ablation, and sputtering. These processes can produce high-quality results but tend to come with hefty price tags for the initial setup and ongoing maintenance. On the brighter side, more affordable and easier methods have recently emerged, such as spray pyrolysis deposition, spin coating and dip coating. Through this chapter we will go into more details on some fabrications techniques.

III.3.1.Spin Coating:

Spin-coating is a fast and widely used technique for applying thin films onto surfaces. One of the biggest perks of this method is how effortlessly it can create uniform films. It operates on a simple principal when you spin a precursor solution drop by drop onto a substrate at high speeds; the combination of centripetal force and the surface tension of the liquid ensure that the substrate gets covered evenly. After taking away the excess solvent, we end up with a thin film that can range from just a few nanometers to several microns in thickness. This method works well for small substrates, whether they're just a few millimeters across or even a meter in diameter. The ease of setting up the spin-coating process, alongside producing thin and even coatings, makes it a go-to choice in many settings[50].

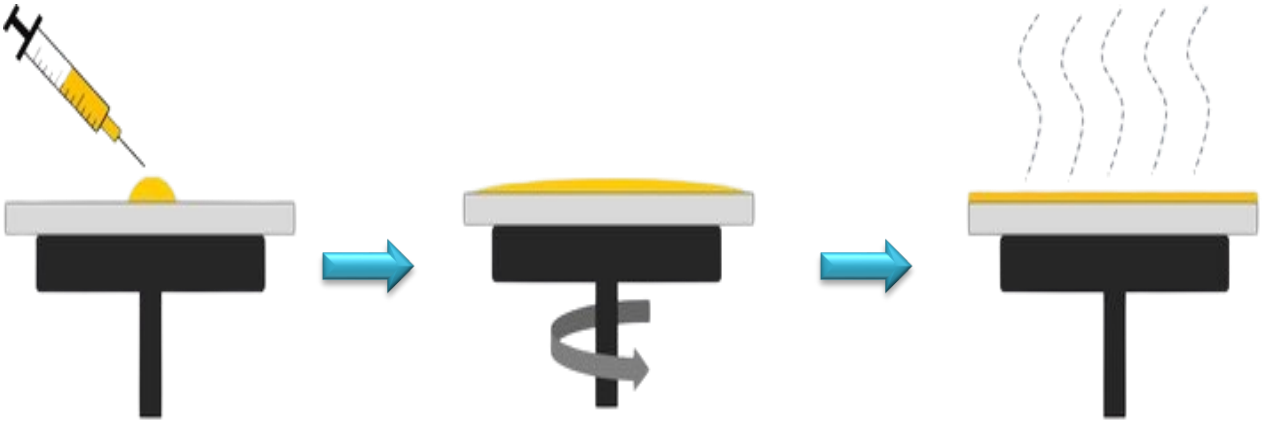

a) Deposition b) Spinning c) Formation of the sample

Figure III.10: ***Schematic Diagram of spin coating process.***

III.3.2.Dip Coating:

On the other hand, dip-coating is another straightforward, cost-effective, and high-quality method for coatings that is popular in both industrial and laboratory environments. In this process, a substrate is dipped into a solution containing the coating materials, and then the solution is allowed to drain away in air or in an oxygen atmosphere[51]. It can be described as depositing an aqueous liquid phase onto the surface of a substrate. Usually, the required materials are dissolved in a solution and applied straight to the substrate.

However, the properties of the solution prepared through dip-coating process involves a number of detailed chemical and physical factors that play a crucial role in determining the film's thickness and shape[50].

- How long you leave the substrate submerged.
- The speed at which you pull it out.
- The number of dip-coating cycles.

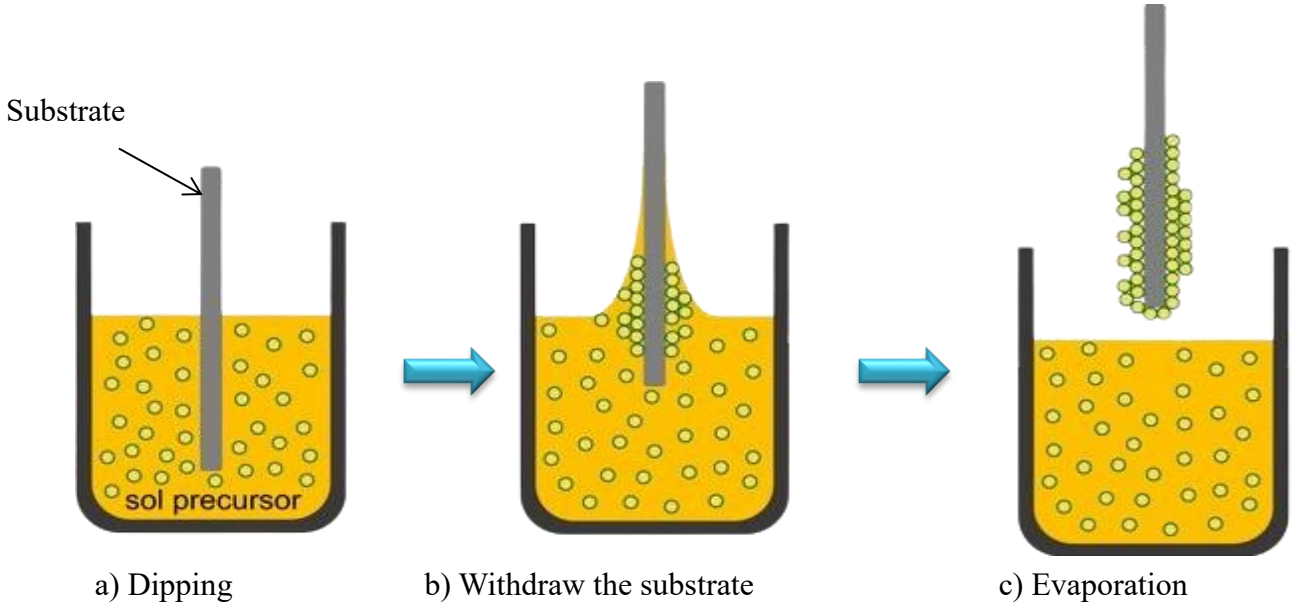

Figure III.11: ***Schematic illustration of the Dip coating process.***

III.3.3.Spray Pyrolysis Deposition:

III.3.3.1.History:

The first use of spray pyrolysis was for depositing metallic and semi-conductor films during 1950 and 1960,after 10 years in 1970-1980 the titanium, zinc and zinc-tin oxide was deposited using this method .more than that, in1990 the spray pyrolysis method is beginning to witness a remarkable progress for applying to deposit different materials including compounds, alloys and multilayer structure.

III.3.3.2.Principe:

The spray pyrolysis (SPD) is a useful technique for depositing thin films of metals oxides and semi-conductor; it is also helpful to get a sample with controlled characteristics including size, morphology and other structural properties. Depending on the kind of pyrolysis reaction and the nozzle used to spray the solutions, it existed many kinds of SP units: Flame Spray Pyrolysis (FSP), Electrostatic Spray Pyrolysis (ESP), Pneumatic Spray Pyrolysis (PSP), Vortex Flame Spray Pyrolysis (VFSP), and Ultrasonic Spray Pyrolysis (USP).

The spray pyrolysis technique is used to produce thin films by dissolving metallic salt in an appropriate solvent is the first step , the preparation of tiny droplets of the solution by forcing them through a nozzle is the second phase it can be also known as droplet formation or

atomization. In the following step a specific amount of the solution will be sprayed in to a disk shape structure onto a substrate and heated to evaporate the solvent .The material result will be obtained in its desired form.[52]

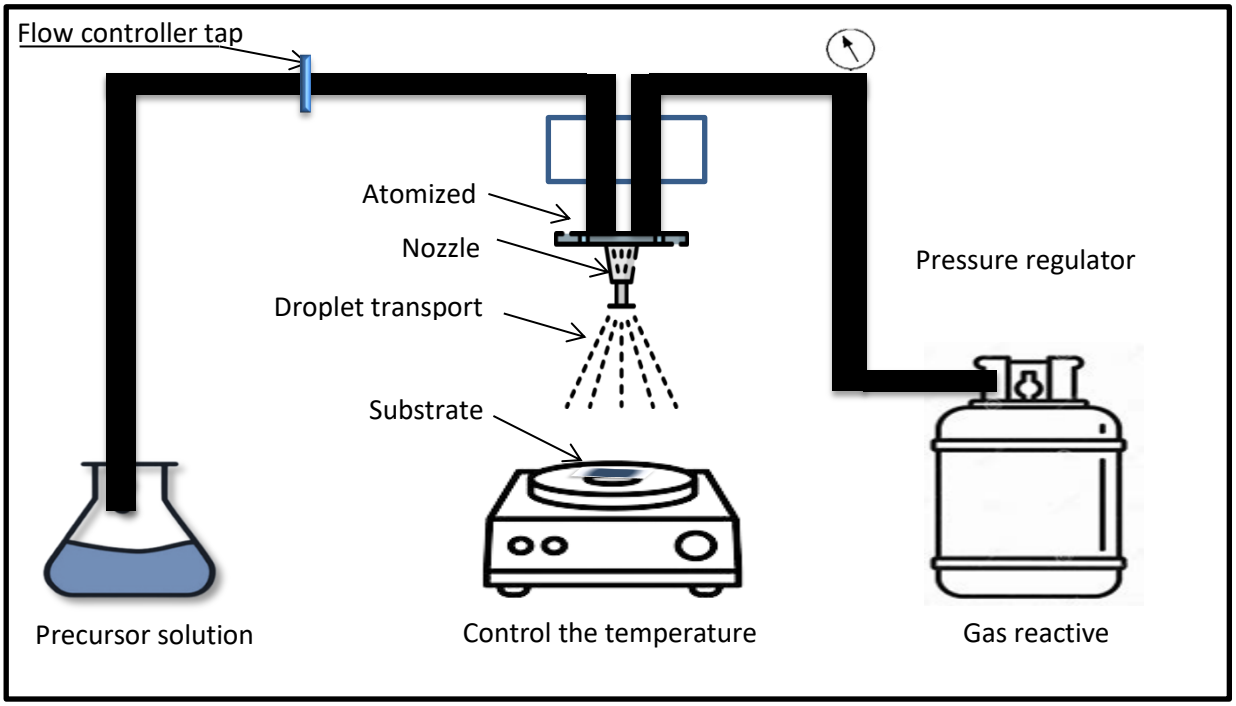

Figure III.12: ***Schematic Diagram of Spray Pyrolysis***

Thin films result can be impact by versatile parameters as shown below:

- The substrate temperature.
- The Spray deposition rate.
- The Spray duration.
- The rotation speed of the hot plate.
- The separation distance between the nozzle and the substrate.

III.3.3.3.The pros and cons of Spray Pyrolysis:

III.3.3.3.1.Advantages of spray pyrolysis:

- The deposition of the thin films is simple with low cost.
- Applicable to large area.
- During this process the high temperature is not required.
- The spray pyrolysis does not require a substrate and chemical product with haut quality.

III.3.3.3.2.Disadvantages of spray pyrolysis:

- The yield of the powdered materials is extremely low
- The sulfides must be converted into oxides.
- A number of challenges are regard in optimizing at growth temperature.

III.3.3.4.thermal annealing

Thermal treatment is necessary to have a good quality thin film. It consists of two steps:

First, drying is carried out at a low temperature of 100°C to evaporate the solvent, and then thermal annealing is applied in a NaberTherm oven as mentioned in the following figure. The gel undergoes an annealing treatment in which it is carried out at a wide range between 300°C and 700°C, also there are annealing treatments up to 1000°C, called high temperature heat treatment with variable durations. In our case, the thin films were treated at 500°C from 30 min to 4 hours; this method subsequently induces the contraction of the material with a reduction in volume (reduction in the thickness of the layer). Following densification, this method allows the elimination of residual organic species.

Figure III.13: Nabertherm oven

In this chapter we aim to optimize the deposition parameter of cobalt sulfide using ultrasonic spray pyrolysis method.

III.4.Synthesis of cobalt sulphide thin films

Elaboration of thin layers is carried out in two stages:

- The synthesis of solutions using sol-gel method
- The preparation of the substrates and the deposit of the films by the ultrasonic spray pyrolysis technique USP.

III.4.1.Solutions preparation

In this study we use cobalt (II) nitrate with the chemical formula $CoN_2O_6{:}6H_2O$ using distilled water as solvent by the addition to thiourea with the formula CH_4N_2S as source of atom sulphur with ratio of 1:3. The quantities of materials used in this precursor solution are deduced from the following calculations:

m_1 ($CoN_2O_6{:}6H_2O$) = C.V.M =0.8*291.02*50*10^{-3} =11.641 g

m_2 (CH_4N_2S) = C.V.M =2.4*76.12*50*10^{-3}=9.134 g

Molar mass of cobalt nitrate ($CoN_2O_6{:}6H_2O$) = 291.02 g/mol

Molar mass of thiourea (CH_4N_2S) = 76.15 g/mol

Solvent volume (distilled water) = 100 ml

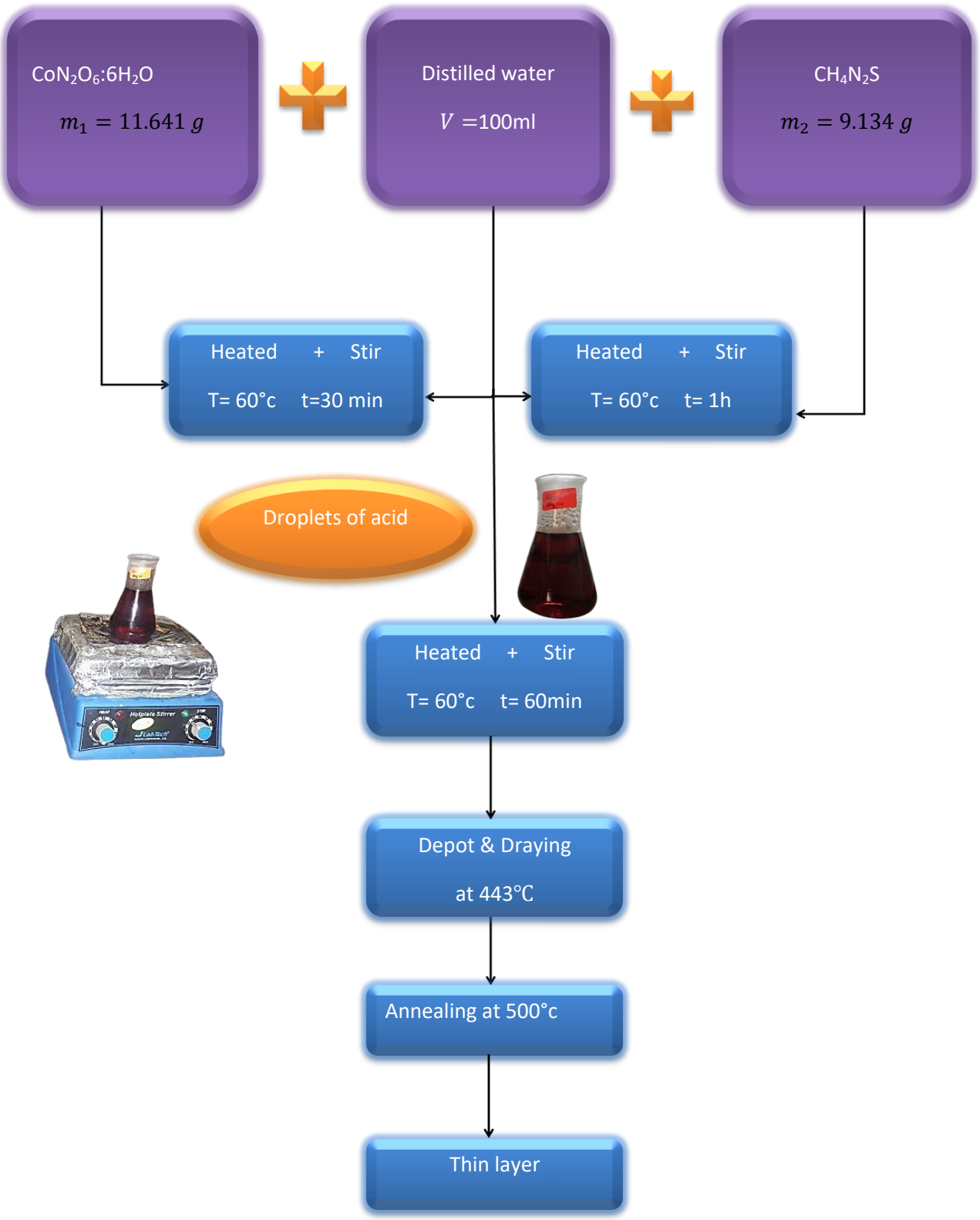

Figure III.14: ***Thin layer production protocol.***

III.4.2.Substrate choice

The thin films of cobalt sulphide were deposited on two different substrate due to the characterization technique requirement. We use glass slides cut by a diamond pen with the dimensions are (25.4, 76.2, 1) nm this type was chosen for its economic viability and transparency which adapted well for the optical characterisation of the films in ultra-visible analysis in addition to the electronic measurement. However, the silicon substrate (100) was used for characterisation by infrared absorption spectroscopy due to its transmission in the IR radiation and allowing for the analysis of the materials deposited on the substrate.

III.4.2.1.Cleaning of substrates:

The surface condition and property of the substrate determine the quality of the deposited layers. As a result, cleaning is a crucial step to eliminate any traces of grease and dust and to make sure that the substrate's surface is free of imperfections, rayures.Also, to ensure a uniform deposit thickness throughout the whole surface. These requirements are essential for the deposit to adhere well to the substrate.

The steps below are used to clean the substrates using ultrasonic bath:

1) Cleaning and rinse with distillation water in an ultrasonic for 15 minutes.

2) Cleaning in a trichloroethylene bath for 15 minutes.

3) Cleaning in an acetate bath for 15 minutes.

4) Cleaning in an ethanol bath for 15 minutes.

5) Drying substrate with the assistance of a dryer (Josephson paper).

III.4.3Layer Deposition:

The ultrasonic spray pyrolysis method is a deposition process that depends on various conditions which could separate into two categories:

Parameters related to the fluid precursor: the concentration of the solution, its viscosity and the surface tension.

Parameters related to the equipment: the distance between the nozzle and the substrate, the duration of the deposition, the frequency of the ultrasonic generator, and the substrate temperature.

Nevertheless, temperature and deposition time remain the main influential parameters on the quality of the layer.

The solution prepared according to the protocol in Figure III.15 is placed in a special glass container submerged in an ultrasonic bath. The aerosol vapour is subsequently transported by an injection of a carrier gas flow from the air pump. It requires slightly higher substrate temperatures to cause the aerosol droplets to thermally decompose on the substrate surface, which in turn promotes the growth of the highly adhesive layer.then,the thin films deposited undergo a thermal treatment at 500 °C for various duration.

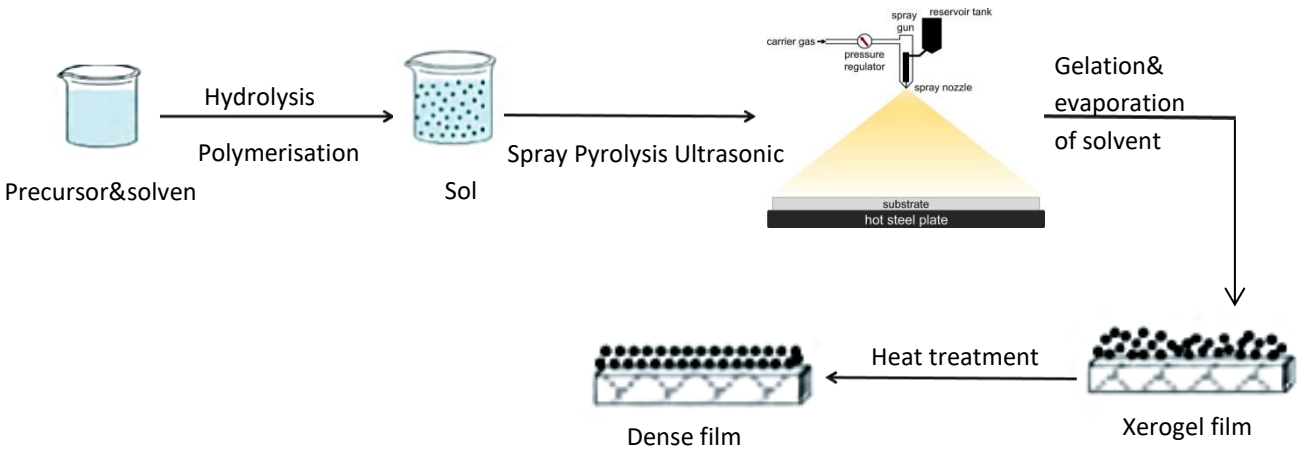

Figure III.15: ***Scheme of depositing samples by Ultrasonic Spray Pyrolysis (USP) method: from colloidal solution.***

III.4.4. Elaboration of an Ultrasonic Spray Pyrolysis (USP) Device

Device for Ultrasonic Spray Pyrolysis was shown in the figure III.16 it contain a heating plate, a precursor solution, air pump,arduino controller and an ultrasonic bath where the ultrasonic sensor was merged. After being put on the plate, the sample is heated to 443°C.

Figure III.16: ***Instrument used to create thin cobalt sulphide layers using ultrasonic spray pyrolysis (USP).***

III.4.4.Deposition parameters:

The following are the deposition parameters:

Solution: C = 1.6 mol/L

Substrate: glass (25.4, 76.2, 1) nm, Silicon (100)

Substrate-nozzle spacing: d=10 cm

Deposition time varied 30 min to 60min

Temperature of the substrate: T = 443°C

Arduino controller has the role to turn on the air pump for 40 second and then turn off for 15 second along deposition duration

The main topics in this section are the various characterisation techniques utilised to describe the newly formed layered materials.

III.5.Characterisation techniques:

Over the years, Spectroscopy has developed as a potential instrument for experiments and analyses carried out in both companies and research labs. This technique investigates how an electromagnetic field interacts with matter. It originated as a study of how visible light is dispersed by a prism dependent on wavelength. The concept was broadened to cover all interactions involving radioactive energy variation with wavelength or frequency.[53]

III.5.1.Principles and instrumentation for UV-Vis-IR:

Ultraviolet (UV) spectroscopy is an essential physical instrument that uses light in the visible, ultraviolet, and near-infrared portions of the electromagnetic spectrum. The concentration of absorbers (or absorbing species) in the solution, absorbance, and path length are all linearly related according to the Beer-Lambert law [54] .This can be used to analyze liquids, gases and solids, Thus, the following predefined wavelengths have been established for these regions: UV: 300–400 nm; Vis: 400–765 nm; and NIR: 765–3200 nm.

It has the feature to provide a qualitative and quantitative analysis.

Qualitative analysis:

Qualitative inorganic analysis seeks to determine whether a certain element or inorganic compound is present in a sample.

Qualitative organic analysis seeks to determine whether a specific organic component or functional group is present in a sample.

Quantitative analysis:

The goal of quantitative analysis is to determine how much of a particular element (or compound) is present in a sample.

III.5.1.1.Principles

Instrument employed for ultraviolet−visible (or UV-Vis) spectroscopy is called UV−Vis−NIR Spectrophotometer, it’s based on a light beam which passed through an object and wavelength of the light reaching the detector is measured. The measured wavelength provides important information about chemical structure and number of molecules (present in intensity of the measured signal). Information may be obtained as transmittance, absorbance or reflectance of radiation in 160 to 3500 nm wavelength range .Thus; both quantitative and qualitative information can be gathered[55].

The UV-Vis spectrum can by recorded via the following types of instruments:

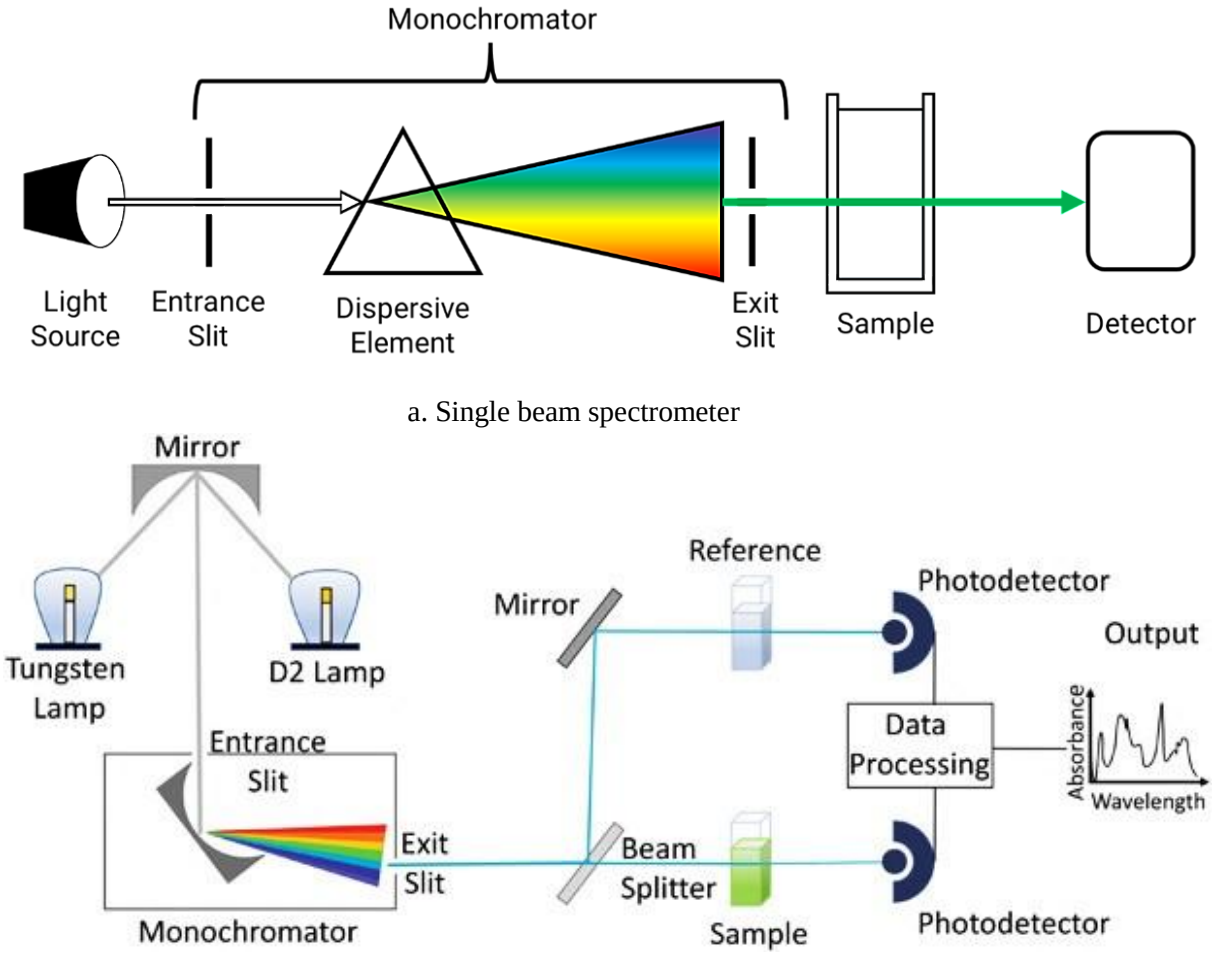

a. Single beam spectrometer

b. Double beam spectrometer

Figure III.17: ***Various types of UV-VIS-IR spectrophotometry.***

III.5.1.2.Instrumentation:

A spectrometer's fundamental parts are the detector, sample stage, monochromator (wavelength selection), and light source (visible and UV). The most widely used kind of light source is a continuous tungsten filament operating in the ultraviolet spectrum. A photodiode or Charge-Coupled Devices (CCD) usually acts as detector.

To filter light of a specific wavelength before feeding it to the detector, photodiodes work in tandem with monochromators. The visible lamp must be switched off while the UV spectrum absorption is being monitored, and vice versa. The UV-Vis-NIR Spectrometer concept can be observed in Figure III.17.[53]

Using this technique, we were able to follow curves that represent how transmittance varied in the UV-VIS-NIR region as a function of wavelength. As result, the determinations of optical properties like the absorption coefficient α and the optical gap are allowed.

Our samples' UV-VIS spectra are measured using the SHIMADZU (UV-1650) double beam spectrophotometer type, which is represented in the picture.

Figure III.18: ***Spectrophotometer of double beam type SHIMADZU (UV-1650PC).***

III.5.2. Fourier Transform Infrared Spectroscopy (FTIR):

The photons with energies in the infra-red range of the spectrum interact mostly with phonons and molecular vibrations and rotations, which are heavily influenced by the atomic structure of the material. FTIR is therefore a helpful method for examining the structural characteristics of materials. However, towards a material to be active for absorption (IR active), or to produce an absorption peak on its spectrum, a certain vibration mode must alter the material's dipole moment. As a result, symmetric vibrational modes typically do not result in absorption.

III.5.2.1.Principle:

This operation based on the interference between light passings through the interferometer's two distinct arms, as seen in Figure III.19. A monochromatic light beam will interfere constructively when the path difference (Δl) between the interferometer's two arms is an integer multiple of the wavelength; when it is an integer multiple plus half of the wavelength, the beams will interfere destructively and cancel each other out. As a result, the detector will produce an oscillating signal over time. For specific locations of the moveable mirror, different wavelengths interfere in different ways. Monochromatic light causes an oscillating reaction on the detector as it travels through the interferometer. In addition, We apply a Fourier transform on the interferogram in order to obtain the frequency domain spectrum.

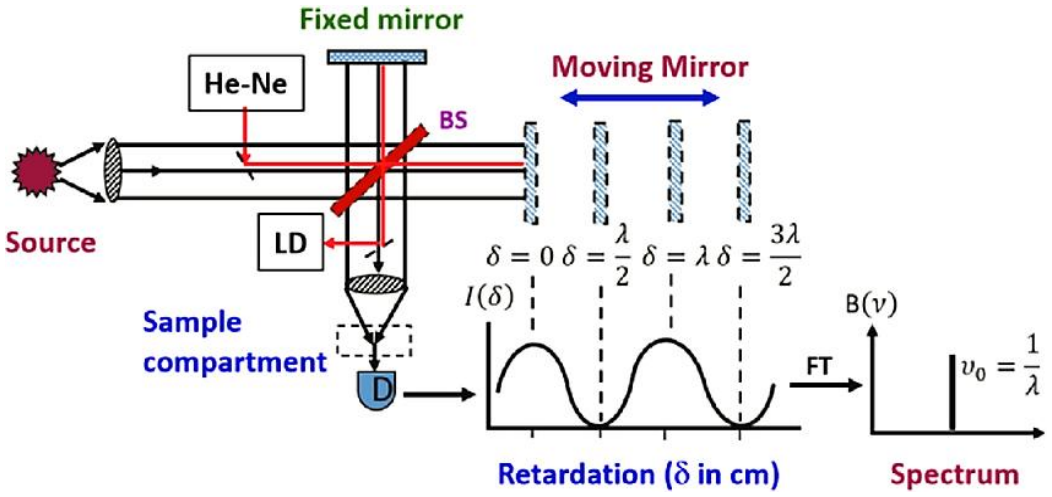

Figure III.19: ***Schematic diagram of Michelson interferometer.***

Employing an FTIR spectrometer to evaluate light transmission through a sample as a function of wavelength is the most popular experiment. The absolute transmittance (T), which represents the contribution attributed exclusively to the sample, is calculated by dividing the raw spectrum (T_0) by the background (B).

$$T = \frac{T_0}{B}$$

IR spectrum classic is plotted in the mid-infrared (wavenumber ν between 400 and 4000 cm^{-1}). It represents the ratio at each point of the transmitted intensities with or without a sample. This ratio, called transmission (T), can be replaced by its percentage (T%) or by its absorbance: A = log(T) = log(1/T)

The absorption radiation of frequency v from the IR radiation causes a molecule to transition from an energy state E_1 to a higher energy state E_2 such that the Bohr condition (resonance condition) is met: $E_2-E_1=h\nu= hc/ \lambda$. The absorption of IR radiation increases the amplitude of molecular vibrations.

However, there are several methods of measuring the infrared transmission for powder samples, such as the Nujol Method and KBr Pellets.

In this case, we make use of the FTIR-8400 infrared spectrometer SHIMADZU, which is set up in the physical genius laboratory and offers a spectral range of [4000-400 cm^{-1}].

Figure III.20: ***Infrared Spectroscopy set up type SHIMADZU -8400.***

III.5.2.2.Applications:

The well-known application of IR spectroscopy is identification of chemical compounds in a diversity of samples; it has also other uses as shown below.

- Determination of concentration of chemical components (quantitative analysis).
- Determination and observation of reaction kinetics, phase transition, and process evolution.
- Structural characterization of materials.
- Atmospheric studies (trace gases, analysis of fires and smoke, automotive emission analysis, etc.)
- Criminal forensic analysis.
- Vibrational spectroscopy of materials.
- Explosive and controlled substances detection and identification.
- Non-invasive clinical diagnosis.
- Food and drug analysis.[56]

III.5.3. X-Ray diffraction (XRD):

X ray analysis include two sub methods X ray diffraction XRD (non-destructive method) and X ray reflectometry XRR ,in our case we will focus on XRD technique.

III.5.3.1.Principle:

The Principe that based on this method the postulate of William Lawrence Bragg in 1913:

The reflection is done on the inter planar spacing d and the spots are formed following the constructive interference between the rays reflected by the different plan which can be mathematically demonstrated using the following formula:

$$2d_{hkl} \sin\theta = n\lambda$$

Where:

d_{hkl}: Interspacing between atomic planes

θ: Bragg angle (angle between the incident or diffracted ray and the relevant crystal planes)

$\boldsymbol{n}$: Integer number

λ: Wavelength

The determination of a microscopy entity (atomic inter planar spacing) d can be obtain by measuring angular 2 θ position from the outgoing diffracted beam relative to a fixed incident direction of the various diffraction peaks observed in a material.

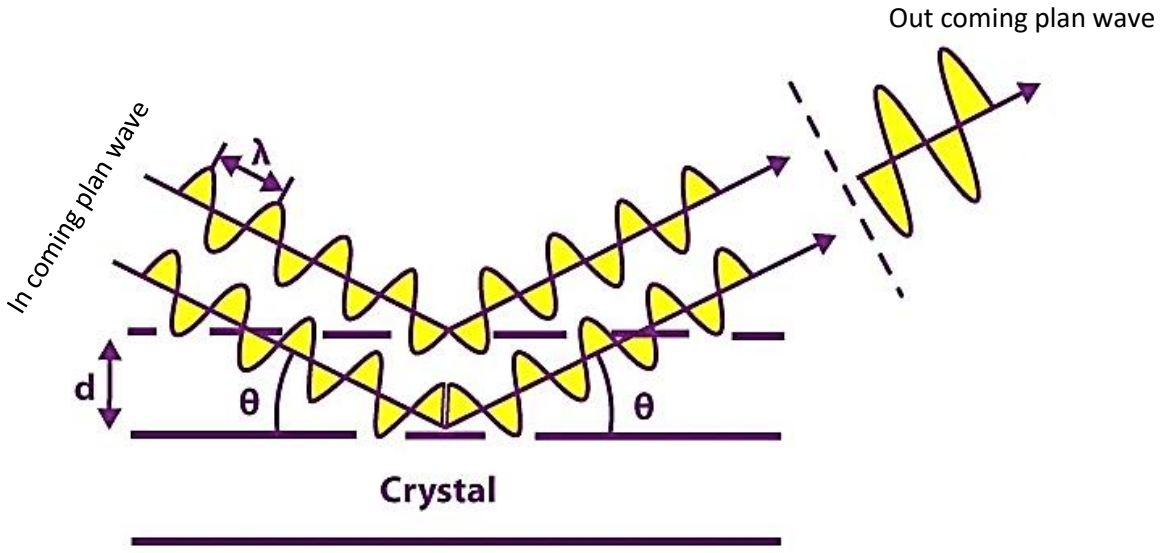

Figure III.21: ***W.L.Bragg low demonstration.***

III.5.3.2.Instrumentation of (XRD):

Understandings of XRD instruments are essential for the data interpretation; the useful machine called diffractometer consists of five main parts as mentioned in figure III.22:

1) the X-ray source which generates X-rays with a specific beam Cu,Mo,Cr or Ag are monochromatic sources ,the most useful is Cu with k_α line with energy of 8.05 Kev and wave length $\lambda = 1.5418$ Å .however, Cr is involved for steel material and Mo,Ag for applications that require deeper penetration.
2) the primary optics which collimate and limit the size and angular spread of the X-ray beam before it reaches the sample for analysis
3) the sample stage which holds the material for analysis and offers rotation and translation options
4) the secondary optics which collimate and limit the size and angular distribution of the diffracted X-ray beam
5) Detector which has a specific sensitivity and resolution to the specific wavelength/energy that is utilised in the experiment[56]

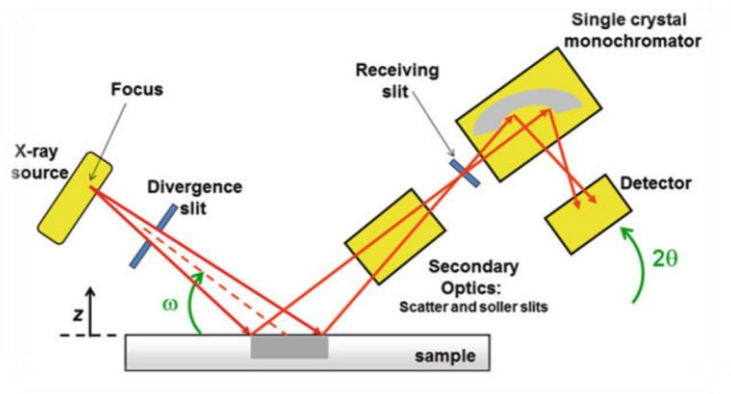

Figure III.22: ***Diagram of XRD setup*****[56].**

III.5.3.3.Applications of (XRD):

Simplicity of this technique bring out the identification of the crystalline structure including unit cell parameters, each crystalline phase has a unique finger print which is presented in diffractogramme due to the positions of peaks that depend strongly on the atoms arrangement in crystal ,the difficulty of peaks identification refer to the presence of different phases in a sample.

Our thin films were elaborated in the synthesis and catalyze laboratory in the university ibn khaldoun tiaret by the use of difffractocrame Rigaku MINIFLEX 600 WITH RADIATION (Cu$-k_\alpha$) with wave length used is λ=1.5418 Å shown in figure III.23:

Figure III.23: ***XRD instrument (Rigaku MINIFLEX 600).***

III.5.4.Profilometry:

A profilometer or surface profilometer is a metrology instrument for topographical characterization of a product's uppermost layers. It is a simple techniques allow to obtain the thickness (d) of the layers up to the nanometer (nm) scale their assembly is simple it based of a metallic cylinder whose end is formed of a cone or a pyramid in diamond, the sample oscillates according to the topology of the layer and the diamond point which always remains in contact with the surface of the substrate therefore the height of the step represents the thickness of thin layer as it shown in the following figure III.24.

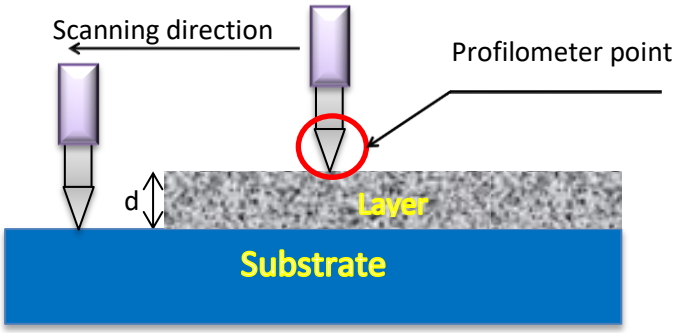

Figure III.24: ***Profilometer process.***

CHAPTER IV

RESULTS & DISCUSSION

This chapter was divided into two parts the computational modelling and laboratory synthesis to allow a clear comparison between the predicated and observed out comes in order to enhance the knowledge on their structural and electronic properties.

The first section presented on the results from density functional theory (DFT) with special attention to the band structure and density of state (DOS) of our structures. This method is important to get initial understanding of its electronic behaviour and stability for further experimental validation.

The second section gives out the results of laboratory work such as the X-Ray Diffraction (XRD), Ultra violet-Visible Spectroscopy (UV-VIS), Infrared radiation spectroscopy (FTIR) and profilometry. These approaches validate the phase composition, bonding properties and optical characteristics of the synthesis material as it was discussed in details in the previous chapter, revealing a notable deviation from expected cobalt sulphides phases, where this process yielded a hexagonal phase of Co_9S_8.

IV.1 Calculation methods and details:

Cobalt Sulfide has received a very special interest due to several properties that are well adapted for applications in energy storage, which is a topic of current scientific interest.

Our main objective is to deepen our understanding of structural properties, such as lattice parameter, compressibility modulus and its derivative, as well as electronic properties, including band structure of TMS cobalt sulfide compound using the pseudopotential method which is implemented in the Quantum ESPRESSO code [30], based on density functional theory (DFT) [21].The exchange and correlation energy is parameterized by the generalized gradient approximation (GGA) proposed by Perdew-Burke-Ernzerhof [31]. Electronic wave functions are expanded in a pseudo wave basis set with the kinetic energy cutoff of 70 eV. The denser k-points were adopted for integration in the Brillouin zone. The convergence criterion of energy was set as 10^{-5}Ry . The maximum number of fully self-consistent field iteration steps is set to 200.

IV.2 Structural properties:

In order to determine the structural properties at static equilibrium (such as lattice parameter a_0, compressibility modulus B and its derivative with respect to pressure B'), we performed a self-consistent calculation of the total energy for several lattice parameters *a,b,c* and then deduced these values using the Murnaghan equation of state [32] given by the following relation:

$$E(V)=E_0+\frac{B}{B'(B'-1)}\left[V\left(\frac{V_0}{V}\right)^{B'}-1\right]+\frac{B}{B'}(V-V_0) \quad \text{.....IV.1}$$

Where

E_0: Total energy.

B: Modulus of compressibility.

V_0: Equilibrium volume.

The modulus of compressibility is determined at the minimum of the E (V) curve by the relation:

$$B=V\frac{\partial^2 E}{\partial V^2} \quad \text{..... (IV.2)}$$

And in terms of its derivative with respect to pressure at constant temperature:

$$B'=\left(\frac{\partial B}{\partial P}\right)_T \quad \text{..... (IV.3)}$$

The minimum of the total energy E_{tot} as a function of volume gives the equilibrium lattice parameter a_0 . Figure IV .25 depicts the variation of total energy as a function of volume in various phases of cobalt sulfide. In addition, Table IV.10 show the structural variables at static equilibrium, including the lattice parameter (a_0), the modulus of compressibility (B), and its derivative (B'), as determined using the GGA-PBEsol approximation.

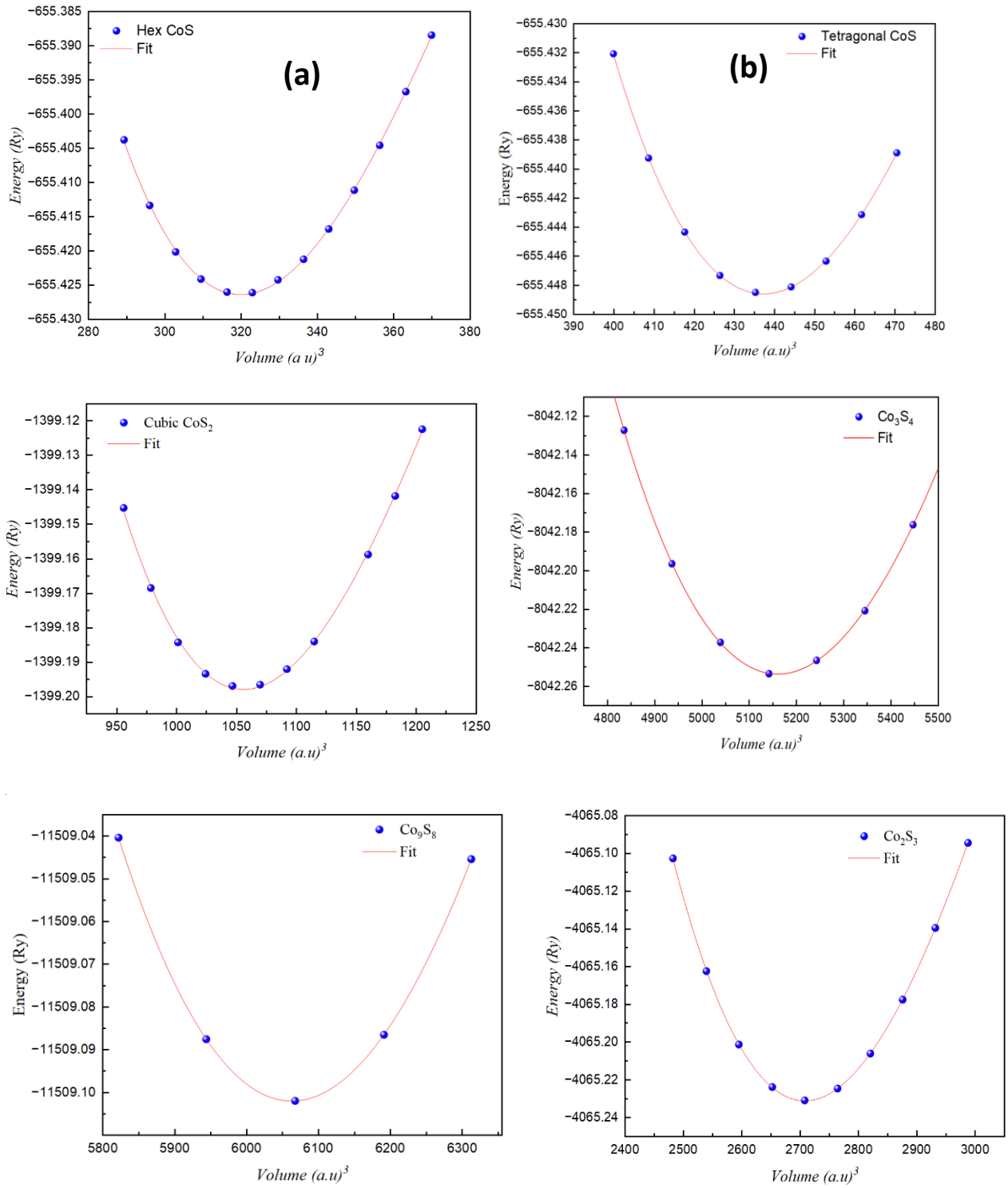

Figure IV.25: ***Variation of the total energy as a function of the unit-cell volume of various phases of cobalt sulfide***

Table IV.10: ***Lattice parameters a,b,c(Å), compressibility modulus B(GPa) and its derivative Bp .***

phases	Lattice parameters(Å)			E_{min} (Ry)	V0 Ang^3	B(GPa)	Bp
	A	b	C				
Co_2S_3	5.5969	5.5969	14.7903	-4065.23	401.24	167.945	4.9806
CoS_2	5.3869	5.3869	5//.3869	-1399.2	156.33	133.947	5.0729
Cos hex	3.3055	3.3055	5.0038	-655.426	47.36	183.453	5.3892
CoS tetra	3.5582	3.5582	5.1188	-655.4486	64.81	128.568	4.2647
Co_3S_4	9.1447	9.1447	9.1447	-8042.25	764.73	158.915	4.8721
Co_9S_8 cub	9.6474	9.6474	9.6474	-2877.2622	224.48	175.78	4.7142

Table follow IV.11 present comparison of our results of the lattice parameters for CoS, CoS_2, Co_2S_3, Co_3S_4, Co_9S_8, highlighting both simulation and experiment results of this study and other previous research offering valuable contribution into material investigation. Most of simulation values are closely align with previous study including CoS, CoS_2, Co_3S_4, Co_9S_8 cubic structure but there few difference compared with previous simulation results of Cobalt pentlandite (Co_9S_8) and Lineallite (Co_3S_4) , furthermore the new finding of provide a crucial insight into its structural properties.

Table IV.11: ***Comparison between the results of our work with the previous study.***

	Lattice parameters(Å)												
	This work						Previous works						
	Simulation			Experimental			Simulation			Experimental			
phases	a	b	C	a	b	C	a	b	c	a	b	C	Ref
CoS hex	3.3055	3.3055	5.0038				3.347	3.347	5.139	3.371	3.371	5.1809	[57][58]
CoS tetra	3.5582	3.5582	5.1188				3.53	3.53	4.8	-	-	-	[59]
CoS_2	5.3869	5.3869	5.3869				5.506 5.515	5.506 5.515	5.506 5.515	5.5376	5.5376	5.5376	[57][60],[61]
Co_3S_4	9.1447	9.1447	9.1447		/		6.573	6.573	6.573	9.437	9.437	9.437	[57] [18]
Co_2S_3	5.5969	5.5969	14.7903				-	-	-	-	-	-	-
Co_9S_8 hex	-	-					-	-	-	3.183	3.183	4.652	[62]
Co_9S_8 cub	9.6474	9.6474	9.6474				6.933	6.933	6.933	9.4	9.4	9.4	[57][22]

High stable structure was defined by the structure with low energy, figure IV.26 show the variation of total energy versus volume for cobalt monosulfide structures, we deduce that hexagonal CoS is less stable than the tetragonal structure open the door for more experiment investigations.

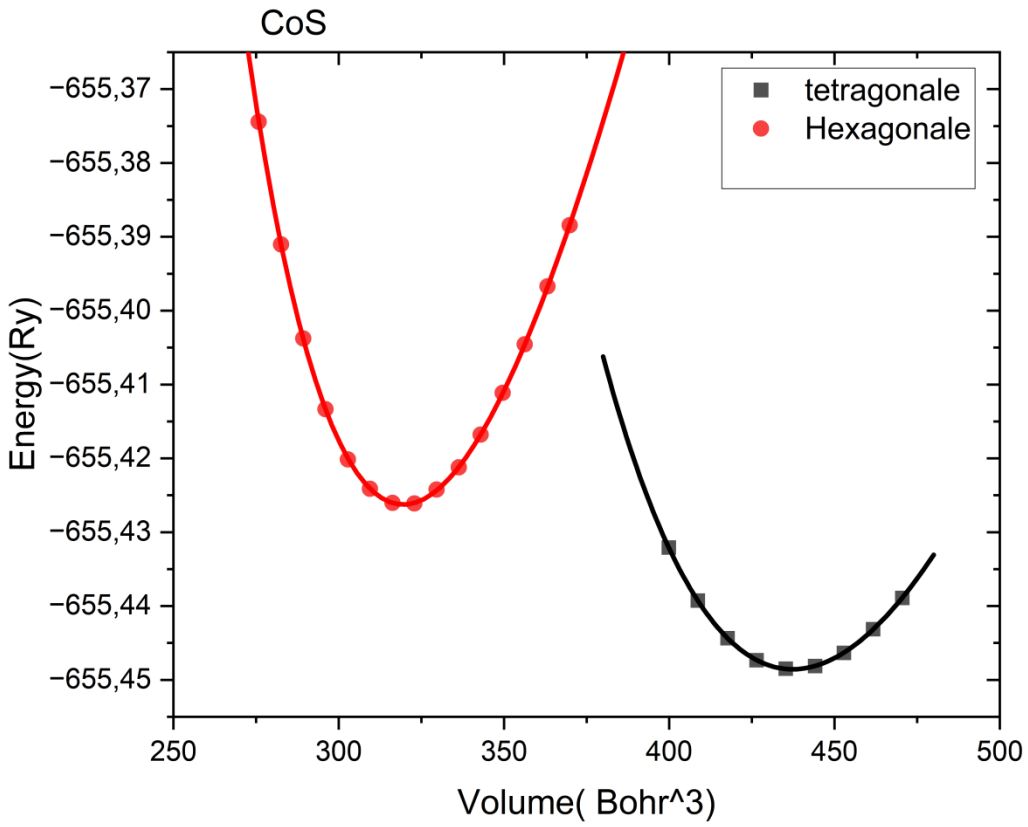

Figure IV.26: ***Energy versus volume of CoS both structure.***

IV.3 Electronic properties:

The concept of energy bands plays an essential role in solid physics, providing critical information about electron levels in ideal structures and the nature of liaison formed between the different compounds. However, electrons can only assume specified energy values which describe by using band theory that include bands separated by banned bands which represented in reciprocal space and to simplify it we use the high symmetry lines of the first Brillouin zone.the electon configuration of the atoms in various components are as follows: Co: [Ar] $4s^2$ $3d^7$ and S: [Ne] $3s^2$ $3p^4$.

IV.3.1 Structure of bands energy:

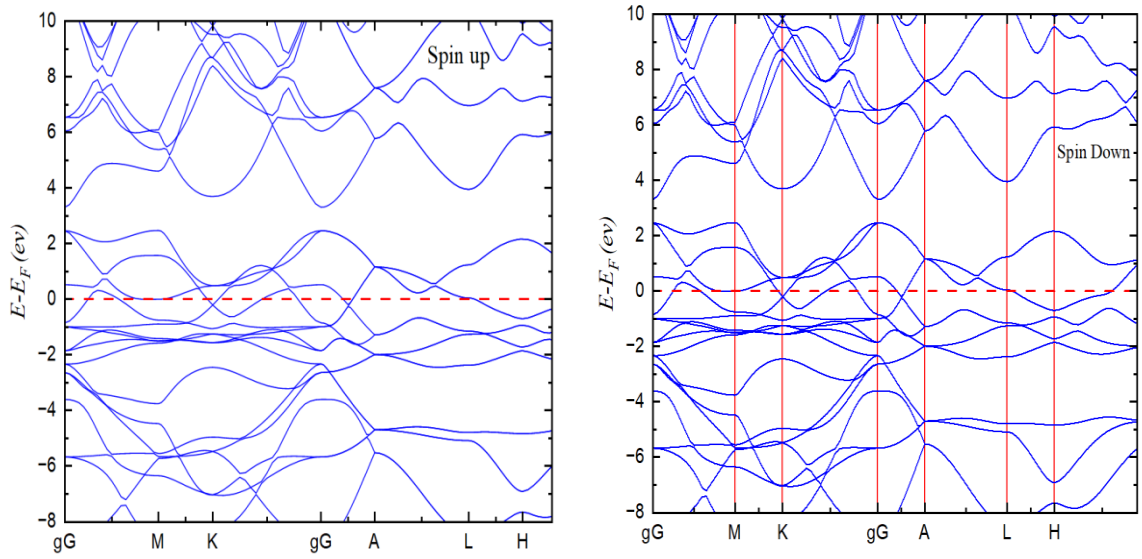

Figure IV.27: Band structure of hexagonal CoS

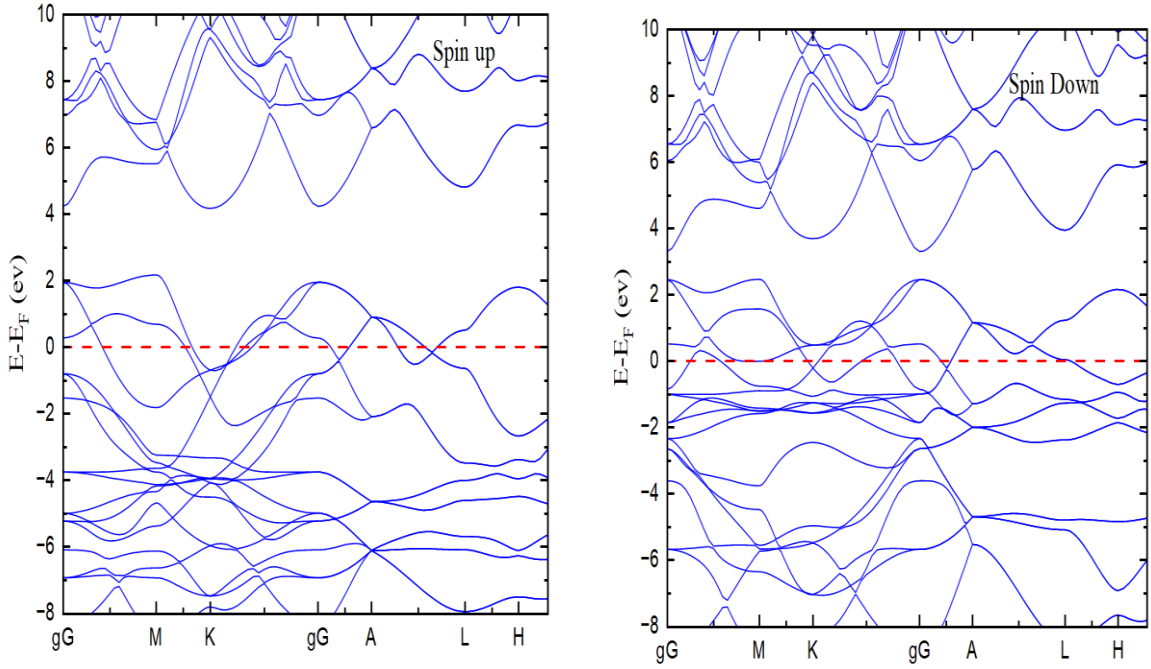

Figure IV.28: Band structure of hexagonal CoS, calculated using GGA+U

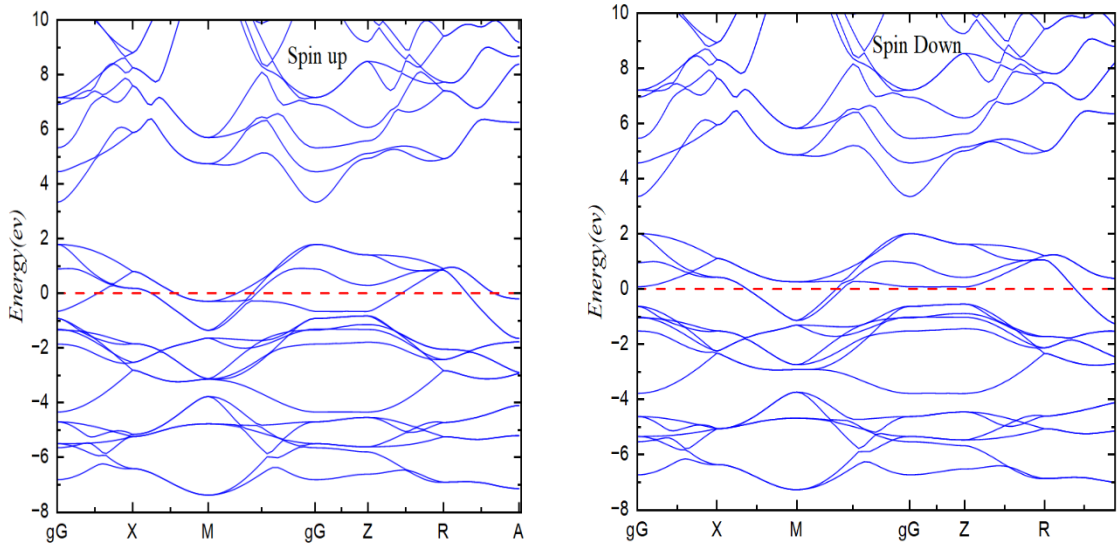

Figure IV.29: Band structure of tetragonal CoS

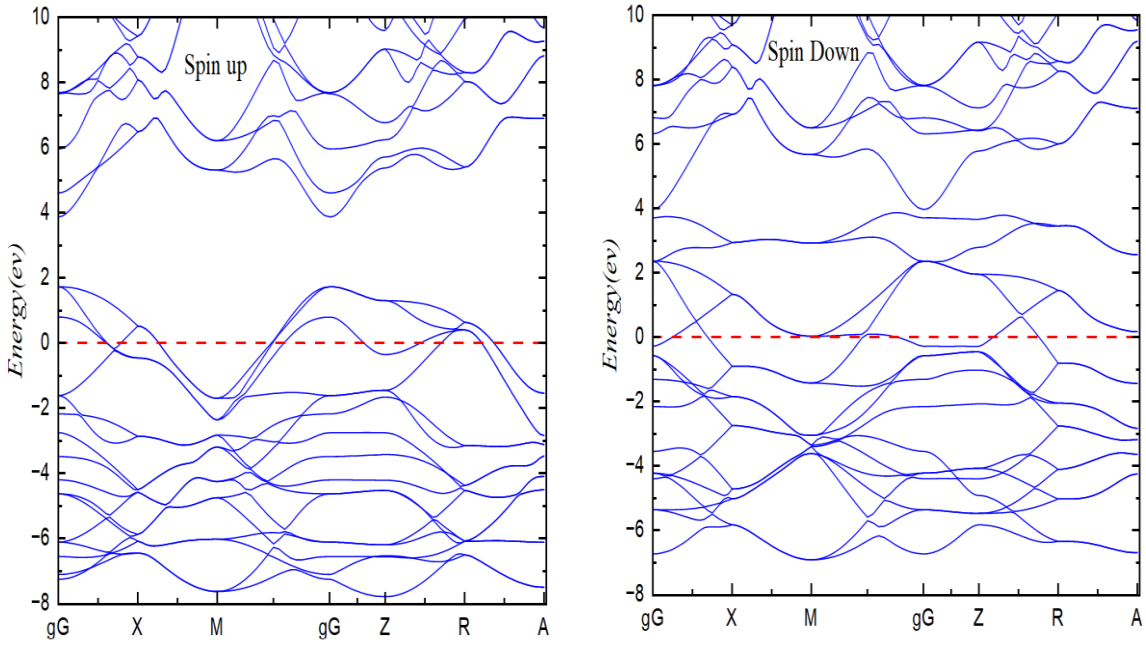

Figure IV.30: Band structure of tetragonal CoS, calculated using GGA+U

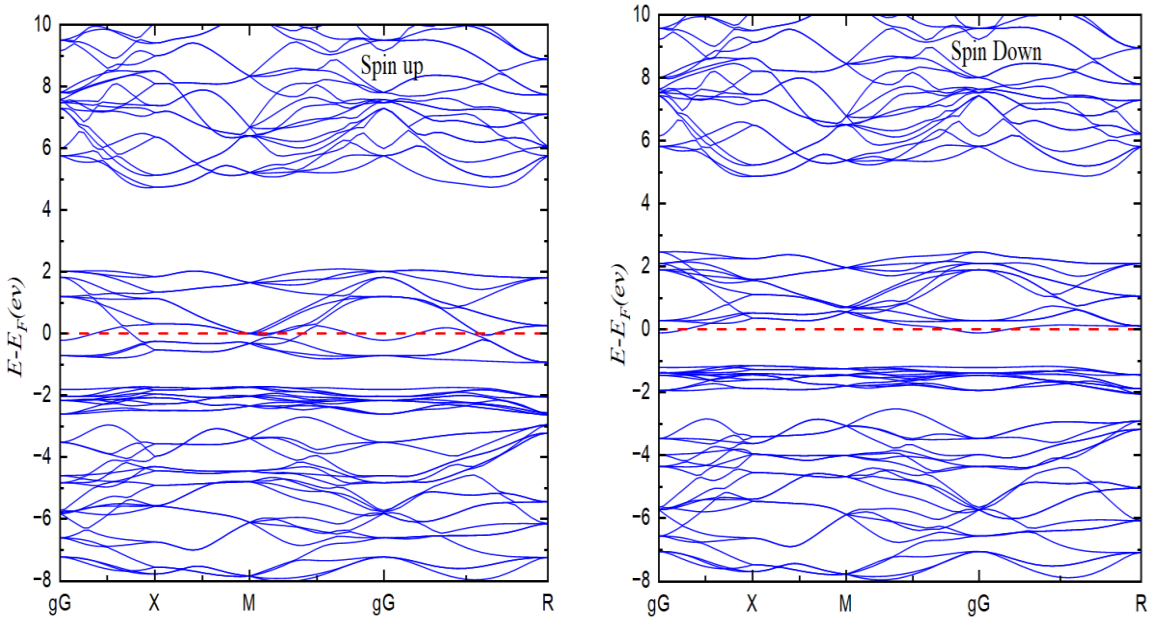

Figure IV.31: Band structure of cubic CoS_2

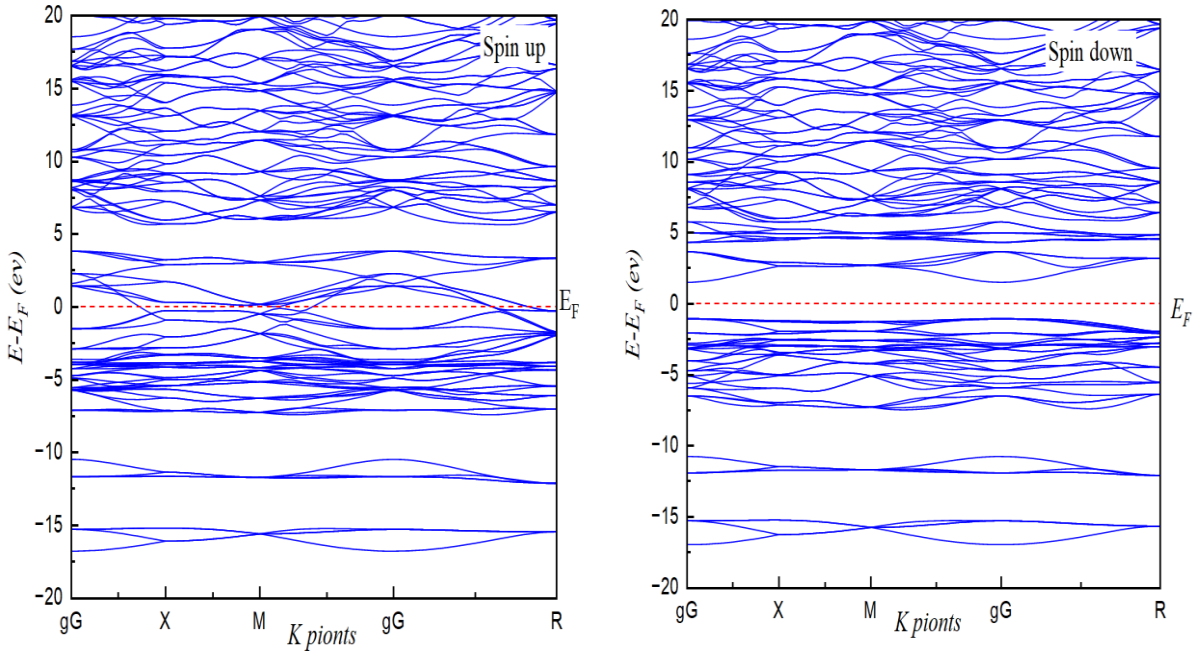

Figure IV.32: Band structure of cubic CoS_2 , calculated using GGA+U

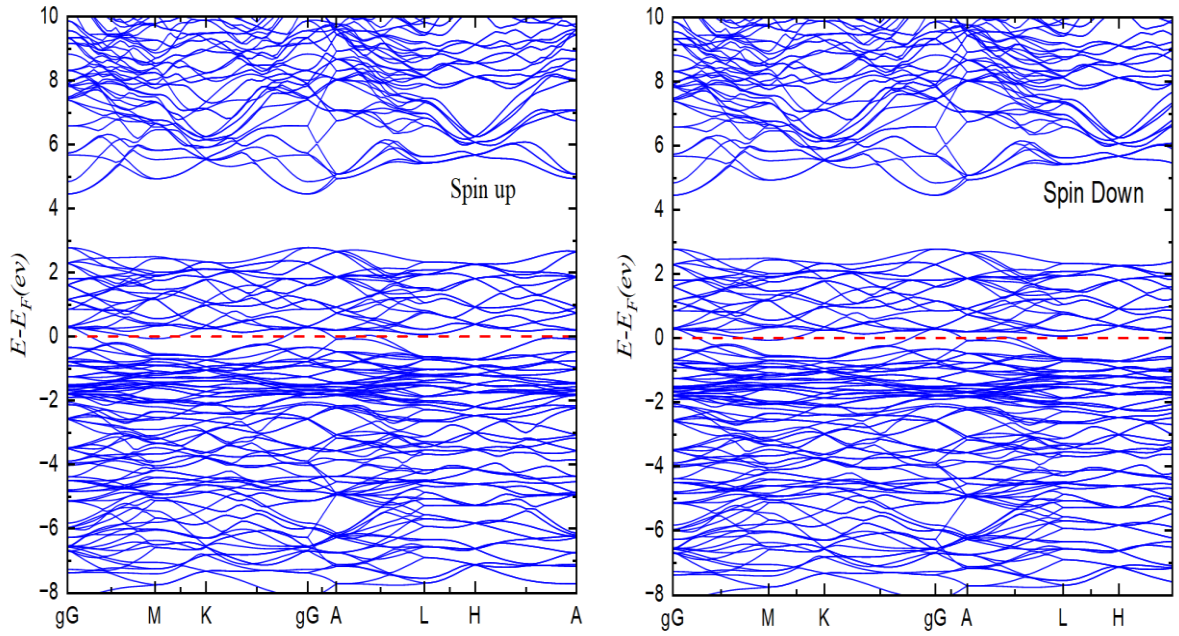

Figure IV.33: Band structure of tetragonal Co_2S_3

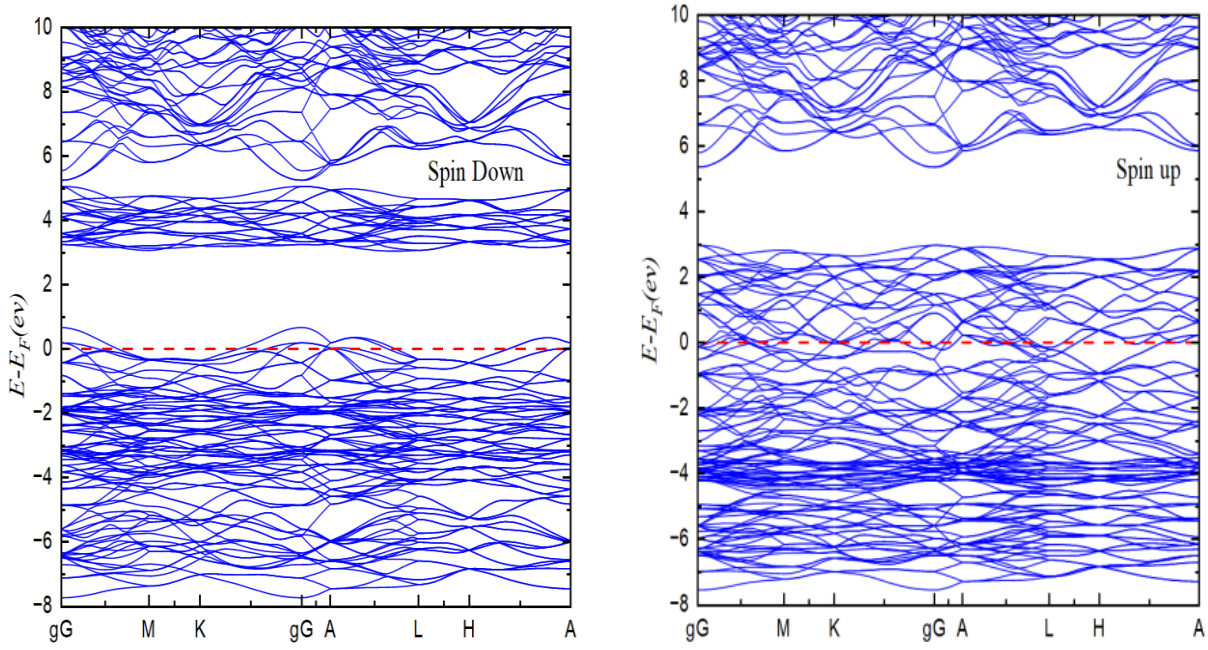

Figure IV.34: Band structure of tetragonal Co_2S_3, calculated using GGA+U

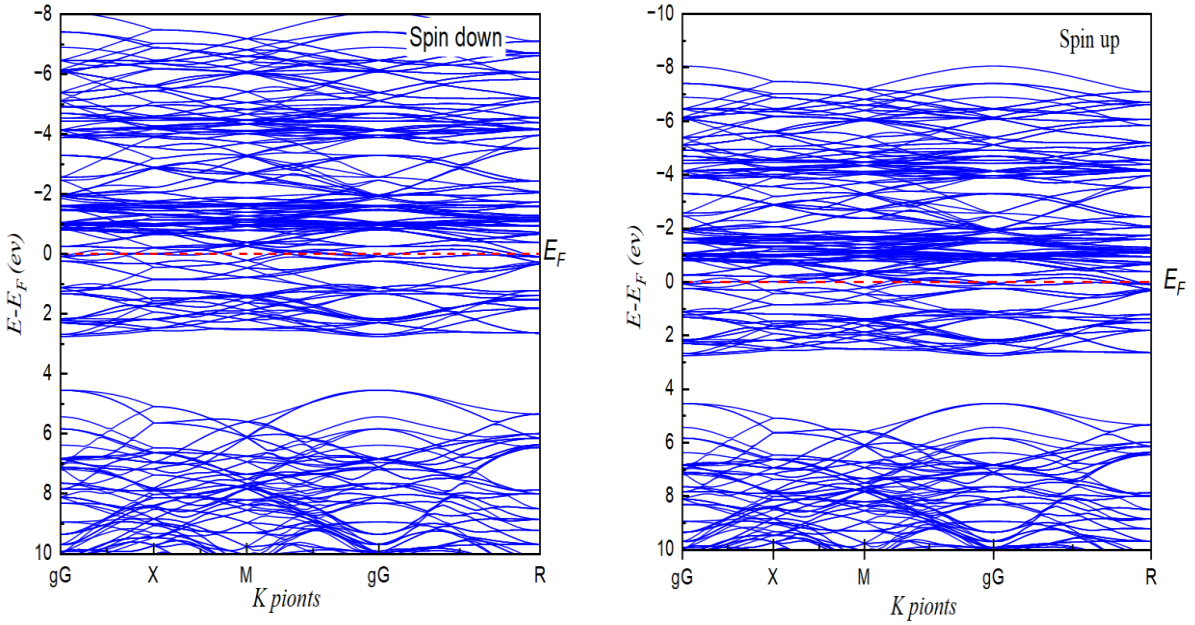

Figure IV.35: Band structure of spinel Co_3S_4

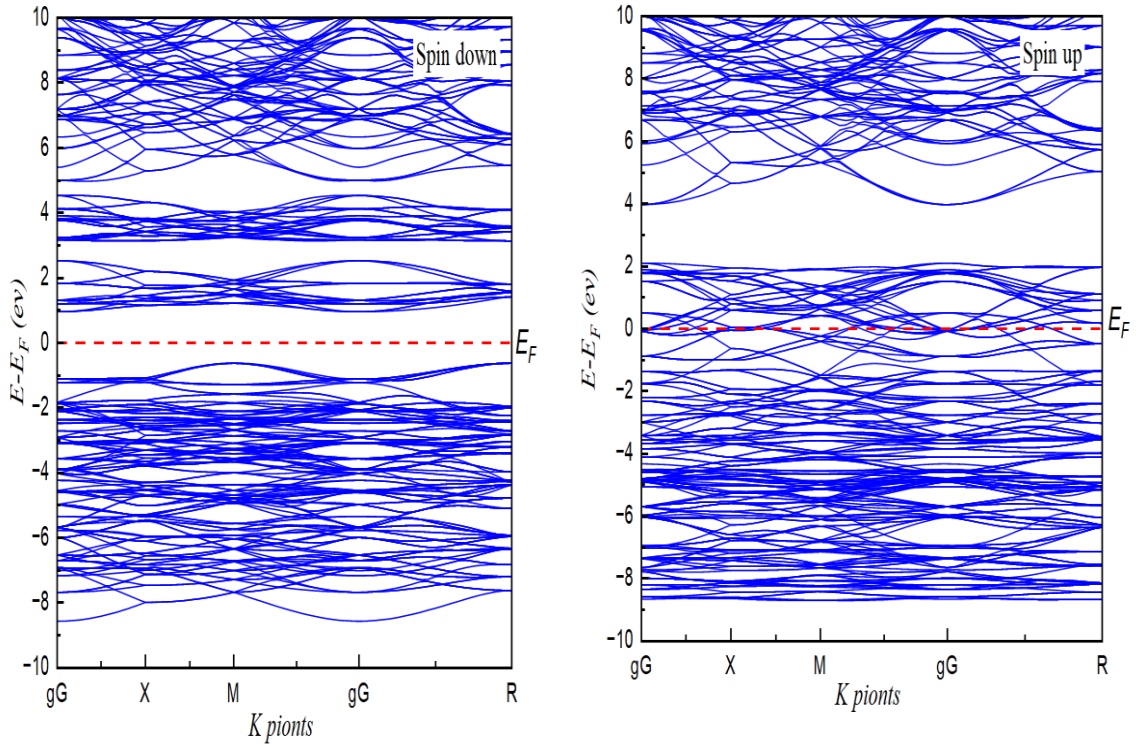

Figure IV.36: Band structure of spinel Co_3S_4, calculated using GGA+U

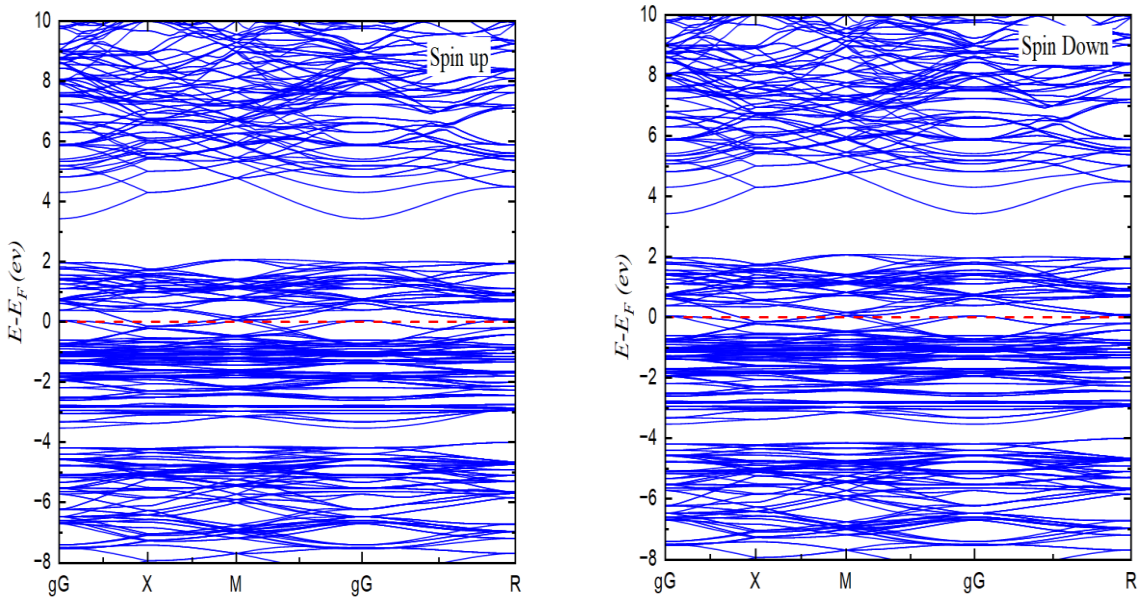

Figure IV.37: Band structure of cubic Co_9S_8

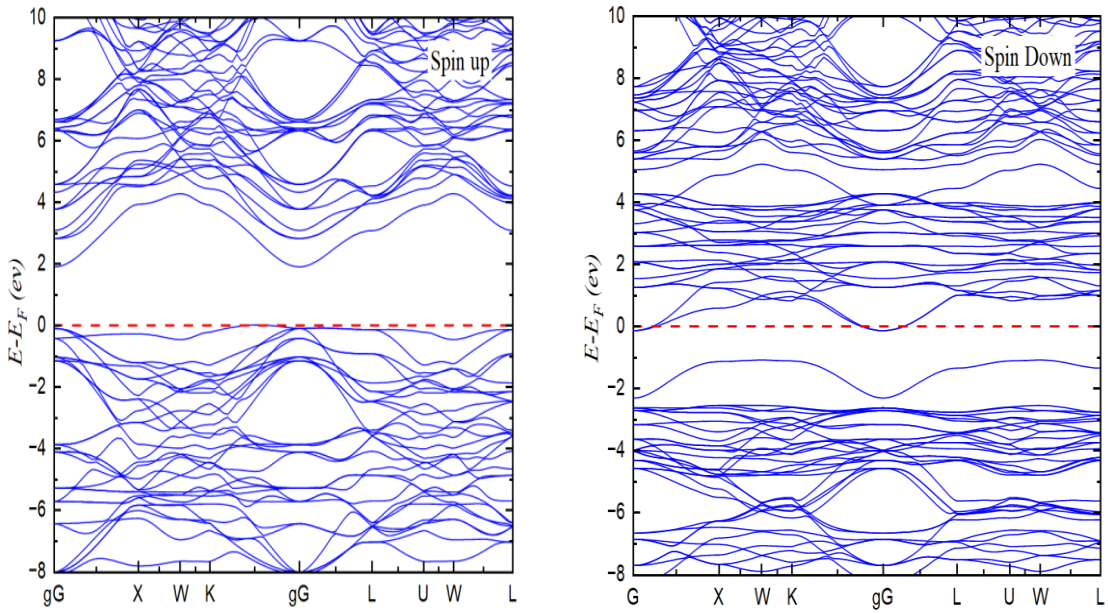

Figure IV.38: Band structure of cubic Co_9S_8 , calculated using GGA+U

The structural topology of spin-up and spin-down bands was calculated using two approximations GGA-PBEsol and GGA-PBEsol+U, the results are presented in the figures

VI-27 to VI-38 , It is clear that the majority of phases have a metallic behaviour due to the overlap of the Valence and Conduction bands.

In other hand CoS , CoS_2, Co_3S_4 and Cobalt pentlandite (Co_9S_8) show direct and indirect transitions describe its half metal behavior using GGA+U. Regarding direct gap for all structures are typically occurring at Γ point (gG) ,while in direct transitions spanned between several K points such as CoS ($\Gamma^V - M^C$) , Co_3S_4($R^V - \Gamma^C$), Co_9S_8 ($K^V - \Gamma^C$);in contrast CoS_2 display only direct gap as it shown in table IV.3.This classification as a semi-metal indicates that the compound has both metallic and semi-conductive properties. In a semi-metallic structure, the conduction and valence bands slightly overlap, allowing certain electrons to circulate freely, as in a metal, while retaining semiconductor-specific electronic properties.

Table IV.12: *Nature of gap for Hex CoS, CoS_2, Co_3S_4 and Co_9S_8*

Phases	Band type	K-path	This work(ev)
CoS	Direct	$\boldsymbol{\Gamma^V - \Gamma^C}$	3.3903
	Indirect	$\boldsymbol{\Gamma^V} - M^C$	3.3867
CoS_2	Direct	$\boldsymbol{\Gamma^V - \Gamma^C}$	2.5551
Co_3S_4	Direct	$\boldsymbol{\Gamma^V - \Gamma^C}$	1.8362
	Indirect	$R^V - \boldsymbol{\Gamma^C}$	1.5825
Co_9S_8	Direct	$\boldsymbol{\Gamma^V - \Gamma^C}$	1.9968
	Indirect	$\mathbf{K^V - \Gamma^C}$	1.8905

IV.4.1. Density of state:

Density of states (DOS) is one of the most important concept for understanding physical properties of materials, because it provides a simple way to characterize complex electronic structures, It also enables us to determine the occupancy rate of each atomic state, which gives us insight into the nature of the chemical bonds in a material and, in turn, the charge transfer between atoms. The density of states can be broken down into a partial local DOS using the DFT approach, as shown by:

$$g(E) = g^{out}(E) + \sum_{l,t} g_l^t(E) \quad \text{.....(IV.4)}$$

Where:

$g_l^t(E)$: is the state number (electron) including spin by Ry and the unit cell at energy E, which resides in the sphere, characterized by harmonics with the azimuthal quantum number.

$g^{out}(E)$: is the number of states (electrons) in the interstitial area, including spin by Ryd and unit cell at energy E.[63]

We began by examine project density of state pdos , where we could bring out that Co-3d has a hugh contribution in the electronic state near Fermi level while a minor contribution of S-2p. we noted that under Fermi level the contribution of Co atoms are higher than S atoms states for all phases. However, when the energy was increased more than E_F the contribution of cobalt minimise and be approximately as the same contribution of sulphur for most structure through figure IV.39.than we moved to analysis total density of state effect on the magnetic feature of numerous phases, the only phase that show a magnetic behaviour was CoS_2.

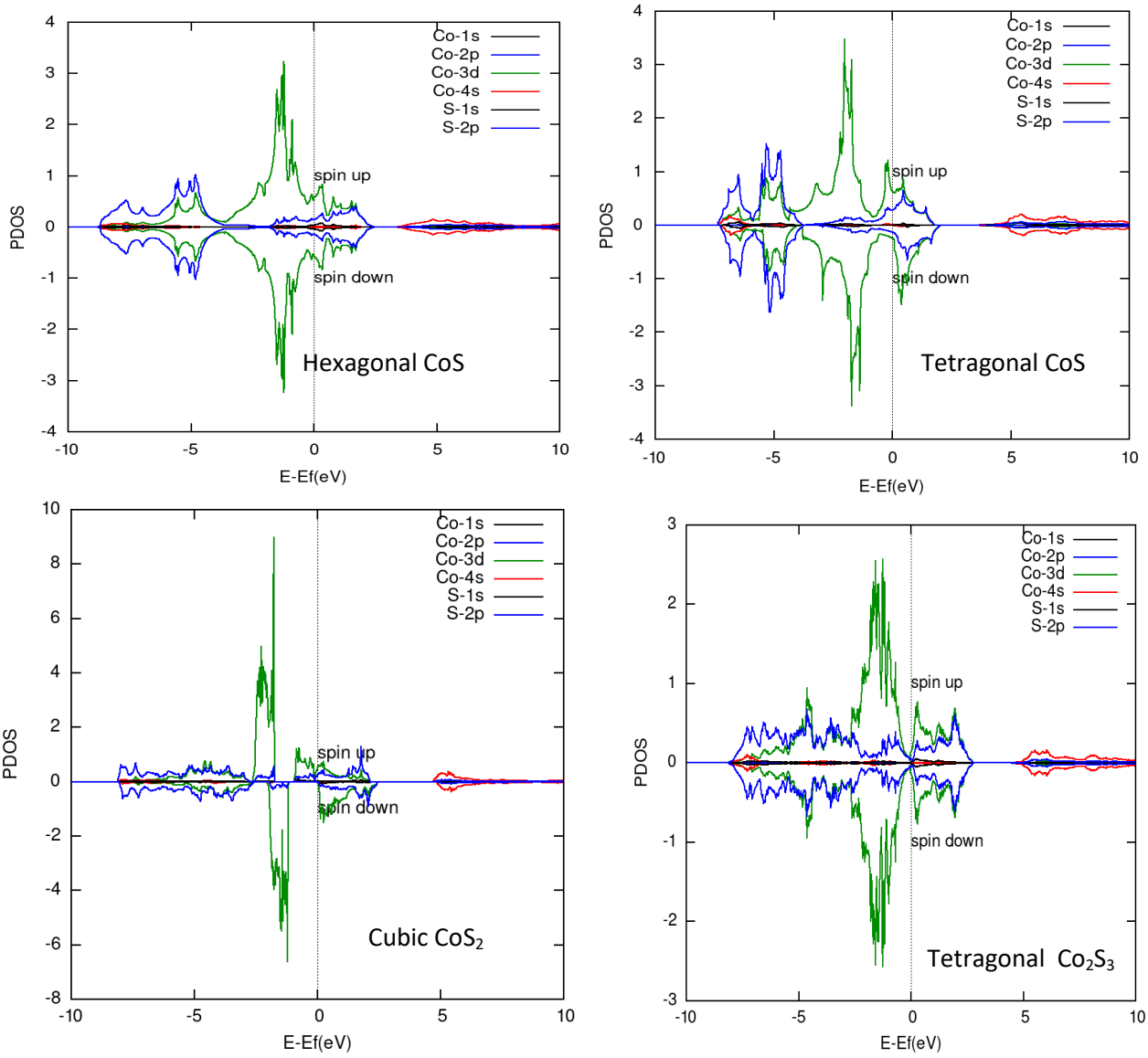

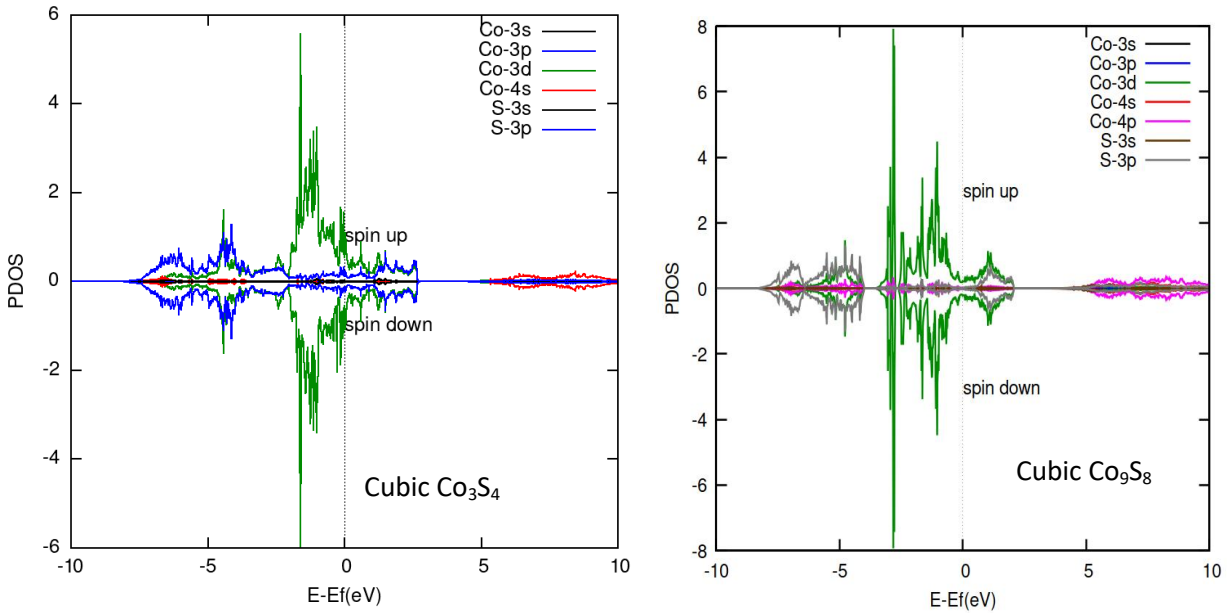

Figure IV.39: ***Partial density of state of cobalt sulfide phases***

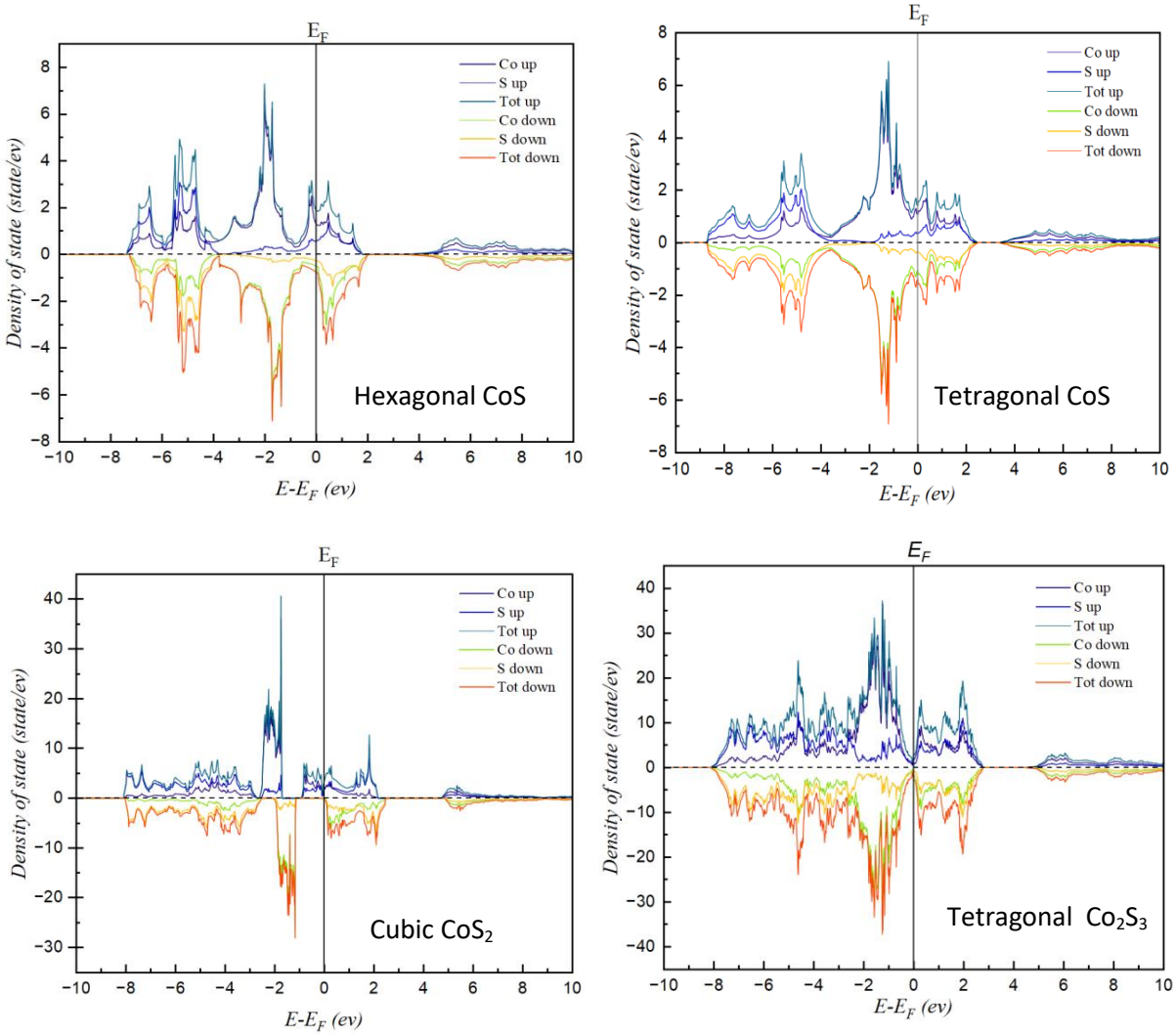

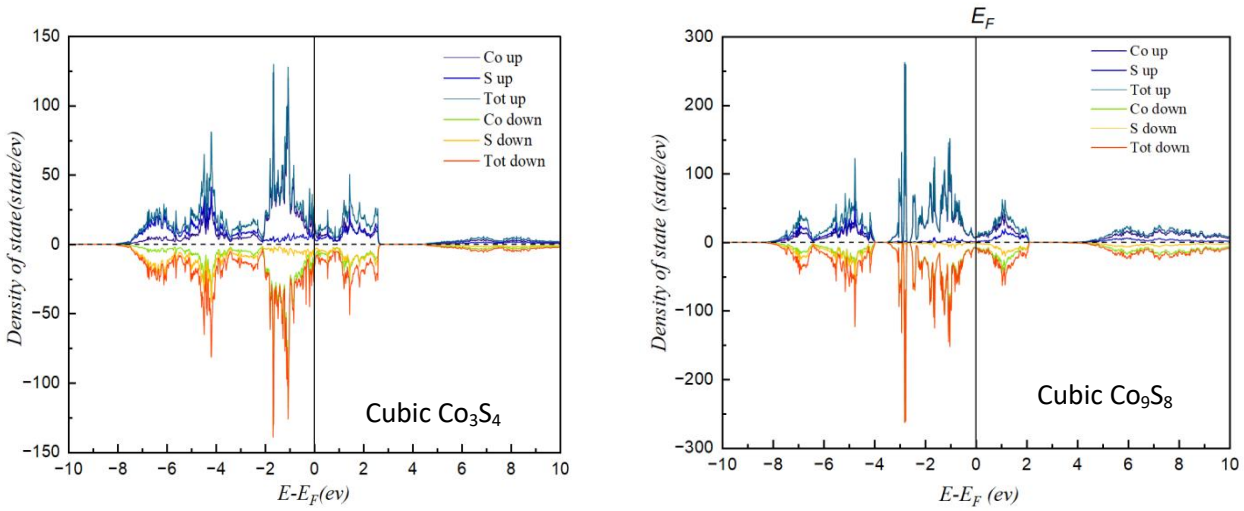

Figure IV.40: *Total density of state plots of cobalt sulfide phases*

IV.2.Expiremental part

IV.2.1.X Ray diffraction (XRD):

The identification of the crystalline phases of cobalt sulfide was compared based on the JCPDS files and the software MATCH. The XRD results shown in figure IV-41 of cobalt sulfide annealing at 500 c for 4 hours.

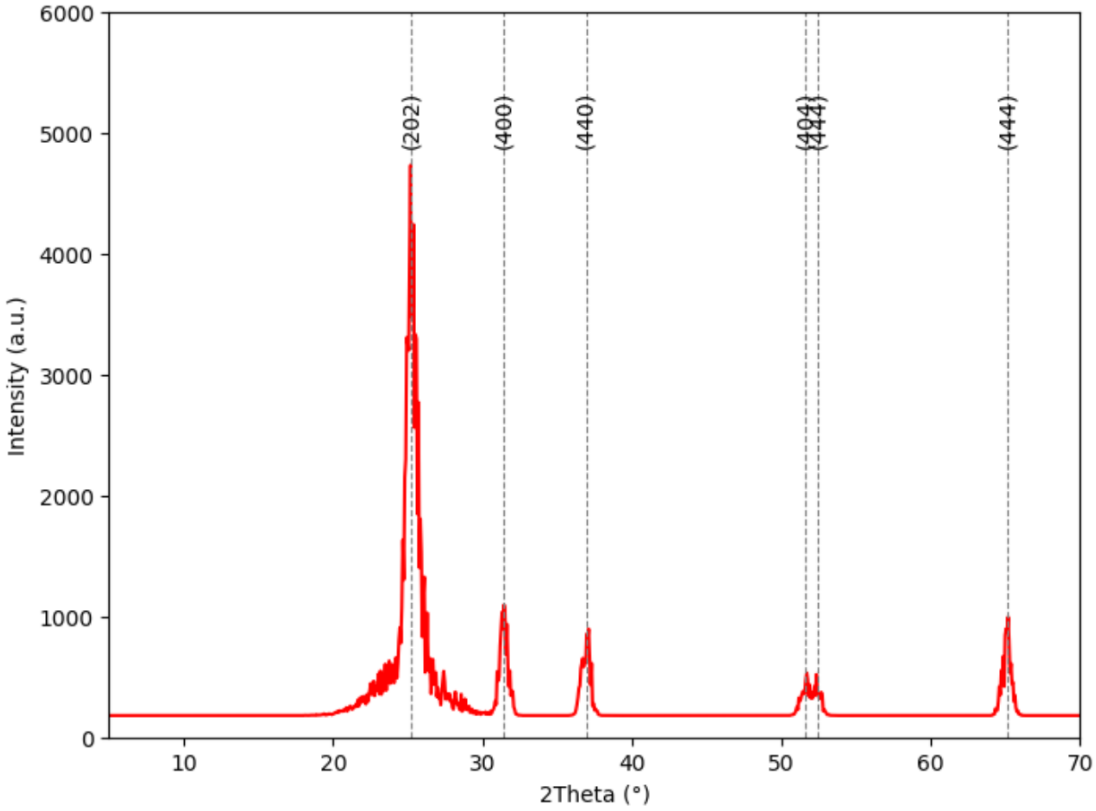

Figure IV.41: *Diffractogramme (DRX) of Co_9S_8*

Calculating grain size is done using the Scherer relation:

$$D = \frac{0.9\lambda}{BCos(\theta)} \quad \text{.....(IV.5)}$$

Where:

λ: The incident wave length (**λ** CuKα = 1.5418 Å)

B: The size of the diffraction peak at the mid height (FWHM) in radian (rd)

θ: The diffraction angle.

Determination of grain size of our material was through these steps:

$$2\theta = 25.59° \longrightarrow \theta = 12.795°$$

With the FWHM in degree is : B=0.3610° =0.0063 rd

$$D = \frac{0.9 \times 0.15418}{0.0063 \times Cos(12.795)} = 22.47\ nm$$

Table IV.13: *Reflection angles with the (hkl) of hexagonal cobalt sulfide Co_9S_8*

$2\theta(^\circ)$	25.59	31.42	36.9	51.61	52.5	65.09
d_{hkl} (nm)	0.348	0.285	0.244	0.177	0.174	0.143
(hkl)	202	400	440	404	444	444

The characteristic peaks are visible in the sample. The Bragg reflections' angles served with the (hkl) mailer index are mentioned in table IV.13 In addition we calculated the d_{hkl} through Bragg low and the lattice parameters was bring out through the following formula

$$\frac{1}{d^2{}_{hkl}} = \frac{1}{\frac{4}{3}\left(\frac{h^2+hk+k^2}{a^2}\right)+\frac{l^2}{c^2}}$$

Using peaks at (202) and (404) it gives us a=b= 0.318 nm and c=0.465 nm

It exist references reported a cubic structure with the following lattice parameter a≈ 0.94 *nm* [22][65][66].However, for the hexagonal structure was mentioned in the following references [62], [64], [65] but they did not turn on its lattice parameters only one studied that agree with our results a=b=0.3183 nm and c=0.4652 nm.interstignly, it existed some studied used identical JCPDS card number corresponds to the cubic structure; for this reasons a direct comparison with the hexagonal structure could not be conducted.

IV.2.2.Profilometry measurements:

The thickness measurements were carried out in the Oran laboratory using the DIKTAK machine and summarized in table IV.14.

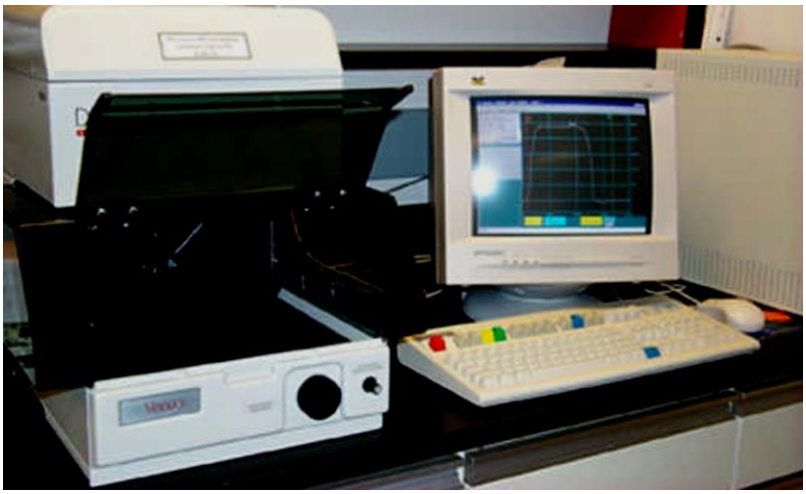

Figure IV.42: DEKTAK profilometry instrument.

Table IV.14: Thickness of different thin films

a) Deposition duration effect on thin films thickness

Samples condition	Thickness (nm)
30 min	237.3
45 min	229.6
60 min	254

b) annealing duration effect on thin films thickness

Samples condition	Thickness (nm)
30 min	245.2
1h	308.7
2h	374.8
4h	294.8

IV.2.3.Fourier Transform Infrared Spectroscopy (FTIR):

FTIR spectrum display the absorption peaks in function with the wave number of cobalt sulfide thin films. A homogenous phase is suggested by the absence of features typical of other phases as it shown in following figureIV.43.

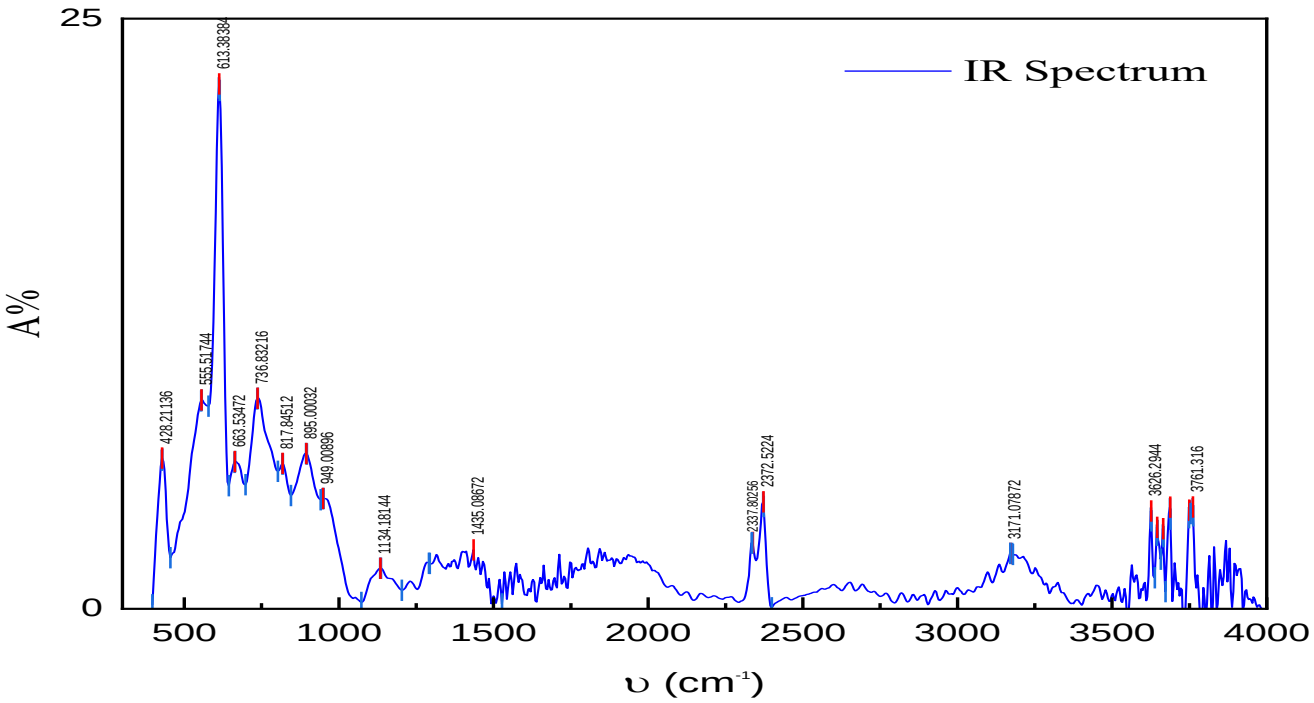

Figure IV.43: *FTIR spectrum of Co_9S_8*

Compared to the previous result the peak with high intensity at 613 cm^{-1} represent the lattice vibrations of Co cations in the surface of Co_9S_8, where the peak at 1113 cm^{-1} shows S-O bonding[65].Meanwhile, the existence peaks ranging between 1500-4000 cm^{-1} represent organic components.

IV.2.4. UV-Vis spectroscopy Analysis:

UV-VIS Spectroscopy provide as well an important idea about the optical properties of cobalt sulfide thin films

Optical transmittance spectrum was despite in figure IV.44 below for the different synthesis condition to provide a visual comparison:

a) A variation in the time of deposition ranging from 30 min to 60 min by the scale of 15 min with a fixed time of annealing at 500 ℃ for 30 min.

b) Fixed deposition time (30 min) with the variation in the duration of its annealing ranging from (non-heated to 4 hours).

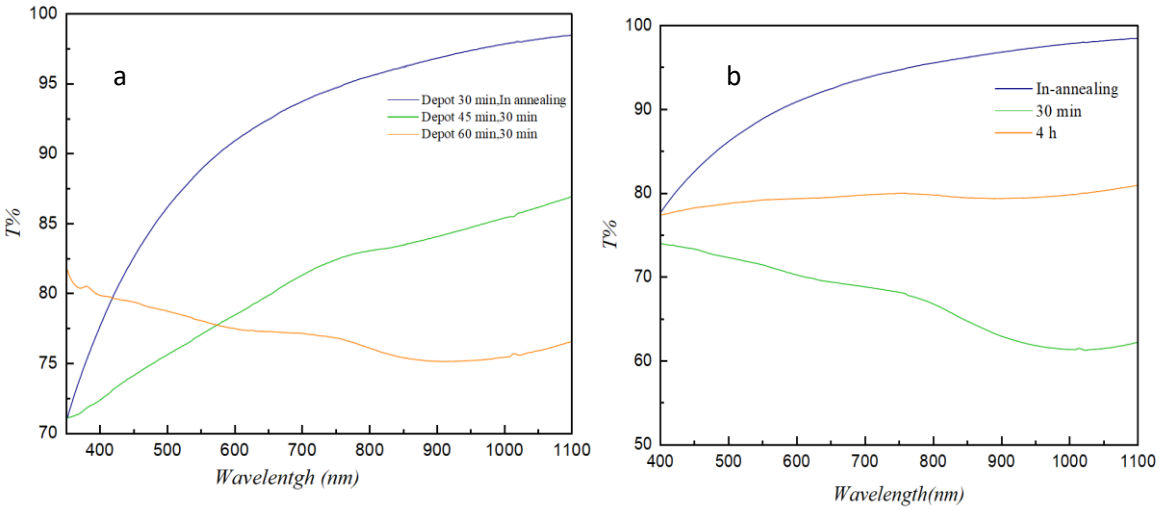

Figure IV.44: *Impact of Annealing and Deposition duration on the Optical Transmittance of Synthesised Films.*

UV-Vis absorption spectra of the synthesised cobalt sulphide phase was recorded and examined in order to find out their optical characteristics. By plotting it using "Tauc plots," the band gap of each phase was determined separately. Enabling the distinction between direct and indirect transitions. To make a comparison evaluation easier, a combined graph with all stages was put together in figure IV.44.

The spectrum of transmittance was shown in figure IV.45 and IV.46 for synthesised phase at specific conditions, and the Tauc method has been employed with the following equation:

$$(\alpha h\nu)^n = A\ (h\nu - Eg) \quad \ldots\ldots\ldots\ldots (IV.6)$$

Where:

- (α) is the absorption coefficient,

- ($h\nu$) is the photon energy,

- (A) is proportionality constant,

- (Eg) is the band gap,

- (n) is 2 for direct transitions and 1/2 for indirect transitions.

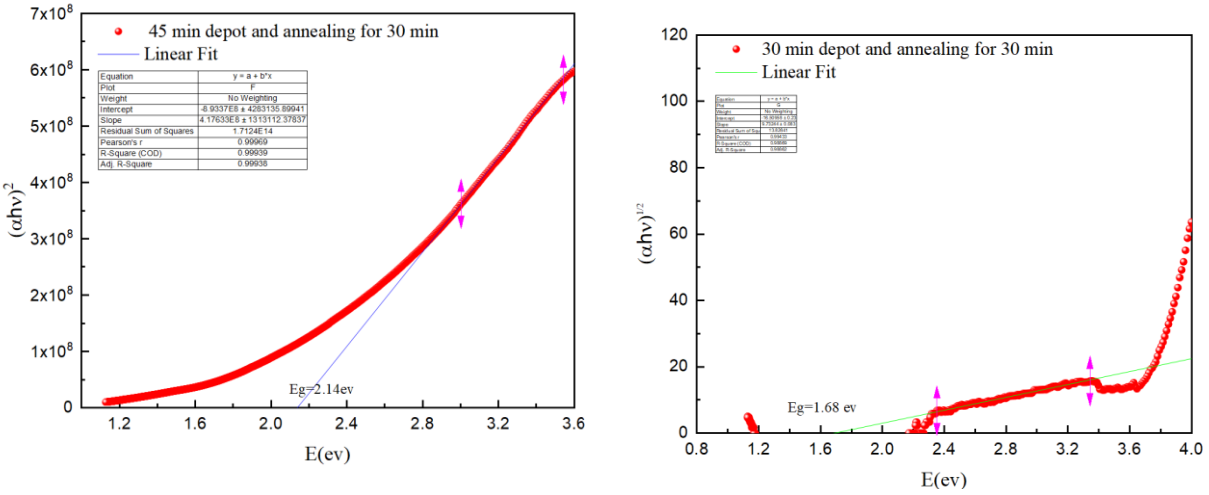

Figure IV.45: *Direct and indirect band gap in variation of deposition duration*

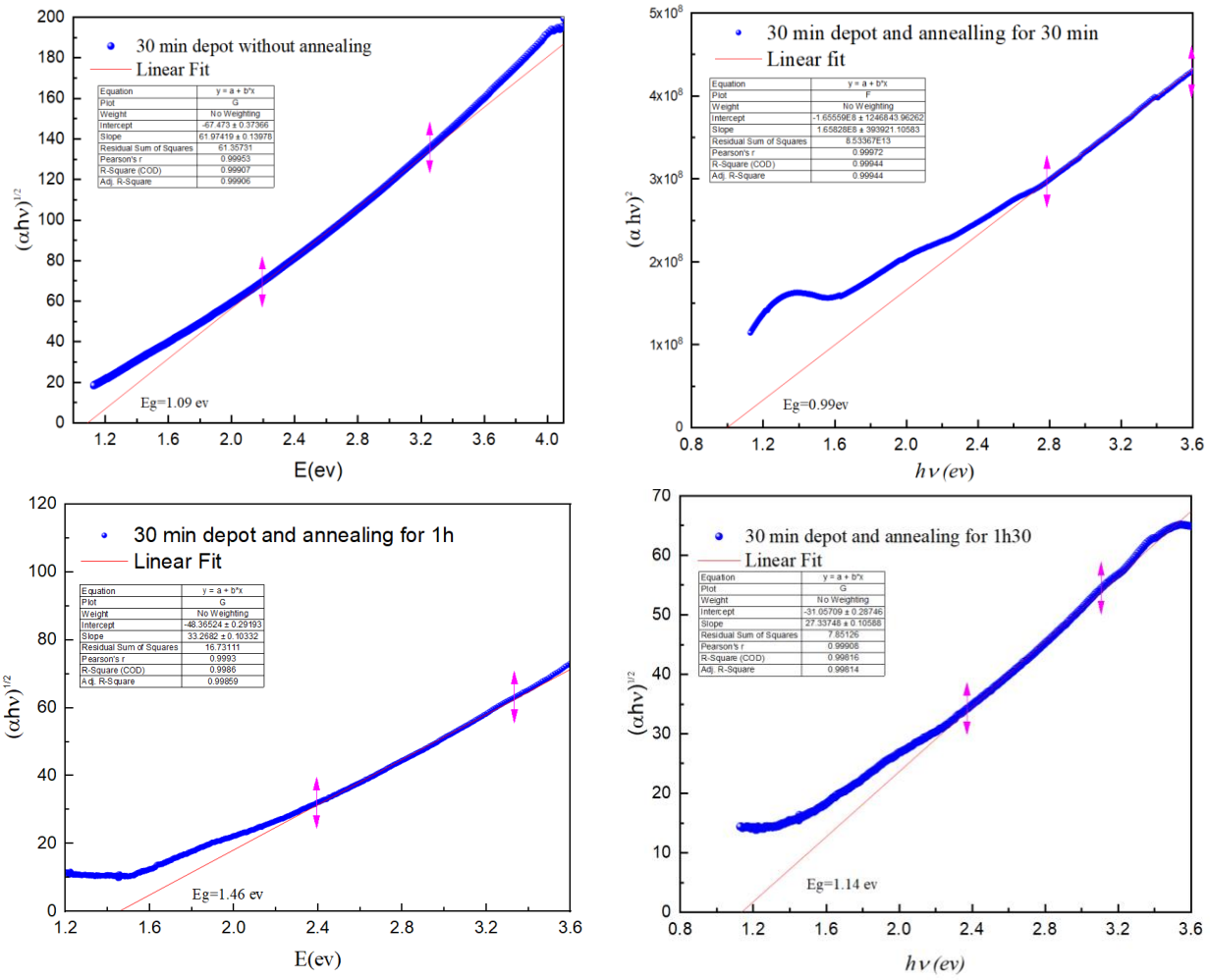

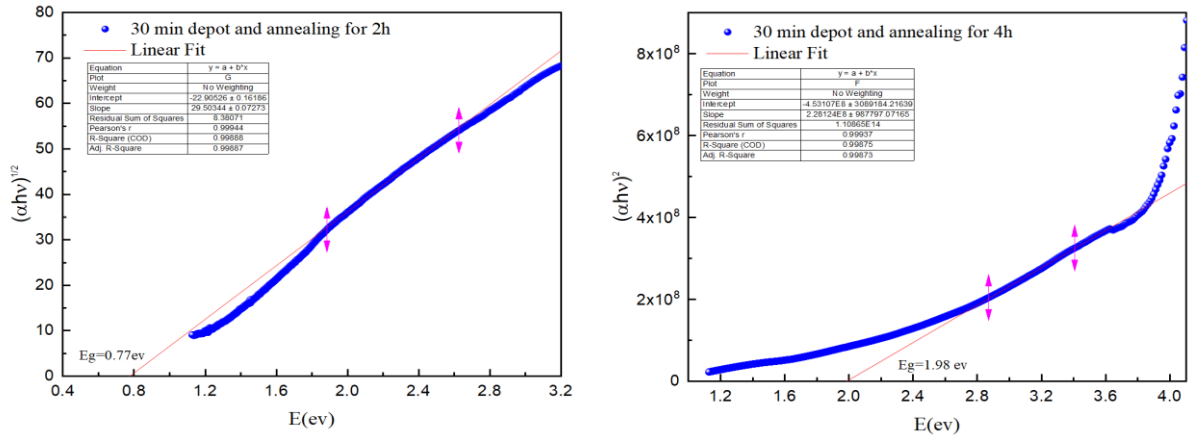

Figure IV.46: *Direct and indirect band gap of variation in annealing duration*

Tauc relation is appropriate for estimating optical band gap. Meanwhile, it is only valid for semiconductors phases. Direct and indirect band gaps shown in figure IV.45-46 were calculated by extrapolating the straight line segment of the Tauc plot, the graphs excluded for versatile condition show high band gap or metallic behavior indicated non stoichiometric phases or poor crystallinity depending on deposition conditions. The findings of this analysis are summarized in table IV.15 indicate that:

Both graphs shows in figure IV.45 bring out the transition from indirect to direct band gap with increased in deposition time suggest phase evolution. For the second condition when thin film was deposited only for 30 min without annealing treatment show indirect gap. However, when we initial annealing for short time 30 min the band gap reduce and shift into direct transition may due to improve in crystallinity also the contrast observed in comparison with gap of previous result at same condition reflect to the effect of film uniformity, phase purity and defect density. Intermediates annealing 1h to 2h reveal indirect gaps, after we extended to 4h Eg increases and restore direct transition could be explain by phase purification.

The refractive index (n) was calculated using Ravindra approximation

$$n = 4.084 - 0.62\,Eg$$

The results of samples turn on that when the band gap narrows, the material become more optically dense, increasing n. In addition, the refractive index adjusts accordingly and This behavior highlights the influence of structural ordering and phase evolution on the films' optical density and electronic polarizability.

Table IV.15: *Table show collectively analysis of the deposition Co_9S_8 at various conditions and its optical behaviour.*

a)The effect of deposition duration on its optical properties

Depot time	Annealing time at 500	Direct gap (eV)	Indirect gap (eV)	n
30	30min	-	2.22	2.7076
45	30min	2.14	-	2.7572

b) The effect of annealing duration on its optical properties

Depot time	Annealing time at 500	Direct gap(eV)	Indirect gap(eV)	n
30 min	0	-	1.09	3.4082
	30 min	0.99	-	3.4702
	1h	-	1.46	3.1788
	1h30	-	1.14	3.3772
	2h	-	0.77	3.6066
	4h	1.98	-	2.8564

CONCLUSION

Conclusion:

This study entailed an exhaustive literature review of cobalt sulfides phases CoS, CoS_2, Co_2S_3,Co_4S_3, Co_3S_4 and Co_9S_8 ,in our study we used the ab initio and experimental technique which provided a new insight into the physical properties of these compounds.

In the first part we investigated the structural , electronic and magnetic properties utilizing the pseudo-potentials plane-wave (PPsPW) methodology within the Quantum ESPRESSO platform. The structure characteristics including the lattice parameter, bulk modulus, and its pressure derivative, exhibit remarkable suitable with previous studies .However ,in electric properties our study is the first that reported the traits of Co_2S_3 which show up a metallic behaviour ,also we noticed that hexagonal CoS, CoS_2, Co_3S_4 and Co_9S_8 shows a Half metallic behaviour after we examined through the Hubbard correction. Interestingly, reveals a remarkable difference that only CoS_2 exhibits magnetic behaviour in contrast with previous results that indicate CoS,Co_9S_8 as magnetic materials.

Furthermore, we performed the experiment study using ultrasonic spray pyrolysis (USP),our XRD analysis confirmed the hexagonal structure of Co_9S_8 with particle size D=22.47 nm ,by using FT-IR analysis shows intense peak that refer to Co-S, on other side the UV-VIS shows that the optical transmittance is above 60% for all samples and the band gap obtained using tauc relation turn up sensitive of cobalt sulfide thin films to subtle synthesis variation these findings highlight the importance of precise control over processing condition. Moreover, the refractive index values reveal a clear inverse relationship with optical band gap.

These combined theoretical and experimental findings have made a huge contribution to fill its gaps and to the understanding of the various phases of cobalt sulfide that gives them a potential to be used in several applications like batteries , DSSC and biomedicine.

References: Introduction

[1] Y. Han, B. Lao, X. Zheng, S. Li, R.-W. Li, and Z. Wang, "Transition metal oxides: a new frontier in spintronics driven by novel quantum states and efficient charge-spin interconversion," *Front. Mater.*, vol. 11, Aug. 2024, doi: 10.3389/fmats.2024.1444769.

[2] R. Ramesh and D. G. Schlom, "Creating emergent phenomena in oxide superlattices," *Nat. Rev. Mater.*, vol. 4, no. 4, pp. 257–268, Mar. 2019, doi: 10.1038/s41578-019-0095-2.

[3] S. Sahoo, K. Y. Wickramathilaka, E. Njeri, D. Silva, and S. L. Suib, "A review on transition metal oxides in catalysis," *Front. Chem.*, vol. 12, May 2024, doi: 10.3389/fchem.2024.1374878.

[4] W. Suchanek and J. Garcés, "Hydrothermal synthesis of novel alpha alumina nano-materials with controlled morphologies and high thermal stability," *Crystengcomm*, vol. 12, Oct. 2010, doi: 10.1039/b927192a.

[5] A. V. Nikam, B. L. V. Prasad, and A. A. Kulkarni, "Wet chemical synthesis of metal oxide nanoparticles: a review," *CrystEngComm*, vol. 20, no. 35, pp. 5091–5107, Sep. 2018, doi: 10.1039/C8CE00487K.

[6] M. Liao *et al.*, "Constructing amorphous/crystalline heterointerface in cobalt sulfide for high-performance supercapacitors," *J. Power Sources*, vol. 625, p. 235663, Jan. 2025, doi: 10.1016/j.jpowsour.2024.235663.

[7] S. R. Shingte *et al.*, "The power trio: CoS-CoFe2O4-rGO ternary composite to enhance energy density of all-solid-state asymmetric supercapacitors," *J. Energy Storage*, vol. 106, p. 114842, Jan. 2025, doi: 10.1016/j.est.2024.114842.

[8] S. Ali *et al.*, "Transition metal sulfides: From design strategies to environmental and energy-related applications," *Coord. Chem. Rev.*, vol. 523, p. 216237, Jan. 2025, doi: 10.1016/j.ccr.2024.216237.

[9] S. Y. Shajaripour Jaberi, A. Ghaffarinejad, Z. Khajehsaeidi, and A. Sadeghi, "The synthesis, properties, and potential applications of CoS2 as a transition metal dichalcogenide (TMD)," *Int. J. Hydrog. Energy*, vol. 48, no. 42, pp. 15831–15878, May 2023, doi: 10.1016/j.ijhydene.2023.01.056.

[10] A. Y. A. Ahmed *et al.*, "Application of cobalt-sulphide to suppress charge recombinations in polymer solar cell," *Mater. Sci. Semicond. Process.*, vol. 185, p. 108917, Jan. 2025, doi: 10.1016/j.mssp.2024.108917.

[11] Q. Zhou *et al.*, "Co3S4-pyrolysis lotus fiber flexible textile as a hybrid electrocatalyst for overall water splitting," *J. Energy Chem.*, vol. 89, pp. 336–344, Feb. 2024, doi: 10.1016/j.jechem.2023.10.015.

[12] L. Zhu *et al.*, "Investigation of CoS2-based thin films as model catalysts for the oxygen reduction reaction," *J. Catal.*, vol. 258, no. 1, pp. 235–242, Aug. 2008, doi: 10.1016/j.jcat.2008.06.016.

[13] Y. Zhao, D. Gao, J. Biskupek, U. Kaiser, R. Liu, and C. Streb, "In situ formation of robust nanostructured cobalt oxyhydroxide/cobalt oxide oxygen evolution reaction electrocatalysts," *Mater. Adv.*, vol. 5, no. 11, pp. 4786–4793, 2024, doi: 10.1039/D4MA00382A.

[14] M. Yu *et al.*, "Fabrication of permselective interlayer with uniform pore structure and in-situ sulfurized Co4S3 for high performance lithium sulfur battery," *Sep. Purif. Technol.*, vol. 341, p. 126664, Aug. 2024, doi: 10.1016/j.seppur.2024.126664.

[15] M. S. Gopika and S. Savitha Pillai, “Investigations of structural, morphological, and optical properties of CoS/Fe3O4 composites,” *Mater. Today Proc.*, vol. 66, pp. 3334–3339, Jan. 2022, doi: 10.1016/j.matpr.2022.06.540.

[16] G. Abdelouahab, C. Zaouche, A. Maouane, A. Ammari, and L. Dahbi, “Substrate Temperature Effect on the Structural, Optical and Morphological Proprties of Cobalt Sulfide Thin Films Deposited Using Spray Pyrolisis,” *Ann. West Univ. Timisoara - Phys.*, May 2024, doi: 10.2478/awutp-2024-0010.

[17] X. Tang *et al.*, “Self-templating approach to Co9S8 hexagonal sheets via Kirkendall effect with efficient photocatalytic performance,” *Inorg. Chem. Commun.*, vol. 161, p. 112055, Mar. 2024, doi: 10.1016/j.inoche.2024.112055.

References: Chapters

[1] D. G. Dadi, M. W. Shura, and F. Gochole, "Density functional theory study of cobalt sulfide as a counter electrode material for dye-sensitized solar cells," *Mater. Res. Express*, vol. 11, no. 10, p. 105506, Oct. 2024, doi: 10.1088/2053-1591/ad87b2.

[2] Dr. S. Patil *et al.*, "Template-free synthesis of one-dimensional cobalt sulfide nanorod array as an attractive architecture for overall water splitting," *Int. J. Energy Res.*, vol. 45, Sep. 2020, doi: 10.1002/er.5973.

[3] A. Alshoaibi, "Investigating the Supercapacitive Performance of Cobalt Sulfide Nanostructures Prepared Using a Hydrothermal Method," *Materials*, vol. 16, no. 13, Art. no. 13, Jan. 2023, doi: 10.3390/ma16134512.

[4] M. S. Gopika and S. S. Pillai, "Impact of morphology on the magnetic and optical properties of cobalt sulfide," *J. Mater. Res.*, vol. 38, no. 8, pp. 2097–2111, Apr. 2023, doi: 10.1557/s43578-023-00954-6.

[5] T. Abza *et al.*, "Characterization of Cobalt Sulfide Thin Films Synthesized from Acidic Chemical Baths," *Adv. Mater. Sci. Eng.*, vol. 2020, no. 1, p. 2628706, Jan. 2020, doi: 10.1155/2020/2628706.

[6] P. H. Edwards, J. R. Bairan Espano, and J. E. Macdonald, "Rational Phase Control in the Synthesis of Cobalt Sulfides," *Chem. Mater.*, vol. 36, no. 15, pp. 7186–7196, Aug. 2024, doi: 10.1021/acs.chemmater.4c00911.

[7] P. O. Agboola, I. Shakir, Z. A. Almutairi, and S. S. Shar, "Hydrothermal synthesis of Cu-doped CoS2@NF as high performance binder free electrode material for supercapacitors applications," *Ceram. Int.*, vol. 48, no. 6, pp. 8509–8516, Mar. 2022, doi: 10.1016/j.ceramint.2021.12.061.

[8] Y. Wang *et al.*, "Controlled synthesis of van der Waals CoS2 for improved p-type transistor contact," *Nanotechnology*, vol. 35, Oct. 2023, doi: 10.1088/1361-6528/ad0059.

[9] "CoS2 Nanoparticles Embedded in Covalent Organic Polymers as Efficient Electrocatalyst for Oxygen Evolution Reaction with Ultralow Overpotential | Request PDF." Accessed: Nov. 17, 2024. [Online]. Available: https://www.researchgate.net/publication/354184824_CoS2_Nanoparticles_Embedded_in_Covalent_Organic_Polymers_as_Efficient_Electrocatalyst_for_Oxygen_Evolution_Reaction_with_Ultralow_Overpotential?_tp=eyJjb250ZXh0Ijp7ImZpcnN0UGFnZSI6InNlYXJjaCIsInBhZ2UiOiJzZWFyY2giLCJwb3NpdGlvbiI6InBhZ2VIZWFkZXIifX0

[10] X. Chen *et al.*, "Recent advances in cobalt disulfide for electrochemical hydrogen evolution reaction," *Int. J. Hydrog. Energy*, vol. 48, no. 25, pp. 9231–9243, Mar. 2023, doi: 10.1016/j.ijhydene.2022.11.352.

[11] R. Ivanauskas, K. Vaičiukynaitė, S. Zalenkiene, and I. Ancutiene, "Structural, Morphological, Compositional and Optical Properties of Cos2 Thin Films Synthesized by Adsorption-Diffusion Method," Oct. 28, 2023, *Rochester, NY*: 4616247. doi: 10.2139/ssrn.4616247.

[12] A. Pandey *et al.*, "Structural, morphological and electrical properties of hydrothermally synthesized cobalt disulfide (CoS2) nanoparticles," *Ferroelectrics*, vol. 618, no. 2, pp. 451–463, Jan. 2024, doi: 10.1080/00150193.2023.2273722.

[13] K. Vaiciukynaite, S. Zalenkiene, I. Ancutiene, and R. Ivanauskas, "Structural, morphological, compositional and optical properties of CoS2 thin films synthesized by adsorption-diffusion method," *Curr. Appl. Phys.*, vol. 68, pp. 1–11, Dec. 2024, doi: 10.1016/j.cap.2024.08.004.

[14] R. Xu *et al.*, "Study on modification and electrochemical properties of COS2-based cathode materials," *RSC Adv.*, vol. 15, no. 15, pp. 11337–11342, Apr. 2025, doi: 10.1039/D5RA01620G.

[15] M. Zhu, Y. Yang, X. Zhang, Y. Liang, and J. Tang, "Cobalt-based zeolitic imidazole framework derived hollow Co3S4 nanopolyhedrons for supercapacitors," *Appl. Organomet. Chem.*, vol. 38, no. 8, p. e7533, 2024, doi: 10.1002/aoc.7533.

[16] G. Abdelouahab, C. Zaouche, A. Maouane, A. Ammari, and L. Dahbi, "Substrate Temperature Effect on the Structural, Optical and Morphological Proprties of Cobalt Sulfide Thin Films Deposited Using Spray Pyrolisis," *Ann. West Univ. Timisoara - Phys.*, May 2024, doi: 10.2478/awutp-2024-0010.

[17] H. C P, G. A, I. I G K, V. S, and B. S, "Synthesis and Application of Titanium Carbide (Ti3C2)-Cobalt Sulfide (Co3S4) Nanocomposites in Amino Acid Biosensing," *Cureus*, vol. 16, no. 7, p. e63582, doi: 10.7759/cureus.63582.

[18] H. Li, H. Yang, Z. Sun, Y. Shi, H.-M. Cheng, and F. Li, "A highly reversible Co3S4 microsphere cathode material for aluminum-ion batteries," *Nano Energy*, vol. 56, pp. 100–108, Feb. 2019, doi: 10.1016/j.nanoen.2018.11.045.

[19] X. Li, K. Zheng, J. Zhang, G. Li, and C. Xu, "Engineering Sulfur Vacancies in Spinel-Phase Co3S4 for Effective Electrocatalysis of the Oxygen Evolution Reaction," *ACS Omega*, vol. 7, no. 14, pp. 12430–12441, Apr. 2022, doi: 10.1021/acsomega.2c01423.

[20] H. Yang, L. Liu, J. Ma, J. Zhang, and Q. Zhang, "Hydrothermal Synthesis of Hierarchical Cage-like Co9S8 Microspheres Composed of Nanosheets as High-Capacity Anode Materials," *Energies*, vol. 17, no. 22, Art. no. 22, Jan. 2024, doi: 10.3390/en17225553.

[21] X. Tang *et al.*, "Self-templating approach to Co9S8 hexagonal sheets via Kirkendall effect with efficient photocatalytic performance," *Inorg. Chem. Commun.*, vol. 161, p. 112055, Mar. 2024, doi: 10.1016/j.inoche.2024.112055.

[22] T. Munir *et al.*, "Structural, optical and thermoelectric properties of (Al and Zn) doped Co9S8-NPs synthesized via co-precipitation method," *J. King Saud Univ. - Sci.*, vol. 35, no. 7, p. 102836, Oct. 2023, doi: 10.1016/j.jksus.2023.102836.

[23] "Ab initio density functional studies of transition-metal sulphides: I. Crystal structure and cohesive properties - IOPscience." Accessed: May 29, 2025. [Online]. Available: https://iopscience.iop.org/article/10.1088/0953-8984/9/50/013/meta

[24] C. Wang, X. Pang, G. Wang, L. Gao, and F. Fu, "Cobalt Sulfide (Co9S8)-Based Materials with Different Dimensions: Properties, Preparation and Applications in Photo/Electric Catalysis and Energy Storage," *Photochem*, vol. 3, no. 1, pp. 15–37, Jan. 2023, doi: 10.3390/photochem3010002.

[25] G. Abdelouahab, C. Zaouche, A. Maouane, A. Ammari, and L. Dahbi, *Ann. West Univ. Timisoara - Phys.*, May 2024, doi: 10.2478/awutp-2024-0010.

[26] T. Munir *et al.*, "Structural, optical, electrical and thermo-electrical properties of Cu doped Co9S8-NPs synthesized via co-precipitation method," *Chem. Phys. Lett.*, vol. 761, p. 137989, Dec. 2020, doi: 10.1016/j.cplett.2020.137989.

[27] A. Ait-karra *et al.*, "Effect of hydrothermal temperature on the structural, morphological, optical properties and photocatalytic performances of cobalt sulfide nanomaterials," *J. Alloys Compd.*, vol. 999, p. 174946, Sep. 2024, doi: 10.1016/j.jallcom.2024.174946.

[28] W. Kohn and L. J. Sham, "Self-Consistent Equations Including Exchange and Correlation Effects," *Phys. Rev.*, vol. 140, no. 4A, pp. A1133–A1138, Nov. 1965, doi: 10.1103/PhysRev.140.A1133.

[29] "MPHY108.pdf." Accessed: Apr. 24, 2024. [Online]. Available: http://e-biblio.univ-mosta.dz/bitstream/handle/123456789/20532/MPHY108.pdf?sequence=1

[30] "A Theory of Hartree's Atomic Fields | Mathematical Proceedings of the Cambridge Philosophical Society | Cambridge Core." Accessed: Apr. 24, 2024. [Online]. Available: https://www.cambridge.org/core/journals/mathematical-proceedings-of-the-cambridge-philosophical-society/article/abs/theory-of-hartrees-atomic-fields/7BD2B084CD38C4FA05F636396088897A

[31] "Chapitre II Outils Théoriques".

[32] "Phys. Rev. B 53, 3764 (1996) - Generalized Kohn-Sham schemes and the band-gap problem." Accessed: Apr. 03, 2024. [Online]. Available: https://journals.aps.org/prb/abstract/10.1103/PhysRevB.53.3764

[33] "lec11_pseudopotentials.pdf." Accessed: May 20, 2024. [Online]. Available: https://www-users.york.ac.uk/~mijp1/teaching/grad_FPMM/lecture_notes/lec11_pseudopotentials.pdf

[34] "Figure 2.3: Schematic diagram of a pseudopotential. The wave function...," ResearchGate. Accessed: May 20, 2024. [Online]. Available: https://www.researchgate.net/figure/Schematic-diagram-of-a-pseudopotential-The-wave-function-ps-AE-calculated-in-the_fig3_50279135
[35] P. Giannozzi *et al.*, "QUANTUM ESPRESSO: a modular and open-source software project for quantum simulations of materials," *J. Phys. Condens. Matter*, vol. 21, no. 39, p. 395502, Sep. 2009, doi: 10.1088/0953-8984/21/39/395502.
[36] W. A. Bryant, "The fundamentals of chemical vapour deposition," *J. Mater. Sci.*, vol. 12, no. 7, pp. 1285–1306, Jul. 1977, doi: 10.1007/BF00540843.
[37] "GROWTH AND STRUCTURE OF FILMS – Thin film Science and Technology." Accessed: May 23, 2025. [Online]. Available: https://ebooks.inflibnet.ac.in/msp12/chapter/growth-and-structure-of-films/
[38] "6 Types Of Thin Films And Their Uses." Accessed: May 23, 2025. [Online]. Available: https://www.theindustryoutlook.com/manufacturing/news/6-types-of-thin-films-and-their-uses-nwid-3769.html
[39] "Thin Film Deposition | 6 Types Of Thin Films & Applications." Accessed: May 23, 2025. [Online]. Available: https://vaccoat.com/blog/thin-film-and-thin-films-types/
[40] "Dimensionless Analysis to Determine Elastoplastic Properties of Thin Films by Indentation," ResearchGate. Accessed: May 23, 2025. [Online]. Available: https://www.researchgate.net/publication/365623012_Dimensionless_Analysis_to_Determine_Elastoplastic_Properties_of_Thin_Films_by_Indentation
[41] D. N. Jain, "Key Steps in the Sol-Gel Process for Nanoparticle Synthesis," AZoNano. Accessed: May 23, 2025. [Online]. Available: https://www.azonano.com/article.aspx?ArticleID=6857
[42] "📚 Théses-Algérie: Doctorat, Magister, Master..." Accessed: May 23, 2025. [Online]. Available: https://www.theses-algerie.com
[43] E. Cuce, P. M. Cuce, C. J. Wood, and S. B. Riffat, "Toward aerogel based thermal superinsulation in buildings: A comprehensive review," *Renew. Sustain. Energy Rev.*, vol. 34, pp. 273–299, Jun. 2014, doi: 10.1016/j.rser.2014.03.017.
[44] "Preparation, synthesis and application of Sol-gel method," ResearchGate. Accessed: May 24, 2025. [Online]. Available: https://www.researchgate.net/publication/344942631_Preparation_synthesis_and_application_of_Sol-gel_method
[45] P. Vidyapith, "Physics Vidyapith." Accessed: May 24, 2025. [Online]. Available: https://www.physicsvidyapith.com/2023/08/preparation-of-nanostructured-particles-by-sol-gel-method.html
[46] S. Choudhury, "A REVIEW OF THE SOL-GEL PROCESS AND ITS APPLICATION," *Int. Educ. Res. J. IERJ*, vol. 10, no. 7, Jul. 2024, doi: 10.21276/IERJ24449856325648.
[47] D. Bokov *et al.*, "Nanomaterial by Sol-Gel Method: Synthesis and Application," *Adv. Mater. Sci. Eng.*, vol. 2021, no. 1, p. 5102014, 2021, doi: 10.1155/2021/5102014.
[48] "Thio sol–gel synthesis of titanium disulfide thin films and nanoparticles using titanium(IV) alkoxide precursors - ScienceDirect." Accessed: May 24, 2025. [Online]. Available: https://www.sciencedirect.com/science/article/abs/pii/S0022369707001229?via%3Dihub
[49] "Sol-Gel Synthesis Explained | Nanotechnology Material Science." Accessed: May 23, 2025. [Online]. Available: https://www.nanowerk.com/nanotechnology-glossary/sol-gel-synthesis.php
[50] "Thin-Film Dip-Coating Methods." Accessed: Apr. 11, 2025. [Online]. Available: https://encyclopedia.pub/entry/25970
[51] N. Hadjadj, "Etude microstructurale et optique des films minces nanostructurés du SnO2 dopé azote par spray pyrolyse ultrasonique," Thesis, université ibn khaldoun-tiaret, 2018. Accessed: Apr. 11, 2025. [Online]. Available: http://dspace.univ-tiaret.dz:80/handle/123456789/2986
[52] A. B. Workie, H. S. Ningsih, and S.-J. Shih, "An comprehensive review on the spray pyrolysis technique: Historical context, operational factors, classifications, and product applications," *J. Anal. Appl. Pyrolysis*, vol. 170, p. 105915, Mar. 2023, doi: 10.1016/j.jaap.2023.105915.

[53] "1585214485_PHY(H)-VI-NANO_MATERIAL-13-AJAYPRATAP.pdf." Accessed: May 30, 2025. [Online]. Available: https://www.deshbandhucollege.ac.in/pdf/resources/1585214485_PHY(H)-VI-NANO_MATERIAL-13-AJAYPRATAP.pdf

[54] R. Gandhimathi, S. Vijayaraj, and M. P. Jyothirmaie, "ANALYTICAL PROCESS OF DRUGS BY ULTRAVIOLET (UV) SPECTROSCOPY – A REVIEW," vol. 2, no. 2, 2012.

[55] "Introduction to spectroscopy/ Donald L. Pavia, Gary M. Lampman, George S. Kriz, and James R. Vyvyan," ResearchGate. Accessed: May 30, 2025. [Online]. Available: https://www.researchgate.net/publication/44372742_Introduction_to_spectroscopy_Donald_L_Pavia_Gary_M_Lampman_George_S_Kriz_and_James_R_Vyvyan

[56] M. Sardela, Ed., *Practical Materials Characterization*. New York, NY: Springer, 2014. doi: 10.1007/978-1-4614-9281-8.

[57] Y. Ding, W. Jiang, and X. Tang, "A DFT study on the mechanical properties of Co9S8 during the lithiation/sodiation process," *Bull. Mater. Sci.*, vol. 45, no. 4, p. 253, Dec. 2022, doi: 10.1007/s12034-022-02839-6.

[58] M. S. Gopika and S. S. Pillai, "Impact of morphology on the magnetic and optical properties of cobalt sulfide," *J. Mater. Res.*, vol. 38, no. 8, pp. 2097–2111, Apr. 2023, doi: 10.1557/s43578-023-00954-6.

[59] "Density functional theory study of cobalt sulfide as a counter electrode material for dye-sensitized solar cells." Accessed: May 16, 2025. [Online]. Available: https://www.researchgate.net/publication/388292057_Density_functional_theory_study_of_cobalt_sulfide_as_a_counter_electrode_material_for_dye-sensitized_solar_cells

[60] "Calculation on surface energy and electronic properties of CoS 2," ResearchGate. Accessed: May 16, 2025. [Online]. Available: https://www.researchgate.net/publication/342606744_Calculation_on_surface_energy_and_electronic_properties_of_CoS_2

[61] "Cos2, jcpds card, Card No.41-1471, find txt data - ECHEMI.com," ECHEMI. Accessed: May 17, 2025. [Online]. Available: https://www.echemi.com/community/cos2-jcpds-card-card-no-41-1471-find-txt-data_mjart2210311640_737.html

[62] X. Tang *et al.*, "Self-templating approach to Co9S8 hexagonal sheets via Kirkendall effect with efficient photocatalytic performance," *Inorg. Chem. Commun.*, vol. 161, p. 112055, Mar. 2024, doi: 10.1016/j.inoche.2024.112055.

[63] M. Y. Toriyama *et al.*, "How to analyse a density of states," *Mater. Today Electron.*, vol. 1, p. 100002, May 2022, doi: 10.1016/j.mtelec.2022.100002.

[64] "Electrochemical synthesis of 3D hierarchical Co 3 S 4 /Co 9 S 8 nanoparticles as photocatalysts for degradation of Carboxylic acids." Accessed: Jul. 14, 2025. [Online]. Available: https://www.researchgate.net/publication/338356531_Electrochemical_synthesis_of_3D_hierarchical_Co_3_S_4_Co_9_S_8_nanoparticles_as_photocatalysts_for_degradation_of_Carboxylic_acids

[65] P. Liu *et al.*, "Synthesis of poly(m-phenylenediamine)-coated hexagonal Co9S8 for high-performance supercapacitors," *J. Mater. Sci.*, vol. 53, no. 1, pp. 759–773, Jan. 2018, doi: 10.1007/s10853-017-1537-0.

[66] L. Jin, C. Lv, J. Wang, H. Xia, Y. Zhao, and Z. Huang, "Co_9S_8 Nanotubes as an Efficient Catalyst for Hydrogen Evolution Reaction in Alkaline Electrolyte," *Am. J. Anal. Chem.*, vol. 07, no. 02, Art. no. 02, 2016, doi: 10.4236/ajac.2016.72018.

Abstract:

This work used both computational and experimental techniques to investigate different cobalt sulphide phases. In this study preconceived notions about the magnetic properties of compounds CoS_2 and discovered metallic and half-metallic behaviour of the several phases through Quantum ESPRESSO simulations. Co_9S_8 was synthesised experimentally with a hexagonal structure and a particle size of about 22 nm. It demonstrated an indirect band gap and more than 60% optical transmittance. These results provide important new information about the potential uses of cobalt sulphides in solar cells, energy storage, catalysis, and medicine.

Resume:

Ces travaux ont utilisé des techniques informatiques et expérimentales pour étudier différentes phases de sulfure de cobalt. L'équipe a remis en question les idées reçues sur les propriétés magnétiques de composés comme Co_2S_3 et CoS_2 et a découvert un comportement métallique et semi-métallique grâce à des simulations Quantum ESPRESSO. Le Co_9S_8 a été synthétisé expérimentalement avec une structure hexagonale et une taille de particule d'environ 22 nm. Il a démontré une bande interdite indirecte et une transmittance optique supérieure à 60 %. Ces résultats apportent de nouvelles informations importantes sur les utilisations potentielles des sulfures de cobalt dans les cellules solaires, le stockage d'énergie, la catalyse et la médecine.

ملخص:

استخدم هذا العمل تقنيات حسابية وتجريبية لدراسة عدة أطوار من كبريتيد الكوبالت. في هذه الدراسة، تم تحدي المفاهيم السابقة حول الخصائص المغناطيسية لمركبCoS_2 ، كما تم اكتشاف سلوك معدني ونصف معدني لعدة أطوار باستخدام محاكاة .Quantum ESPRESSO تم تصنيع Co_9S_8 تجريبياً بهيكل سداسي وحجم جسيم يقارب 22 نانومتر. وأظهر فجوة نطاق غير مباشرة ونفاذية ضوئية تتجاوز 60٪. توفر هذه النتائج معلومات جديدة مهمة حول الاستخدامات المحتملة لكبريتيدات الكوبالت في الخلايا الشمسية وتخزين الطاقة والتحفيز والطب